Dissecting the composition, dynamics, and regulation of immunoglobulin class switch recombination

Inaugural-Dissertation to obtain the academic degree Doctor rerum naturalium (Dr. rer. nat.)

submitted to the Department of Biology, Chemistry, Pharmacy of Freie Universität Berlin

by

Tannishtha Saha

2023

This study was performed from February 2018 to January 2023 under the supervision of Prof. Dr. Michela Di Virgilio at “Max Delbrück-Center for Molecular Medicine” in the Helmholtz Association, in Berlin.

1st Reviewer: Prof. Dr. Michela Di Virgilio

Charite University - Max Delbrück Center for Molecular Medicine

2nd Reviewer: Prof. Dr. Oliver Daumke

Freie University - Max Delbrück Center for Molecular Medicine

Defended on 21st November 2023

ABSTRACT

Class switch recombination (CSR) is a somatic recombination reaction occurring in mature B lymphocytes, that involves programmed double-strand break (DSB) formation and repair at immunoglobulin heavy chain locus (*Igh*). CSR is essential for adaptive immunity since it diversifies the effector functions of antibody responses. Many key players, including components of the DNA damage response and DSB repair, transcriptional regulators, long non-coding RNAs and chromatin remodelers, have been reported to contribute to the different phases of this complex process. However, how all these DNA-RNA-protein interactions are established and evolve to support the repair dynamics of CSR remains elusive. In order to bridge this knowledge gap, I have established a primary B cell model system that couples locus-specific chromatin purification and proximity labelling to high-resolution mass-spectrometry to identify the factors that selectively bind within the *Igh* locus to support DSB processing and repair during CSR.

53BP1 is a DNA damage response factor that protects DSB ends from nucleolytic processing to promote their repair *via* the nonhomologous end-joining (NHEJ) pathway. Because of this activity, 53BP1 is not only crucial for CSR, but also facilitates toxic mis-repair (toxic-NHEJ) of DSBs in BRCA1-deficient cells. Phosphorylation of 53BP1 on its N-terminus by the DSB repair kinase ataxia telangiectasia mutated (ATM) is essential for DNA end-protection, and, as a consequence, for both these physiological (CSR) and pathological 53BP1 (toxic-NHEJ) repair events. Through a SILAC-based mass-spectrometry approach, we identified acidic leucine-rich nuclear phosphoprotein 32B (ANP32B) as a potential interactor of 53BP1 under unphosphorylated conditions. I tested the hypothesis that ANP32B might interact with 53BP1 and negatively regulate it during DSB repair, which on further assessment I confirmed is dispensable for repair-associated activity.

Rap1-interacting factor 1 (RIF1) is a multi-functional protein that, together with 53BP1, acts as a pro-NHEJ protein because of its ability to mediate DSB end-protection. As a consequence, RIF1 promotes both CSR in mature B cells and toxic-NHEJ reactions on BRCA1-deficient backgrounds. However, the post-translational regulation of RIF1 DNA end-protection function has not yet been elucidated. To this end, I implemented label-free mass-spectrometry in primary B lymphocytes to define potential phosphorylation events supporting RIF1 DNA end-protection activity. I identified a serine residue (S2138) that is phosphorylated upon DSB induction; however, this post-translational modification was dispensable for regulating RIF1 function during DSB repair and CSR.

Altogether, CSR repair components, including 53BP1 and RIF1, define a crucial balance between immunity and lymphomagenesis in B cells. Therefore, identifying novel factors and

post-translational modifications involved during CSR break repair will expand our understanding of the mechanisms preserving genome stability during antibody diversification in mature B cells.

ZUSAMMENFASSUNG

Die Klassenwechsel-Rekombination (CSR) ist eine somatische Rekombinationsreaktion, die in reifen B-Lymphozyten auftritt und die Bildung und Reparatur von programmierten Doppelstrangbrüchen (DSB) am Locus der schweren Kette des Immunglobulins (Igh) umfasst. Die CSR ist für die adaptive Immunität von wesentlicher Bedeutung, da sie die Effektorfunktionen der Antikörperreaktionen diversifiziert. Es wurde berichtet, dass viele Schlüsselakteure, darunter Komponenten der DNA-Schadensreaktion und der DSB-Reparatur, Transkriptionsregulatoren, lange nicht-kodierende RNAs und Chromatin-Remodeler, zu den verschiedenen Phasen dieses komplexen Prozesses beitragen. Wie jedoch all diese DNA-RNA-Protein-Interaktionen zustande kommen und sich entwickeln, um die Reparaturdynamik der CSR zu unterstützen, ist nach wie vor ungeklärt. Um diese Wissenslücke zu schließen, habe ich ein primäres B-Zell-Modellsystem etabliert, das die ortsspezifische Chromatinreinigung und Proximity-Markierung mit hochauflösender Massenspektrometrie verbindet, um die Faktoren zu identifizieren, die selektiv innerhalb des Igh-Lokus binden, um die DSB-Verarbeitung und -Reparatur während der CSR zu unterstützen.

53BP1 ist ein DNA-Schadensreaktionsfaktor, der DSB-Enden vor nukleolytischer Verarbeitung schützt, um ihre Reparatur über den NHEJ-Weg (nonhomologous end-joining) zu fördern. Aufgrund dieser Aktivität ist 53BP1 nicht nur entscheidend für die CSR, sondern erleichtert auch die toxische Fehlreparatur (toxische NHEJ) von DSBs in BRCA1-defizienten Zellen. Die Phosphorylierung von 53BP1 an seinem N-Terminus durch die DSB-Reparaturkinase Ataxia telangiectasia mutated (ATM) ist für den Schutz des DNA-Endes und folglich sowohl für diese physiologischen (CSR) als auch für die pathologischen 53BP1-Reparaturereignisse (toxische NHE) unerlässlich. Mithilfe eines SILAC-basierten Massenspektrometrie-Ansatzes identifizierten wir das saure leucinreiche Kernphosphoprotein 32B (ANP32B) als potenziellen Interaktor von 53BP1 unter unphosphorylierten Bedingungen. Ich testete die Hypothese, dass ANP32B mit 53BP1 interagieren und es während der DSB-Reparatur negativ regulieren könnte, was sich bei weiterer Prüfung als entbehrlich für die Reparatur-assoziierte Aktivität erwies.

Rap1-interacting factor 1 (RIF1) ist ein multifunktionales Protein, das zusammen mit 53BP1 als Pro-NHEJ-Protein fungiert, da es den Schutz von DSB-Enden vermitteln kann. Infolgedessen fördert RIF1 sowohl die CSR in reifen B-Zellen als auch toxische NHEJ-Reaktionen auf BRCA1-defizienten Hintergründen. Die posttranslationale Regulierung der DNA-Endschutzfunktion von RIF1 ist jedoch noch nicht aufgeklärt worden. Zu diesem Zweck habe ich markierungsfreie Massenspektrometrie in primären B-Lymphozyten eingesetzt, um

potenzielle Phosphorylierungsereignisse zu definieren, die die DNA-Endschutzaktivität von RIF1 unterstützen. Ich identifizierte einen Serinrest (S2138), der bei der DSB-Induktion phosphoryliert wird; diese posttranslationale Modifikation war jedoch für die Regulierung der RIF1-Funktion während der DSB-Reparatur und CSR entbehrlich.

Insgesamt bestimmen die CSR-Reparaturkomponenten, einschließlich 53BP1 und RIF1, ein entscheidendes Gleichgewicht zwischen Immunität und Lymphomagenese in B-Zellen. Die Identifizierung neuartiger Faktoren und posttranslationaler Modifikationen, die an der Reparatur von CSR-Brüchen beteiligt sind, wird daher unser Verständnis der Mechanismen erweitern, die die Genomstabilität während der Diversifizierung von Antikörpern in reifen B-Zellen erhalten.

Table of Contents

1. INTRODUCTION

1.1. DNA damage and repair

DNA gets constantly damaged by different ways either by replication error or by exogenous factors like irradiation (IR). But cells also have various mechanisms to repair theses lesions in order to maintain genome integrity. If they remain unrepaired then this can lead to harmful ramifications like oncogenic transformation or even apoptosis[1-3]. One of the most common damages is double strand breaks (DSBs), which involves complete disruption of the sugar phosphate backbone in both the strands of DNA[4-5]. DSBs can be a result of external factors like IR and genotoxic drugs or even programmed internally like during antibody diversification reactions, V(D)J recombination and Class Switch recombination (CSR)[6-8]. Since DSBs are highly deleterious kind of damage causing frameshift mutations, translocations etc., their repair pathways are very tightly controlled.

DSBs are initially detected by MRE11-RAD50-NBS1 (MRN) complex that activates ataxia telangiectasia-mutated kinase (ATM). ATM then gets autophosphorylated and also phosphorylates numerous other downstream factors like H2A.X to γH2AX, that promotes assembly of repair proteins at the DSBs, therefore beginning the signalling cascade of repair[9-10]. Mammalian cells have four diverse DSB repair mechanisms, classical nonhomologous end-joining (c-NHEJ), alternate-end joining (A-EJ), homologous recombination (HR) and single-strand annealing (SSA).

1.1.1 c-NHEJ

c-NHEJ (classical nonhomologous end-joining) is active throughout the cell cycle but mostly dominate in G1 phase[11]. It involves either direct ligation of the blunt DNA ends or use of small stretches of homology (e.g. 1-4 nucleotides in Activation-induced deaminase- (AID) mediated programmed DSBs) for ligation (Figure 3)[12-15]. Direct ligation occurs when the ends are blunt or have compatible overhangs. However, when there are incompatible ends, exo or endonucleolytic processing can help the ligation process (Figure 1)[16-17].

c-NHEJ pathway initiates with Ku70/80 heterodimer rapidly coming to the broken DNA ends that promote the recruitment of x-ray repair cross complementing 4 (XRCC4)-Ligase 4 complex to ligate the ends. These factors make up the core-NHEJ component. Reports suggest that XRCC4-like factor (XLF4) and paralog of XRCC and XLF (PAXX) might be stabilizing XRCC4-Ligase 4 complex at incompatible ends to facilitate it's activity. In case nucleolytic processing is required, then DNA-dependent protein kinase catalytic subunit (DNA-

PKcs) and Artemis also come into play. Artemis requires DNA-PKcs for its activation, following which together they can recognize several types of DNA substrates like 3' overhangs, 5' overhangs, hairpin and also blunt ends, for endo and exonucleolytic activity. In the presence of Mn+ cations Artemis can also process DNA ends independently of DNA-PKcs *in vitro*. Artemis can degrade certain blunt ends created by chemotherapeutic drugs or IR to expose very short stretches of microhomologies (up to four nucleotides) for microhomology-mediated joining[16-17]. DNA ends can also be modified to gain microhomologies by polymerases like POLλ and POLμ during c-NHEJ. POLλ adds nucleotides to overhangs in a template dependent manner. POLμ can fill-in 3' overhangs, with template dependent manner being the canonical pathway. When the overhang is not base-paired to another DNA molecule, then to a limited extent POLμ can function independently of a template[18-19].

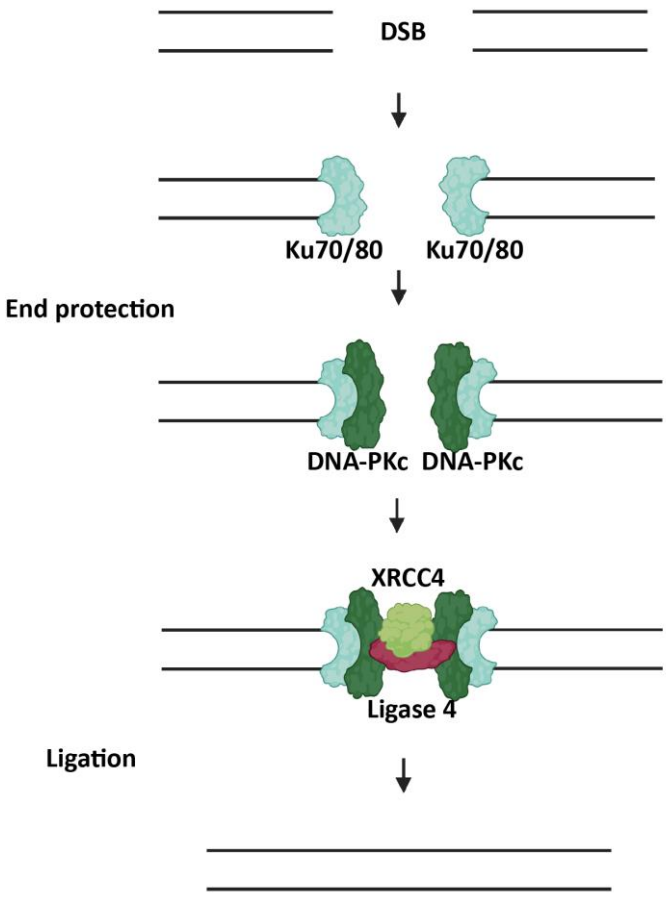

Figure 1. Schematic representation of the c-NHEJ pathway. Ku70/80 goes to DSB ends to recruit XRCC4 and Ligase 4, which ligate the broken ends. For the DSB end processing step, DNA-PKcs is loaded before the recruitment of XRCC4 and Ligase 4. c-NHEJ, Classical nonhomologous end-joining.

1.1.2. HR

HR (Homologous Recombination) is based on long nucleolytic resection on both DNA strands (>100 nucleotide 3' overhangs) on the DSB ends followed by utilization of sister-chromatid as the template for filling in the lost genetic information (Figure 3). Thus, the pathway is predominant in S/G2 phase and also characterized as the one with highest fidelity[11].

HR initiates with resection at 5' end by MRN complex along with CtBP (carboxy-terminal

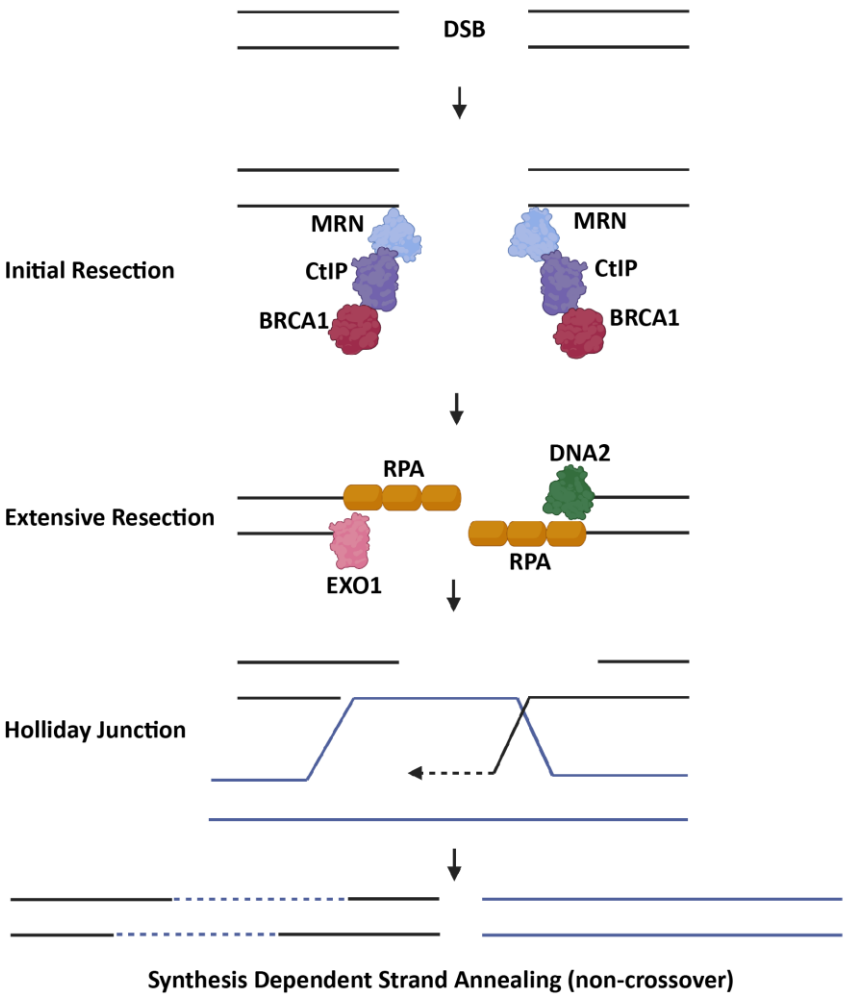

Figure 2. Schematic representation of homologous recombination HR pathway. DSBs are loaded with resection mediators like MRN complex. CDK phosphorylates CtIP upon which it is recruited by MRN to begin nucleolytic end processing. Moreover, CtIP is also ubiquitinated by BRCA1 that further enhances its activity. Long range resection is continued by nucleases EXO1 and DNA2. ssDNA overhangs generated upon resection is immediately bound by RPA until it is displaced by RAD51 for homology search and strand invasion. This forms Holliday junction which is resolved into either crossover or non-crossover products. Somatic cells mostly undergo synthesis dependent strand annealing pathway to generate non-crossover products. Homologous Recombination, HR.

binding protein) interacting protein (CtIP) and BRCA1. MRN, CtIP and BRCA1 bind to the DNA break ends and processes through both endonucleolytic followed by 3' exonucleolytic activity to form short 3' overhangs. These 3' overhangs can be further resected in an additional step by 5' exonuclease EXO1 (Exonuclease 1) and/or by endonuclease DNA2 together with DNA unwinding helicase BLM (Bloom Syndrome Protein). Replication protein A (RPA) has high affinity for ssDNA overhangs and stabilizes them until it is replaced by RAD51 for homology search, leading to strand invasion for DNA synthesis from the sister-chromatid template[20-22]. The resulting double Holliday junction (dHJ) is resolved by the BTR (BLM–TOP3A–RMI) complex to segregate the sister-chromatids without crossover. However, persistent dHJs are resolved later in the cell cycle by SLX4/SLX1/Mus81/EME1 complex, and GEN1, with or without crossover (Figure 2)[23-26].

1.1.3. A-EJ

A-EJ (alternate end-joining) also requires resection mediated by MRN-CtIP pathway. During repair of AID-induced programmed DSBs, it is can generate 2-20 nucleotide 3' overhangs (Figure 3). Nucleolytic resection in A-EJ generates short stretches of homologies to be exposed and thereby the pathway is biased towards terminal strand pairing and ligating DNA ends with microhomologies (longer than in c-NHEJ). Albeit, sometimes it also can also generate overhangs without any homology. It is active throughout the cell cycle and thus, resection also occurs outside S/G2 phase[11,16,28].

A-EJ begins with Poly (ADP-ribose) polymerase 1 (PARP1) competing with Ku to bind at DSBs. PARP1 then recruits MRN-CtIP complex to initiate the resection process, although more limited than HR (and Single Strand Annealing), to expose short overhangs with homology[16,27-28]. RPA on ssDNA is displaced by POLθ that has RAD51 binding motif which in turn restricts RAD51 loading on ssDNA in order to inhibit HR and promote microhomology search. POLθ expression is usually downregulated in HR-proficient condition. It anneals DNA breaks by error-prone gap filling at the DSBs and also by degrading 3' non-complementary tails[27,29-31]. Lastly, ligation is carried out by LIG 3-XRCC1 complex recruited to DSBs *via* MRN complex. LIG3 constitutively associates with MRN complex under undamaged conditions and dissociates only upon DNA damage. However, in the absence of NHEJ, their association is unperturbed[27-28,32-34]. LIG1 also has a role in A-EJ as a back-up protein, although its function doesn't rely on microhomology usage[35]. LIG1 and LIG3 seem to have overlapping function and compensate for each other in the absence of one of them in some situations[36-37].

1.1.4. SSA

This process also initiates with PARP1 immediately binding to DSB ends. SSA (single strand annealing) repair mechanism involves extensive resection on both strands of DNA (less than HR), exposing >25 nucleotides of homology, *via* MRN-CtIP and also by DNA2 and/or EXO1-BLM (Figure 3). RAD52 is one of the main components of SSA that replaces RPA on ssDNA stretches. It facilitates efficient pairing and annealing large sequences of homologous ssDNA on the same DNA molecule. Begore ligation, the residual non-homologous 3' flaps are removed by nucleotide excision repair and the mismatch repair complexes XPF–ERCC1 and MSH2–MSH3 respectively[16,38]. Ligases acting in this repair pathway are still obscure. SSA seems to be predominant during S/G2 phase[11]. However, since it doesn't require sister-chromatid template, it can in theory be active throughout all cell cycle phases. This repair process is error-prone and mutagenic.

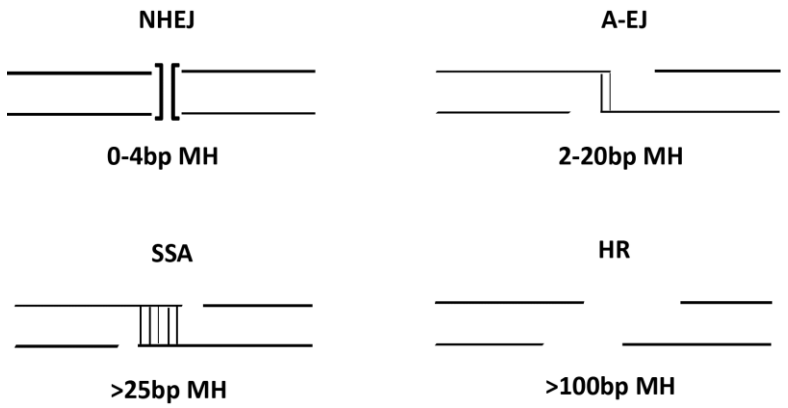

Figure 3. Schematic representation of MH usage in different DSB repair pathways operating in mammalian cells. The approximate length of MH used in each pathway is indicated. MH, Microhomology.

1.2. Class Switch Recombination

B cells are part of the adaptive immune system that produces various types of antigen specific antibodies or immunoglobulins (Igs) with different effector functions. Igs are composed of two heavy and two light polypeptide chains assembled together to form a Y-shape structure. Each of the chain contains a pathogen recognition/binding variable region. However, only heavy chains have a pathogen removal constant region[40-41]. The variable region comprises of three segments: variable (V), diversity (D) and joining (J). In naïve B cells, each V, D and J segment is flanked by a special sequence called recombination signals (RSS). During the process of naïve B cells developing into mature B cells, recombination activating genes-1 and -2 (RAG1 and RAG2) proteins initiate DSBs at the RSS sequences, followed by their repair through c-

NHEJ that eventually results in recombination of V(D)J genes (V and J segments for immunoglobulin light (*Igl)* locus). Productive assembly of *Igh* and *Igl* variable region exons permits the expression of *Igh* and *Igl* chains as cell surface IgM antibody[42]. V(D)J recombination is one of the two antibody diversification mechanisms that is regulated through programmed DSBs, with Class Switch Recombination (CSR) as the other one. Both the processes bear tightly controlled DSB formation and repair pathways and deregulation at any step can not only result in immune-deficiency but also lymphomagenesis[43-44].

The *Igh* locus, located on chromosome 12 in mouse, comprises of eight constant genes that determine the type of immunoglobulin to express on the cell surface (Figure 4). After V(D)J recombination, mature B cells express IgM antibody at its surface since the rearranged V(D)J exons are in juxtaposition to Constant μ gene (Cμ) at the *Igh* locus[45]. CSR is a process occurring after antigen encounter presented by T cells, whereby a mature B cell can switch from IgM to IgG, IgA and IgE, depending on which Constant gene is in juxtaposition to the V(D)J (γ, α, ϵ). Each different isotype mediates a different effector function, thus diversifying the effector component of antibody responses[46-47].

Cμ is known as the donor constant region and all the other constant exons downstream of it are called acceptor constant regions. Each C gene, except for C_δ, is preceded by intronic sequences called switch (S) regions. S regions are highly repetitive sequences spanning from 1 to 12 Kb of DNA. During CSR, Sμ and one of the downstream acceptor S regions (depending on the stimulus) recombine, resulting in the deletion of the intervening sequences, including Cμ, thereby expressing the corresponding acceptor Constant exon. IgD antibody is a result of alternative splicing of a long primary transcript containing both Cμ and Cδ genes[46-47].

At the molecular level, CSR is initiated by Activation-Induced Cytidine Deaminase (AID) expression and germline transcription (GLT) (Figure 4). AID is a B cell-specific cytosine deaminase protein encoded by the *Aicda* gene, which targets the S regions and triggers CSR. GLT starts from a promoter I-exon, located upstream of each S-C unit, proceeds through the S-C regions and terminates downstream of the C exon. Transcription across these regions is essential for AID targeting since AID can only act on single-stranded DNA. AID deaminates cytidine residues within the S regions, thus creating U:G mismatches that are then converted to DSBs *via* the Base Excision Repair (BER) and Mismatch repair (MMR) pathways[48]. A productive CSR event relies on accurate repair of DSBs at Sμ and one of the acceptor S region by the NHEJ pathway (Figure 4). In the absence of core NHEJ factors like Ku80, DNA-PKCs and Ligase IV, CSR is compromised[49]. GLT, and CSR as a consequence, is regulated

by a 25 kb super enhancer region located at the 3' of the *Igh* locus, known as 3' Regulatory Region (3'RR)[50].

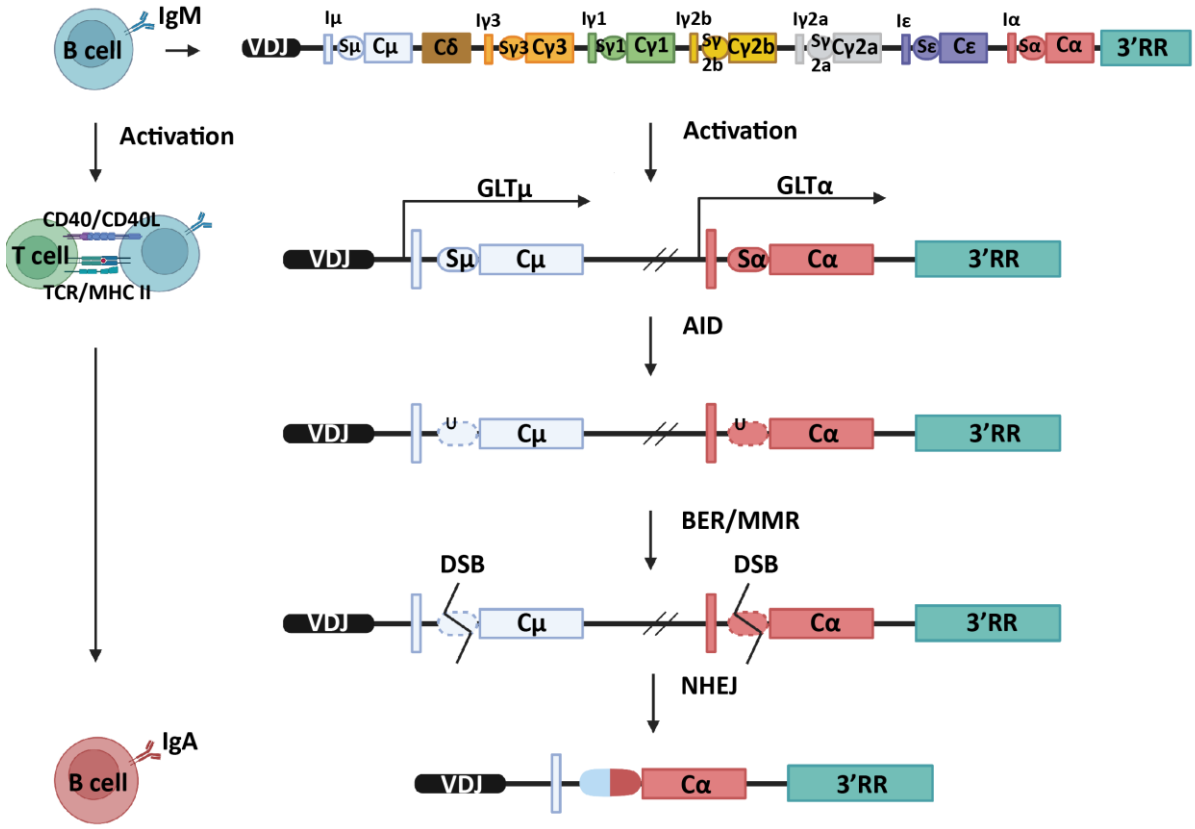

Figure 4. CSR is a multi-step deletional recombination reaction. Top: Schematic representation of mouse *Igh* locus. In a mature mouse B cell, *Igh* locus comprises a rearranged VDJ exon and eight constant regions, each encoding for different antibody isotypes. Each C exon, except for Cδ, is preceded by the respective S region. Bottom: Schematic representation of class switch recombination (CSR). After B cells are stimulated with activation signals (by T cell in physiology and by cytokines *in vitro*), CSR initiates with GLT of acceptor region (GLTμ is mostly constitutively expressed). AID is induced in activated B cells and targets S regions undergoing GLT expression to mutate cytosines to uracil residues. These mismatches are processed into DSBs by BER/MMR pathway that are repaired by NHEJ, deleting the intervening sequences and expressing new C region (Cα here) region juxtaposed to the V(D)J exon. CSR, class switch recombination; GLT, germline transcription; AID, activation-induced cytidine deaminase; DSB, double-strand break; 3′RR, 3′ regulatory region.

1.2.1 Switch regions

As mentioned earlier, each constant gene (except for Cδ) is preceded by the corresponding intronic S region. Each S region has different length with a distinct repetitive unit which are of

different sizes (Table 1)[39]. S regions repeat units are G-rich in the nontemplate strand. AID deaminates the C residues into U on the template strand and the U:G mismatches are eventually converted into nicks by BER or MMR pathway. Dissolution of closely spaced nicks develop into DSBs[46-48]. It has been observed that repair of staggered DSBs are more biased towards A-EJ, like DSBs that are CRISPR/Cas9-mediated at S regions. Similarly, reduced amount of AID-deamination also forms more staggered DSBs and the repair is shifted towards A-EJ[51]. Moreover, effect of loss of A-EJ factor is more prominent in IgA isotype than others, most likely due to longer microhomologies in Sμ-Sα junction than other Sμ-Sx junctions. This observation strongly suggests that CSR to IgA is more dependent on A-EJ than any other isotype[39,52-54].

	Total Size	Repeat Size
Sμ	3.2* Kb	10-40 bp
Sγ3	2.5* Kb	49 bp
Sγ1	10* Kb	49 bp
Sγ2b	5 Kb	49 bp
Sγ2a	2.5 Kb	52 bp
Sε	1 Kb	40-50 bp
Sα	4.2 Kb	80 bp

Table 1. The table indicates approximate length of each S region at mouse *Igh* locus (the asterisk designates that the S region length varies in different mice strains) along with size of each S region repeat units in nontemplate strand.

1.2.2. 3'RR

The 3'RR is located downstream of Cα (last C exon) and has four lymphoid-specific transcriptional core DNAse I hypersensitive enhancer sites (hs3a, hs1,2, hs3b, and hs4). The core enhancers as well as the surrounding sequences within the 3'RR are crucial for GLT[55]. Our lab had found that the chromatin reader ZMYND8, binds at the 3'RR and contributes to efficient CSR by modulating transcription of acceptor S regions. Specifically, ZMYND8 deletion results in enrichment of RNA polymerase II at the 3'RR, significantly at hs1,2 and hs3b, and increased enhancer RNAs transcription, while reducing acceptor S region transcription[50].

1.2.3. Formation of the DSBs

Introduction of double strand breaks are facilitated by AID. It is a B cell specific enzyme that is expressed only in germinal center B cells undergoing CSR and Somatic Hypermutation

(SHM). During CSR, GLT enables recruitment of AID by mechanisms like[56-57]; (1) generation of RNA:DNA hybrid that exposes S region stretches for AID recruitment, (2) transcription-coupled modifications at S regions for AID access[58-59] (3) Spt5 and RNA polymerase II dependent targeting of AID to S regions[60], (4) and tethering AID to intronic Switch RNA *via* Debranching enzyme (DBR1) to target S region[61]. AID generates mismatches at the S region by converting deoxycytidine to deoxyuridine. The mismatches are further processed into DSBs by Base excision repair pathway (BER) and Mismatch repair pathway (MMR)[48].

1.2.4. Pathways in DSB repair during CSR

AID induces breaks at G1 phase of cell cycle and therefore, DSBs during CSR are repaired predominantly by NHEJ and partly by A-EJ[62-65]. Large proportion of the S region junctions display direct joins and the remaining bear 1-4 bp microhomologies, albeit a few still have microhomologies longer than 4bp[12-15]. Deletion of any of the core NHEJ components not only significantly impairs CSR, but also increases chromosomal translocation involving *Igh* locus. Loss of DNA-PKcs reduces CSR to varying efficiencies. Depletion of XLF4 mildly reduces CSR and Artemis can maintain CSR almost to *WT* levels[16-17,66-68]. B cells lacking a core NHEJ protein still exhibit some residual CSR. Moreover, S region junctions of B cells deficient of XRCC4, LIG4, Ku, XLF, and Artemis display lesser direct joins and are skewed towards having longer microhomologies. These observations suggest that A-EJ also plays a role during DSB repair of CSR, but more as a secondary repair mechanism[16,27-28].

MRE11 deletion considerably reduces CSR, most likely due to its upstream role in DSB repair signalling cascade[29,52-53,69-71]. Other A-EJ factors like CtIP effected CSR to varying degrees with mild implications on CSR junctions. Loss of PARP1 has no effect in CSR, however it causes lesser usage of microhomologies. Polθ-deficiency neither effects CSR nor S region junctions[72]. 5hmC binding embryonic stem cell-specific protein (HMCES) has been defined recently as a novel A-EJ factor involved in repair of CSR breaks. Its abrogation mildly reduces CSR, specifically to IgA, and favours more direct joins at S region junctions. It has been proposed that it binds to ssDNA to promote A-EJ and also to protect it from extensive resection[54]. Deletion of either LIG1 or LIG3 doesn't affect CSR. However, abrogation of either ligases further reduces CSR in Ligase 4-depleted cells, indicating their redundant roles in A-EJ during CSR. Furthermore, LIG1 and LIG3 mediate CSR with tenfold slower kinetics[36-37]. A-EJ also increases chromosomal translocation frequency[16,27-28]. Altogether, these data imply that NHEJ is the predominant repair pathway for AID-induced programmed DSBs and A-EJ is an additional pathway. CSR is a great tool to dissect these pathways, although these pathways could act in a more distinct way at *Igh* locus than non-programmed DSBs.

Since CSR is a G1 phase process, HR is dispensable for isotype switching. However, it has been observed that B cells lacking RAD51 paralog XRCC2 and therefore inefficient in HR, accumulate AID-induced DSBs at *Igh* locus and at some off-targets. This observation could suggest that the DSBs that remain unrepaired during G1 by NHEJ get subsequently repaired by HR[73-75]. Since HR requires a sister-chromatid for the repair, in principle the *Igh* locus sequence is completely restored. It gives B cells the possibility for an additional round of activation induced DSB formation and repair for successful CSR. Furthermore, the non-*Igh* DSBs generated by AID are repaired with high fidelity by HR and shields B cells from genomic instability. Interestingly B cells have the capacity to activate checkpoints during DSBs induced by IR, but CSR induced DSBs supress checkpoint activation. This hypothesis comes from a study that showed suppression of p53 during germinal centre reaction in spleen that induces CSR post immunization[76]. These evidences imply that exogenous sources of DSBs can activate checkpoint but programmed DSBs somehow have a mechanism to bypass this phenomena for antibody diversification.

In theory, SSA is active in all cell cycle phases since it doesn't require sister-chromatid as a template for repair mechanism. B cells lacking any of the core NHEJ factor have reduced CSR but show high frequency of intra-switch recombination. Intra-switch recombination is a product of same switch region recombining back together with some internal sequence deletion, but without deleting the intervening constant exons. Even though it could be mediated by A-EJ, RAD52, a SSA protein, was recently reported to execute intra-switch recombination. In general, it competes with Ku to bind to DNA break ends and hence in *WT* condition some repair is also directed towards intra-switch recombination. Additionally, loss of Ku and RAD52 almost completely diminishes CSR that could also indicate contribution of RAD52 in A-EJ[49,77].

1.2.5. Influence of AID-induced breaks in pathway choice

Distal mismatches generated by AID are processed by MMR pathway to create staggered DSBs. Mice deficient in core NHEJ protein XRCC4 and a MMR factor (EXO1, MSH2 or MLH1), significantly reduce CSR when compared with depletion of any of the individual protein. Although except for MLH1/XRCC4 double deficient mice, none of the other double deficient genotype (with XRCC4) exhibited increase of direct end-joining frequency at S regions compared to XRCC4-deficiency alone[78]. Consistent with this observation, a study further showed that decrease in AID-induced deamination shifts the preference towards MSH2-dependent MMR for processing of DSBs and CtIP dependent A-EJ for DSB repair. AID^{low} CH12 cell line generated by shRNA, where AID was not completely depleted, displayed increased use of microhomology in switch junctions. Knockdown of CtIP in AID^{low} CH12,

significantly reduced CSR and intra-switch recombination at Sμ. Besides, Ku70 recruitment was reduced and CtIP recruitment was increased in AID^{low} cells. AID^{low} cells showed a significant increase of EXO1 at Sμ and RPA at *Igh* for DNA resection to enable microhomology-mediated joins. MSH2 knockdown leads to 80% reduction of IgA in AID^{low} cells and 45% reduction in WT[79]. The study proposed that DSBs formed by SSBs with close proximity would be preferentially repaired by c-NHEJ and staggered DSBs generated by MMR after processing of distant uracils, will skew the repair towards A-EJ[48,79]. The relationship between the type of DNA breaks induced by AID and repair pathway was further characterized by a study using CRISPR/Cas9-mediated generation of DSBs that mimicked AID-induced ones. It demonstrated that repair of staggered DSBs with 5′ overhangs display more microhomology at switch junctions than blunt DSBs, suggesting A-EJ as the pathway choice for the repair of staggered DSBs. In support of these data, it was speculated that staggered DSBs with overhangs would be poor substrate for Ku[80]. A similar study using CRISPR/Cas9-mediated AID-modeled DSBs in human B cells also showed that 5' DSB exhibits more microhomologies than blunt or 3' DSB[81]. Although it was previously determined that AID generates more staggered DSBs than blunt lesions, the idea of blunt DNA breaks resolving into staggered ends and vice versa was not ruled out[82]. The C-terminal AID domain encoded by exon 5 was also associated with DNA repair during CSR. Deletion of exon 5 allowed efficient deamination of switch regions, but failed to recruit NHEJ repair proteins and protect DNA ends from resection[83]. Overall, these findings indicate that not only AID can act as a scaffolding protein for repair factors, but the polarity and density of AID-induced breaks also have a significant impact on the repair pathway choice.

1.2.6. CH12

CH12 are lymphoma B cells that can be stimulated by certain cytokines to express AID and undergo CSR to IgA *in vitro* with high efficiency and mimicking the physiological process[84]. Given their clonal origin, high proliferation capability, diploid genome for chromosomal studies, and ability to tolerate a wide range of selection marker concentrations, they represent a versatile model system amenable to genetic engineering and experimental scale-up[85].

B cells (and T cells) undergo a procedure known as allelic exclusion. This means that Ig transcript of only one allele will encode a functional Ig on the surface. The Ig transcript from the other allele is expressed but is non-functional[86]. CH12 cell line seems to have the recombined Sμ-Sα in the non-productive allele[87].

1.3. 53BP1

53BP1 was discovered as p53 binding protein, but over the years it has been described and established more for its role in DSB repair. It is a large protein consisting of various domains that display separation of functions. It has a Tudor domain that promotes its constitutive association to the chromatin through the histone marker H4K20me2[88]. A protein known as TIRR (Tudor Interacting repair regulator) binds to Tudor domain of 53BP1 and limits its interaction with H4K20me2. Only upon DNA damage, TIRR dissociates from 53BP1 and thereby restoring the complete ability of 53BP1 to bind to H4K20me2[89]. During DDR, ATM phosphorylation events marks the beginning of the signaling cascade. γH2AX gets phosphorylated, MDC1 gets recruited and E3 ubiquitin ligase RNF8 and RNF168 ubiquitinates histone marker H2AK15. The UDR domain of 53BP1 recognizes and bind to histone damage marker H2AK15-Ub. Oligomerization domain (OD) and LC8 domain help to multimerize the protein and also to form DSB induced foci[88]. The BRCT domain of the protein is still not completely functionally determined, but it has been observed to not have any implications on DSB repair. It has been reported to enhance p53 apoptotic mechanism, although this function is also partially mediated by the OD[90]. This function is independent of its role in DNA repair. 53BP1 has N-terminus 28 S-T/Q sites that are phosphorylated upon DNA damage by ATM. It can be divided into two domains- Pro (Protection) and Mob (Mobility). Pro contains the binding sites of proteins in the DSB repair pro-NHEJ pathway, RIF1 (ortholog of yeast Rap1-interacting factor 1), that in turn recruits Sheildin complex (SHLD 1,2,3 and REV7), CST (CTC1, STN1, TEN1) complex, POLα and Primase. Together they promote end-protection of DNA breaks from nucleolytic resection and fill-in of gaps[91-98]. Pro domain also has binding motif for Pax2 transactivation domain-interacting protein (PTIP) at S25 site. Interaction of PTIP to 53BP1 is necessary to block HR, but the mechanism is still elusive[99]. Finally, the Mob domain is crucial for mobility of the DNA break ends to encounter each other, a function also important for end joining (Figure 5)[100].

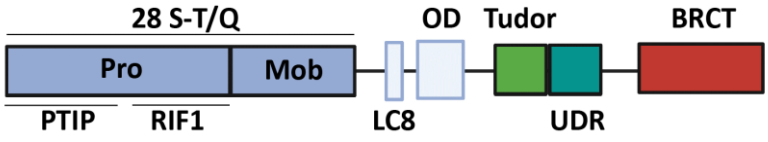

Figure 5. Schematic representation of human 53BP1. Recruitment of 53BP1 to DSBs depends on Tudor, UDR, LC8 and OD domains. The N-Terminal S-T/Q phosphorylation sites comprise of the Pro and Mob domains. The Pro domain mediates end-protection function that includes PTIP and RIF1 interacting motifs. The Mob domain mediates chromatin end mobility. LC8, (8 kDa light chain

dynein)-binding motif; OD, oligomerization domain; Tudor, Tudor domain; UDR, ubiquitylation-dependent recruitment motif; Pro, Protection domain; Mob, Mobility domain.

1.3.1 Role of 53BP1 during CSR

53BP1 is very vital for CSR and in its absence CSR is abrogated that makes CSR as one of the beneficial phenotypic read-outs to dissect the mechanism of 53BP1. One of the key determinant step of CSR is end-protection and it is exerted by 53BP1-RIF1-Sheildin-CST axis (CTC1 in CST complex). Deletion of any of the interaction partners or mutating the 28 S-T/Q sites (mutation of the 28 S-T/Q motifs to Alanine; mutant 28A or 53BP1^{28A}) significantly reduces CSR[91-98,101]. However, deletion of 53BP1 has a more severe impact on the process than its interactors suggesting that 53BP1 has additional role in CSR apart from imparting end-protection. Studies have reported that 53BP1-deficient B cells randomizes the break order compared to *WT* scenario, where the first breaks are biased at Sμ region[102]. Furthermore, in *WT* B cells, inversion to deletion ratio (Inv:Del) of the intervening *Igh* sequence after DSBs is biased towards deletion. In the absence of 53BP1 the biasness is lost and the ratio is almost 50:50. However, it has been established that the above two phenotypes are not through the end-protection mechanism[87,103]. Tudor, UDR and OD domains are also crucial for CSR due to their role in accumulation of 53BP1 at chromatin and/or DSBs, although mechanism through OD is still not clear[88,93]. The PTIP interacting motif or Mob domain do not have any role in CSR, despite their importance in DSB repair.

1.3.2. Role of 53BP1 in synthetic lethality

The importance of 53BP1 got highlighted in the generation of PARPi chemotherapeutic drug for BRCA1-depleted breast and ovarian cancers[88]. PARPi is the first clinically approved drug that was developed to exploit the principle of synthetic lethality in tumors. Synthetic lethality is defined as when the alteration of two genes causes cell death, but mutation of either one doesn't. PARPi induced DNA damage can be only repaired by HR. *WT* cells that are proficient in HR remain viable whereas cells with BRCA1-deficiency are unable to repair it and instead use the NHEJ repair machinery to compensate. In this case NHEJ pathway is more error prone and lethal to the cells. Therefore, PARPi drives the cells to use another repair pathway and henceforth pushing them towards apoptosis[104].

During HR nucleolytic resection occurs in two phases: the first phase is mediated by BRCA1, CtIP, MRN and leads to the formation of short tracks of 3' ssDNA, which are further processed in a second step by EXO1 and/or DNA2/BLM proteins to generate the long 3' overhangs for RAD51 loading and homology search[105-108]. 53BP1 is a DNA damage response factor known for protecting DNA ends from nucleolytic processing. As a consequence, 53BP1 inhibits the formation of the 3' overhangs by inhibiting BRCA1, and promotes NHEJ repair of DSBs, for which protection of DNA ends is crucial. But during S phase, 53BP1 is displaced by BRCA1 in order to promote resection[109]. PARPi is the inhibitor of ssDNA break sensor protein PARP1. It traps PARP1 at replication induced single strand breaks (SSBs) during S phase. When replication fork collides with the trapped PARP1-PARPi complex, SSBs get converted into DSBs. In BRCA1-proficient *WT* cells, these DSBs are repaired efficiently by HR. In the absence of BRCA1, these breaks are repaired by 53BP1 that leads to the fusion of two or more chromosome ends. These structures are called chromosomal radials and are highly toxic to the cells. This pathological outcome is due to aberrant NHEJ, called toxic-NHEJ, and it became the basis for synthetic lethality by PARPi. However, when 53BP1 is also depleted in BRCA1-deficient cells, formation of toxic chromosomal radials is reduced almost to *WT* levels and thus cell viability is also rescued. This is because in the absence of 53BP1 in BRCA1-depleted cells, HR end resection is again re-wired

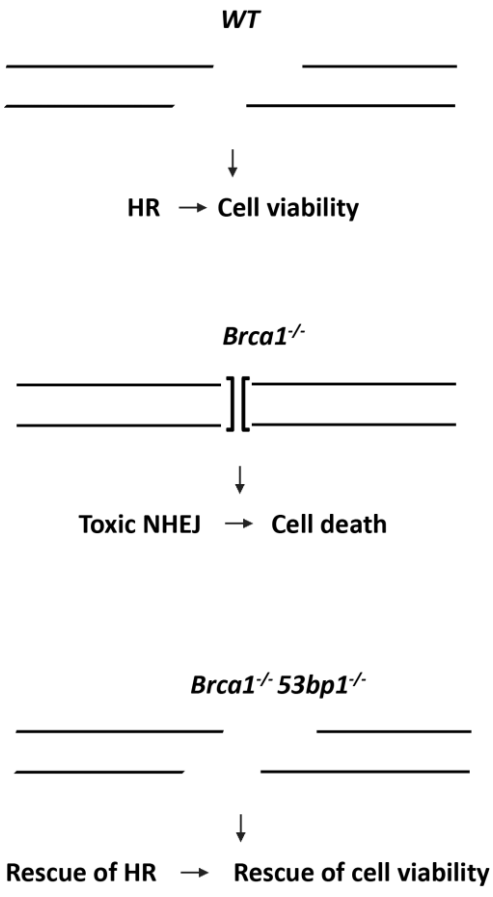

Figure 6. Genomic instability by 53BP1 in BRCA1-depleted cells. Schematic representation of PARPi induced genomic instability in WT, BRCA1-deficient and BRCA1-, 53BP1-double-deficient cells. CSR, class switch recombination; NHEJ, Nonhomologous end-joining.

through EXO1 and/or DNA2/BLM to generate the 3' overhangs (Figure 6). Similarly deletion of RIF1, Shieldin or CST or abrogating their interaction with 53BP1 (mutant 28A or 53BP1^{28A}) promotes rescue of HR and cell viability due to absence of end-protection function[91-98]. Mutation of S-T/Q sites on 53BP1 Mob domain abrogates chromatin mobility which is also crucial for radial formation during toxic-NHEJ[100]. Absence of PTIP or abrogating its interaction with 53BP1 also promotes rescue of HR and cell viability, albeit the mechanism is still not elucidated (Table 2)[99].

	PTIP	RIF1	Mob
CSR	No	Yes	No
Toxic-NHEJ	Yes	Yes	Yes

Table 2. Role of PTIP- interacting, RIF1- interacting and Mob domains on CSR and toxic-NHEJ.

1.3.3. 53BP1-RIF1 relationship

Earlier it was reported that RIF1 interacts with 53BP1 at 7 S-T/Q sites located within the Pro domain and the mutant was named 53BP1^{7A}. Recently it was observed that this mutant is able to recruit RIF1 sufficiently, however it can't not recruit Sheildin complex. Another mutant was developed named 53BP1^{3LA}, which bear dileucine motifs of LxL[xx](pS/pT)xpS where [xx] represents the possible presence of two residues in between. 53BP1^{3LA} does not recruit RIF1 to DSBs, however Shieldin can still accumulate. The combination of 7A and 3LA (53BP1^{7A3LA}) abolished the recruitment of both RIF1 and Sheildin. Both 53BP1^{7A} and 53BP1^{3LA} reconstituted in *53bp1*$^{-/-}$ B cells can rescue CSR, but 53BP1^{7A3LA} cannot. The individual mutants displayed some amount of radial formation whereas 53BP1^{7A3LA} can rescue radial formation equivalent to mutant 53BP1^{28A} in *Brca1*$^{-/-}$. Rescue of viability experiments suggest that the amount of radials accumulated in 53BP1^{7A} and 53BP1^{3LA} are not toxic enough for the cells to undergo cell death. It was suggested that 53BP1 can independently regulate RIF1 and Shieldin, with a non-linear 53BP1-RIF1-Shieldin axis. Although it is possible that trace amount of RIF1 or Shieldin is still recruited at the damage sites in the individual mutants[110].

1.3.4. Inhibitors of 53BP1 DSB repair function

TIRR has been established to bind to 53BP1 Tudor domain and reduces its interaction with H4K20me2. DNA damage dependent phosphorylation of 53BP1 by ATM and subsequent recruitment of RIF1 leads to dissociation of TIRR[89]. A recent study observed that protein ZMYM2 blocks 53BP1 at DSBs through its zinc-finger domain to promote BRCA1 loading and thereby HR[111]. These reports suggest that there are proteins that keep 53BP1 from accessing chromatin to regulate repair process.

1.4. RIF1

RIF1 is a multi-functional protein that was originally described as a negative regulator of telomere length in *Saccharomyces cerevisiae*. However, in higher eukaryotes RIF1 is primarily a DSB repair protein with DNA end-protection function. As an interaction partner of 53BP1, RIF1 is a pro-NHEJ protein for programmed DSBs during immunoglobulin CSR[91-92]. In the absence of RIF1, switch to any antibody isotype is significantly reduced. It also prevents loading of BRCA1 on DSBs for HR repair. In BRCA1-deficient cells it promotes toxic-NHEJ for PARPi-mediated replication induced DSBs[85,92].

Apart from DSB repair, RIF1 has another evolutionary conserved role which is regulation of origin firing during replication initiation in yeast and control of replication timing in humans[112]. RIF1 also protects nascent DNA from degradation at stalled replication forks which are a consequence of replication stress[85].

1.4.1 RIF1 domains

Mammalian RIF1 is a large protein with approximately 2426 amino acids. RIF1 comprises of 21 HEAT (Huntingtin, Elongation factor 3, protein phosphatase 2A, Tor1)-like repeats at the N-terminus end (Figure 7). This region is conserved through mammals to yeast[85]. HEAT repeats provides the domain for protein-protein interactions[112]. It is also essential for recruitment to phosphorylated 53BP1 and foci formation at DSBs during DDR. HEAT repeats are also required for impeding BRCA1 foci at DSBs in G1 cell cycle phase[113].

The HEAT repeats are followed by intrinsically disordered region (IDR) which is poorly conserved and do not acquire a stable secondary or tertiary folded structure (Figure 7). Proteins possessing IDR have the ability to change conformation and hence, modify its interactions with other proteins. Mammalian RIF1 has several S-T/Q motifs on IDR[85].

The C-terminal domain (CTD) consists of 3 parts- CTD1, CTDII and CTDIII. CTD-I is also disordered/unfolded and CTD-II bear both folded and unfolded regions[112]. RIF1 CTD-I

contains RVxF-SILK motif essential for PP1 binding (Figure 7). RIF1-PP1 suppress untimely activation of the MCM2-7 complex thereby preventing premature origin firing[114]. RIF1-PP1 binding is also indispensable for protection of stalled replication fork after replication stress. RIF1 recruits PP1 through its RVxF-SILK motif which dephosphorylates DNA2 and impedes its activity of extensive degradation of stalled replication forks. Degradation of nascent replication forks can lead to genomic instability[115]. CTD-II is a DNA-binding domain and CTD-III is BLM helicase-interaction domain (Figure 7)[112,116]. Interaction of BLM and RIF1 is crucial for restart of stalled replication forks after exposure to replication stress from agents like aphidicolin. Loading of RIF1 to stalled replication fork relies on BLM and in its absence RIF1 recruitment is delayed[116]. CTD, apart from the RVxF-SILK motif, is also required for inhibiting BRCA1 foci formation during G1 phase for DSB repair[113].

RIF1 contains several S-T/Q sites which are consensus sites for ATM/ATR phosphorylation[85]. RIF1 was reported to be phosphorylated at the human ortholog of S1528 following irradiation[117]. Another mass-spectrometry based study showed that yeast RIF1 was phosphorylated at ATM consensus site S1351 and non-ATM sites S181 and S1637 after telomere specific DNA damage[118]. Recently our lab established that phosphorylation of three S-T/Q sites at IDR (S1387, S1416 and S1528) are consensus of ATM/ATR and promote protection of stalled replication fork from degradation following replication stress in mouse RIF1. Although these three sites were identified after irradiation of activated primary B cells, they are dispensable for DNA end-protection during genome-wide DSBs and CSR. Hydroxy urea treatment recruited RIF1 to stalled replication fork to prevent fork degradation[85].

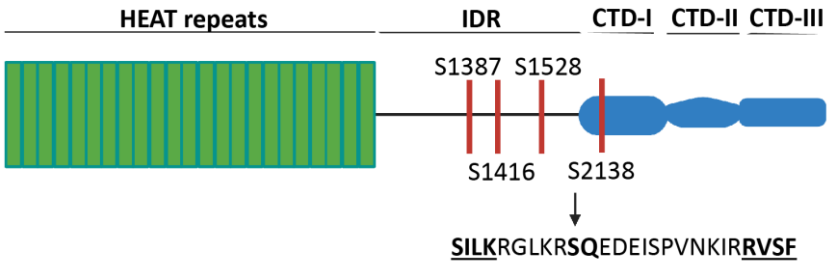

Figure 7. Structure of mouse RIF1. Schematic representation of RIF1 protein which comprises of the following domains. 21 N-terminal HEAT repeats domain for protein-protein interaction and DSB induced foci formation; IDR; CTD-I has RVxF/SILK motif for PP1 interaction for replication initiation and fork stability, CTD-II is a DNA binding domain and CTD-III is BLM interaction domain for replication fork stabilization. Red lines indicate serine (S) residues within ATM/ATR phosphorylation sites (SQ/TQ); S1387, S1416, S1528, S2138. HEAT, Huntingtin, Elongation factor 3, protein phosphatase 2A, Tor1; IDR, Intrinsically disordered region; CTD, C-terminal domain.

1.5. Targeted chromatin purification

Identification of transcription factors, chromatin remodellers, DNA damage response (DDR) factors or even RNAs that are actively binding at specific genomic loci is crucial for studying the course of events for gene expression, cellular identity etc. spCas9 (CRISPR (Clustered Regularly Interspaced Short Palindromic Repeats) associated protein 9) is a protein from *Streptococcus Pyogenes* that is utilized by bacteria for defence mechanism against viruses. It has been now used very commonly for genetic engineering. The protein can create DSBs on gene of interest with the help of a 20bp single guide RNA (sgRNA or gRNA) that is complementary to the target locus sequence. However, the target site must be preceeded by a specific sequence known as PAM (protospacer adjacent motif) which is NGG for spCas9 (or referred as *WT* Cas9 here). PAM provides the motif for recognition by Cas9 and gRNA which means if a sequence that has high homology to the target but lacks the PAM will not be cleaved by Cas9, reducing the off-target effects of the system[119].

CRISPR based locus pull-down with nuclease-deficient Cas9 (dCas9) is a highly specific technique to explore DNA-Protein/RNA interactions. Using locus specific gRNA, dCas9 can be targeted to any gene of interest for a comprehensive analysis. However, the technique also involved biochemical cross-linking of the samples before lysis that may generate false positive results[120]. To this point CRISPR coupled with proximity labelling with Biotin ligase became a more sophisticated technique for that purpose. Biotin ligase (BirA, TurboID) in the presence of biotin can biotinylate proximal proteins and the sample preparation doesn't require any additional biochemical reaction prior to lysis. CRISPR based proximity labelling combines the advantages of CRISPR-based specificity as well as proximity labelling-based conservation of the native state of the samples (Figure 8)[121-122].

dCas9-TurboID-mediated chromatin isolation uses nuclease-deficient Cas9 protein (dCas9) fused to a mutated form of Biotin ligase (TurboID), to label proteins within a 10 nm radius of a specific targeted genomic sequence. Precisely, in the presence of biotin, the biotin ligase enable the formation of biotin-5′-AMP anhydride, which disperses out to biotinylate proximal proteins on nucleophilic amino acids[121-122]. In order to precipitate the locus-specific biotin labelled proteins and the interacting RNAs streptavidin-based pull-down is employed. Streptavidin or neutravidin is a modified form of avidin protein that couples high specificity for biotin with low non-specificity and thus can be used for immunoprecipitation. Because of these features, dCas9-TurboID-mediated chromatin isolation considerably increases the pull-down efficiency of a single loci. The pulled-down protein/RNA interactome can be analysed by high resolution mass-spectrometry and RNA-Seq. Although TurboID provides a great advantage to the technique, it gives some background biotinylation that increases the possibility of getting

false positive hits in mass-spectrometry. To this end, another version of TurboID was developed, called miniTurbo, that reduces total amount of biotinylation and thus the background noise as well. APEX (Ascorbic Peroxidase) is also used for proximity labelling which upon treatment with hydrogen peroxide converts exogenously added biotin-phenol to biotin-phenoxyl radicals that disperses and covalently binds to proximal proteins[123].

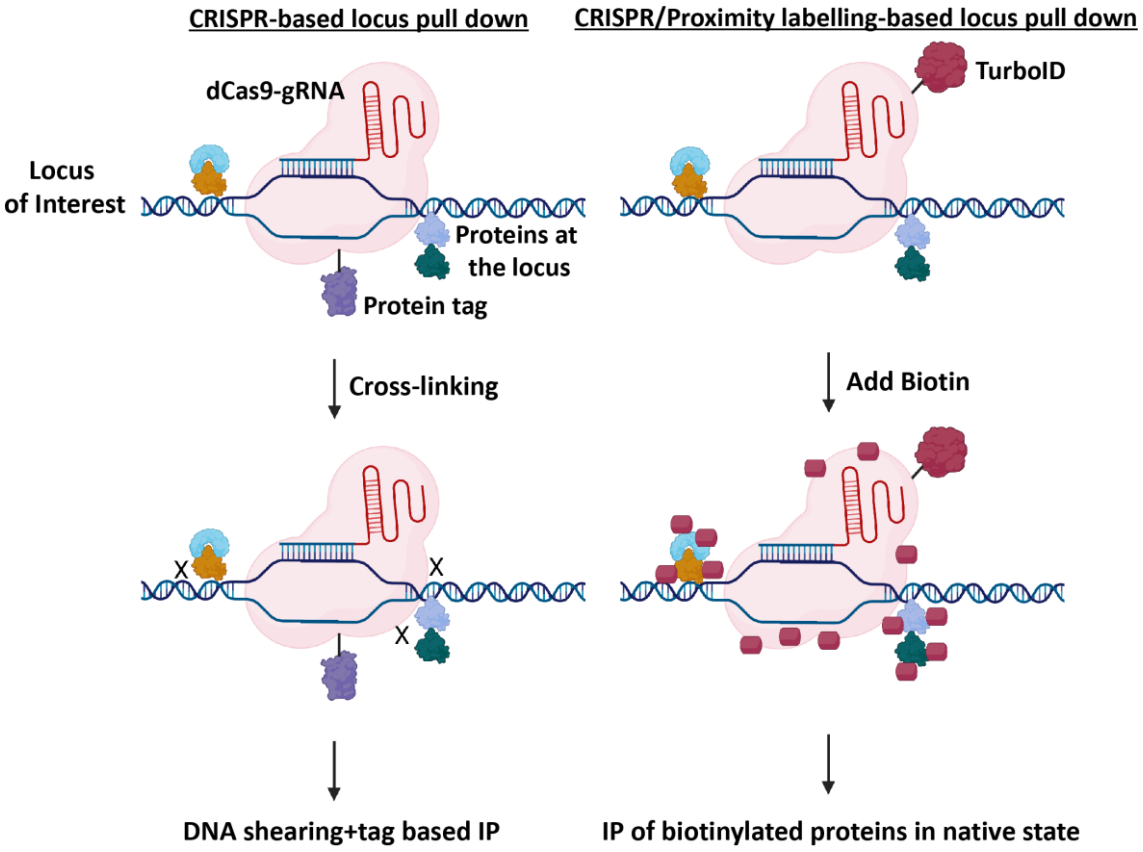

Figure 8. Schematic representation indicating the key differences between CRISPR-based locus pull-down and CRISPR/Proximity labelling-based locus pull down. CRISPR-based locus pull-down involves a protein tag like HA or Flag and cross-linking of DNA-protein-RNA followed by shearing of the cross-linked DNA by methods like sonication. Finally, tag-mediated immunoprecipitation determines proteins interacting at the locus of interest. CRISPR/Proximity labelling-based locus pull-down uses a biotin ligase (or Apex), that biotinylates the proximal proteins and RNA in the presence of biotin. This approach allows for immunoprecipitation of the biotinylated proteins and associated RNAs with streptavidin in native state and provides an advantage of pulling-down even labile interactions. The immunoprecipitated proteins can be analysed using mass-spectrometry and the associated RNAs with RNA-Seq. IP, Immunoprecipitation.

2. AIMS OF THE STUDY

The *Igh* locus comprises multiple key DNA elements and interactomes interconnected in a dynamic web of known and unknown interactions. Despite the work from many groups, decades of research, and the characterization of the roles played by few known CSR factors, a comprehensive picture of the protein and RNA factors that are essential for the process, and how they interact to ensure efficient CSR, is still missing. The identification of novel CSR factors will not only broaden our knowledge of the process, but also add to the translational list of potential candidates that are mutated in patients with CSR immunodeficiencies[43-44]. Furthermore, since AID is a causative factor for chromosomal translocations in B cells, one of the primary oncogenic events in lymphomagenesis[124], the characterization of the mechanistic aspects of its targeting will contribute to advance our understanding of the molecular basis of B cell malignant transformation. Finally, 53BP1 and RIF1 are key DNA end-protection factors during NHEJ and thereby CSR. The identification of their interactors and potential post-translational modifications during the repair process will elucidate the molecular links of the delicate equilibrium in the repair pathway and genomic instability. Therefore, the proposed study will advance our understanding of both B lymphocyte physiology and pathology, as well as of the ubiquitous mechanisms for the preservation of Genome Integrity.

2.1. Aim 1: To comprehensively define the *Igh* interactome, specifically DSB repair factors during CSR

In order to identify proteins and RNA species interacting with the *Igh* locus during CSR, I planned to perform targeted chromatin purification of both S regions and the 3'RR with CRISPR-TurboID system. The major challenge for a single locus-purification approach is the need to maximize the amount of pulled-down material. To do so, I coupled the use of the murine B cell lymphoma line CH12 or primary B cells from mouse spleens as the model systems[84], with CRISPR-TurboID based approach for determining *Igh* locus repair dynamics[21-122].

2.2. Aim 2: To determine if ANP32B is a phospho-dependent regulator of 53BP1 activity in DSB repair and CSR

ANP32B was identified as a protein associating specifically with 53BP1^{28A} mutant (28 Serine-Threonine residues mutated to Alanine) in a SILAC-based mass-spectrometry study[91]. I hypothesized that ANP32B might act as a negative regulator of 53BP1 interaction with the specific DNA damage response/repair factors or 53BP1 activities indicated below:

(1) RIF1: The antagonistic relationship between ANP32B and RIF1 for binding to 53BP1 would interfere with CSR[91-93].

(2) PTIP: The antagonistic relationship between ANP32B and PTIP for binding to 53BP1 would interfere with 53BP1 ability to protect DNA ends in the context of repair of DNA replication-associated DSBs and to promote radials formation in BRCA1-deficient cells[99].

(3) Mob domain interactors: 53BP1 functional interactors required for its activity in DNA end mobility are still unknown. Nevertheless, we hypothesize that ANP32B binding to the Mob domain could inhibit 53BP1-mediated increase in DSB mobility, therefore, negatively impacting radial formation and cell death in the absence of BRCA11[00].

2.3. Aim 3: To identify and validate the DNA damage-induced post-translational regulation of RIF1

I employed Rif1$^{FH/FH}$ mice for our study since they express RIF1 protein tagged with 1x Flag and 2x HA epitopes, which provide additional options for RIF1 pull-downs (Figure 19B). Splenocytes activated with cytokines were exposed to irradiation (IR), which induces DSBs throughout the genome that are primarily repaired by NHEJ. Cytokines not only promote survival in splenocytes but also induce the expression of Activation-induced deaminase (AID). AID activity leads to the formation of DSBs and when repaired by NHEJ, promote CSR[125]. Mass-spectrometry will be employed to define the post-translational modification (PTM) maps. Based on the results of the mass-spectrometry, I employed CRISPR/Cas9 knock-in mutagenesis in either CH12 (mouse B cell lymphoma cell line, that can undergo CSR *in vitro* upon cytokine stimulation) to further analyze the consequences of these PTMs on DSB repair[85].

3. MATERIALS AND METHODS

3.1. Materials

Table 1: Reagents used

LPS	Sigma-Aldrich	L2630
IL-4 (mouse recombinant)	Sigma-Aldrich	I1020
TGFβ-1 (mouse recombinant)	R&D Systems	7666-MB-00
RP105 or RP/14	BD Pharmingen	552128
Purified anti-mouse CD40 Antibody (clone HM40-3)	Biolegend	102902
FBS	Sigma-Aldrich	F7524
RPMI 1640	Life Technologies	21875091
DMEM	Life Technologies	41965062
HEPES	ThermoFisher Scientific	15630056
Sodium Pyruvate	ThermoFisher Scientific	11360039
Antibiotic Antimycotic	ThermoFisher Scientific	15240062
L-Glutamine	ThermoFisher Scientific	25030024
2-Mercaptoethanol	ThermoFisher Scientific	21985023
PenStrep	ThermoFisher Scientific	15140122
Anti-CD43 (Ly-48) microbeads (mouse)	Milteny Biotech	130-049-801
ACK Lysis Buffer	Life Technologies	A10492-01 NEG-502A250UC
Trypsin 0.05% EDTA	Life Technologies	25300-054
Fugene-HD	Promega	E2312
Opti-MEM	Life Technologies	31985062

NuPage LDS Sample buffer	ThermoFisher Scientific	NP0008
Proteinase K	Peqlab	3375501
Phenol:Chloroform:Isoamyl alcohol	Roth	A156.3
PARPi Olaparib/AZD2281, Ku-0059436	Selleckchem	S1060
Biotin	Sigma-Aldrich	B4639-100MG
Crystal Violet	Sigma-Aldrich	C0775
Complete EDTA free Protease Inhibitor Cocktail	Sigma-Aldrich	11873580001
PhosSTOP	ThermoFisher Scientific	04906837001
Benzonase	Sigma-Aldrich	E1014-25KU
RIPA	Sigma-Aldrich	R0278-500ML
NuPAGE 3-8% gel	Life Technologies	EA0375BOX
NuPAGE 4-12% gel	Life Technologies	NP0321BOX
Tris Acetate Buffer	Life Technologies	LA0041
MOPS Buffer	Life Technologies	NP0001
MES Buffer	Life Technologies	NP0002
SeeBluePlus ladder	Life Technologies	LC5925
1X PBS	Life Technologies	10010031
BSA	Roth	3737
PureLink HiPure Plasmid Filter Midiprep Kit	ThermoFisher Scientific	K2100-15
PureLink HiPure Plasmid Filter Maxiprep Kit	ThermoFisher Scientific	K210017
Stbl3 Competent E. coli	ThermoFisher Scientific	C737303
TOP10 Competent E. coli	ThermoFisher Scientific	C404003

Neon Transfection System, 100 mL Kit	ThermoFisher Scientific	MPK10025
TOPO Blunt Cloning Kit	ThermoFisher Scientific	45-0031
NucleoSpin DNA Purification Kit	Macherey-Nagel	740499
QuickExtract Solution	Epicentre	QE09050
HotStarTaq DNA Polymerase	Qiagen	203205
Phusion High-Fidelity DNA Polymerase	ThermoFisher Scientific	F530L
Taq DNA Polymerase with ThermoPol Buffer	NEB	M0267
T4 DNA Ligase	NEB	M0202
T7 DNA Ligase	NEB	M0318
Phase Lock Gel tubes	VWR	2302820
Superfrost slides	VWR	
Mounting media	ThermoFischer Scientific	P10144
Fixation and permeabilization kit	Abcam	185917
QuickExtract™ DNA Extraction Solution (50mL)	Epicenter	QE09050
BamHI	NEB	R3136
AgeI	NEB	R3552
AsiSI	NEB	R0630
SgrAI	NEB	R0603
PciI	NEB	R0655
AscI	NEB	R0558
BsiWI	NEB	R0553
NsiI	NEB	R0127

Table 2. Antibodies used

Antibodies	Company	Catalogue number	Dilution	Preparation
Rabbit αRIF1	In house (# 2034)	1:2500		3% BSA in PBST (Western blot), 5% Horse serum in PBS (IF)
Mouse αCas9	Novus Biologicals,	NPB2-36440	1:1000	2% Milk in TBST
HRP Goat αRabbit	Jackson immunoresearch	111-035-008	1:10000	3% BSA in PBST
HRP Goat αMouse Lc	Jackson immunoresearch	115-035-174	1:10000	3% BSA in PBST
Rabbit αANP32B	Abcam	[EPR14589] (ab184565)	1:1000	3% BSA in PBST
αStreptavidin-HRP	Thermo Fischer Scientific	S911	1:1000	2% Milk in TBST
Goat anti-Rat IgG (H+L), Alexa Fluor 488	Invitrogen	A-11006	1:500	5% Horse serum in PBS
Goat anti-Mouse IgG (H+L), Alexa Fluor 546	Invitrogen	A-11030	1:500	5% Horse serum in PBS
αCas9 Alexa Fluor 647	Cell Signalling technology	48796S	1:1000	Section 3.2.20
Rabbit αHA	Abcam	ab9110	1:1000	2% Milk in TBST
Mouse anti-Flag M2 (HRP conjugated)	Sigma-Aldrich	A8592	1:!000	2% Milk in TBST
Rabbit αTubulin	Abcam	ab4074	1:10000	2% Milk in TBST
Rat anti-IgG1-APC Clone X56	BD Biosciences	550874	1:400	PBS/FBS

Rat anti-IgG2b-PE Clone RMG2b-1	BioLegend	406707	1:400	PBS/FBS
Goat anti-IgA-PE	Southern Biotech	1040-09	1:400	PBS/FBS
Streptavidin-APC	BD Biosciences	554067	1:400	PBS/FBS

Table 3: Plasmids used

Plasmid	Company/Lab/Reference	Catalogue number
pGH125_dCas9Blast	Addgene	85417
Inducible-Caspex	Addgene	97421
3x HA-miniTurbo-NLS-pCDNA3	Addgene	107172
pR26-CAG-AsiSI/MluI	Addgene/Ralf Kuhn lab, MDC	74286
pMSCV-U6sgRNA-PGKPuro2ABFP	Addgene/ Klaus Rajewsky lab, MDC	102796
phr-scfvGCN4-sfGFP-GB1-NLS-dWPRE	Addgene	60906
pMX-235	93	
px-458-GFP	Addgene	48138
px-330-BFP	Klaus Rajewsky lab, MDC	
lenti-GuidePuro	Addgene	52963

Table 4: List of primers for cloning

Primer	Forward/Reverse
GGGAATTCCGTACGATGTACCCCTACGACGTGCCCGACTACGCCGCTGGAGCATACCCCTACGACGTGCCCGACTACGCCGGTGGCAAAAGGCCGGCGGCCACGAAAAAGG	Forward
TCTTCTTGAGACAAAGGCTTGG	Reverse

TTTACTCTGACCAACTTGGGCGCGCCTGCAGCC	Forward
AGAACCCCGCACGTCTCGTTCAGCAGCGGGAT	Reverse
AGACGTGCGGGGTTCTATCCCGCTGCTGAACG	Forward
CTTTTCGGCAGACCGCGCCCTGCTGAATTC	Reverse
GCGGTCTGCCGAAAAGGAATTCAGCAGGGC	Forward
CCTTGCTCACGGTACCAGGGCCGGGATTCTCC	Reverse
AGTGGATCTGCGATCGCTCCGGTGC	Forward
AGGGCCGGGATTCTCCTCCGGCTTGGCCAT	Reverse
GGAGAATCCCGGCCCTATGGCCAAGCC	Forward
TTAGCCCTCCCGTAATCCAGAGGTTGATT	Reverse
GGTTATGTGTGGGAGGGCTAAAATCAACCTCTGG	Forward
AAGAATGCATGCGTCAATTTTACG	Reverse
CTAGACTAGTCGCCGGCGCCTCAGCCGTCTTCAAGAATTCCTCGAG	Forward
CATGGTCTTTGTAGTCCATGG	Reverse
GCAGATCTGCGAAATCGGATCC	Forward
GAATTCCCACGCGTTCAGGCACCGGGCTTGCGGG	Reverse
CGCGGATCCAGGTGGAGGTGGAAGCGGTATCCCGCTGCTGAACGCTAA	Forward
TTGCGGTCCGCTGGATAACGGTCCGACCTCCACCCTTTTCGGCAGACCGCAGAC	Reverse
TATCCGGAGAATTCTCACGCGTGCCACC	Forward
TTTCCGCTCGAGTTACACCTTGCGCTTCTTCTTG	Reverse
TCCACATCCACCGGTAGGCGG	Forward
CACGATGTCGGGGCCCATGGTAAGCTAGCTTGGGCTGC	Reverse
GCAGCCCAAGCTAGCTTACCATGGGCCCCGACATCGTG	Forward
GCAGACTTCCTCTGCCCTCCACCTTGCGCTTCTTCTTGG	Reverse
CCAAGAAGAAGCGCAAGGTGGAGGGCAGAGGAAGTCTGCTAACATGCGGTGACGTGGAGGAGAATCCCGGCCCTGCTAGCATGGCCACAACCATGGTGAG	Forward

CTTTTATTTTATCGACGCGTTTACTTGTACAGCTCGTCC	Reverse
GGACGAGCTGTACAAGTAAACGCGTCGATAAAATAAAAG	Forward
CCTTTTGCTCACATGTTCTTTCC	Reverse
TCCGAATTCGAACAAAAACTTATTAGCGAAGAAGATCTTATGGATATGAAGAGGAGGATCC	Forward
AGCGGCCCTCGAGTTTAATCATCTTCTCCTTCGTCATCT	Reverse
TTCCGGAATTCATGGATATGAAGAGGAGGATCC	Forward
AGCGGCCCTCGAGTTTAAAGATCTTCTTCGCTAATAAGTTTTTGTTCATCATCTTCTCCTTCGTCATCTG	Reverse

Table 5: List of primers for genotyping

Primer	**Forward/Reverse**
GAGGGGAGTGTTGCAATACCT	Forward
GGAGCGGGAGAAATGGATATG	Reverse
CAGGCGGGCCATTTACCGTAAG	Reverse
GTTTTTTAAAGCAAGTAAAACCTCT	Forward
CTGCAGGTCGAGGGACCTA	Reverse
AGAATTGATTTGATACCGCG	Reverse
CGCCATCCACGCTGTTTTGACC	Forward
CAGCCCGGACCGACGATGAAG	Reverse
GGCGGCTTGGTGCGTTTGCGGGGATGG	Forward
CTTTTGCTTCATCAGAAGGCTGTCCAT	Reverse
TACCTTTCTGGGAGTTCTCTGCTGCC	Forward
CCTGTTCAATTCCCCTGCAGGACAACG	Reverse
GATATCAATTTCAAGATTAAGT	Forward
AGCTGGGTCCAGTCCAGAGG	Reverse

Table 6: gRNAs used

Primer	**Forward/Reverse**
CACCGTGGGGTGAGCTGAGCTGAGC	Forward
AAACGCTCAGCTCAGCTCACCCCAC	Reverse
CACCGGGGTGAGCTGAGCTGAGCTG	Reverse

AAACCAGCTCAGCTCAGCTCACCCC	Forward
CACCGAGCTGGAGTGAGCTGAGCTG	Reverse
AAACCAGCTCAGCTCACTCCAGCTC	Reverse
CACCGGGCCAGAACCAGAATCAATT	Forward
AAACAATTGATTCTGGTTCTGGCCC	Reverse
CACCGTGGAATGAGCTGAGCTGAAC	Forward
AAACGTTCAGCTCAGCTCATTCCAC	Reverse
CACCGGGGCTGGGCTGGTGTGAGCT	Reverse
AAACAGCTCACACCAGCCCAGCCCC	Forward
CACCGGAGCTGGAATGAGCTGGGAT	Reverse
AAACATCCCAGCTCATTCCAGCTCC	Reverse
CACCGAGCTCAGCCTAGCCCAGCTC	Forward
AAACGAGCTGGGCTAGGCTGAGCTC	Reverse
CACCGAAGTCCTAGTGGTATGCAGC	Forward
AAACGCTGCATACCACTAGGACTTC	Reverse

Table 7: Softwares used

FACS Diva	BD	N/A
FlowJo v.10	Treestar	N/A
MacVector v15.0	MacVector, Inc.	N/A
Prism v.6	GraphPad	N/A
ImageJ	GitHub	N/A

3.2. Methods

3.2.1. Cell culture

The following CH12 cell lines were used: wild-type (*WT*) CH12, *Zmynd8*$^{-/-}$ CH12, *53bp1*$^{-/-}$ CH12, *AIDER* CH12, *Brca1*$^{mut/mut}$ CH12, *Brca1*$^{mut/mut}$ *Rif1*$^{-/-}$ CH12, *Brca1*$^{mut/mut}$ *Rif*$^{mut/mu-}$ CH12, *Rif1*$^{-/-}$ CH12, *Rif1*^{S2138A} CH12 and *Rif1*^{S2138D} CH12. Cells were grown in RPMI 1640 medium complemented with 10% foetal bovine serum (FBS) (Sigma-Aldrich), 10 mM HEPES (Life Technologies), 1 mM Sodium Pyruvate (Life Technologies), 1X Antibiotic-Antimycotic (Life Technologies), 2 mM L-Glutamine (Life Technologies), and 1X 2 Mercaptoethanol (Thermo Fisher Scientific) at 37°C and 5% CO_2 levels.

The following immortalized Mouse embryonic fibroblasts (iMEFs) were used: *WT* iMEFs, *WT1* iMEFs, *WT2* iMEFs, *53bp1*$^{-/-}$ iMEFs and *Brca1*$^{\Delta 11/\Delta 11}$ iMEFs. Each *WT* iMEFs were immortalized separately in different labs. Cells were grown in DMEM medium containing 10% foetal bovine serum (FBS), 1x PenStrep (Life Technologies) and 2 mM L-Glutamine at 37°C and 5% CO_2 levels.

HEK293T and its derivative BOSC23 were also grown in DMEM medium containing 10% foetal bovine serum (FBS), 1x PenStrep and 2 mM L-Glutamine at 37°C and 5% CO_2 levels.

Mice used for the studies were *Rosa26*$^{dCas9Suntag/+}$, BALB/c-Tg(CMV-cre)1Cgn/J and *Rosa26*$^{dCas9\text{-}Suntag/+}$ *CMV*$^{Cre/+}$ and *Rif1*$^{FH/FH}$, albeit for splenocyte extraction only *Rosa26*$^{dCas9Suntag/+}$ and *Rif1*$^{FH/FH}$ were used. For primary B cells (splenocytes) isolation the spleen was extracted and placed in a 70mm mesh which was in a 100mm dish containing 10 mL PBS/FBS (PBS with 3% FBS). Using a 3 mL syringe plunger the spleen was mashed in the mesh till it was completely grounded. The solution was poured from the dish into a 50ml falcon tube through the same mesh. The cells were centrifuged down for 5' at 1200rpm. Most of the supernatant was removed and the pellet was resuspended by flicking gently on the tube. 1mL/spleen ACK lysis buffer (ThermoFisher Scientific) was added slowly but continuously while gently moving the tubes and was incubated at room temperature for 3 minutes. To dilute the NH_4Cl in ACK 9 mL PBS/FBS was added. Supernatant was transferred in a new tube without collecting the debris. After centrifugation, the pellet was resuspended in 900 uL PBS/FBS and 100 uL of anti-CD43 magnetic beads (Milteny Biotech) following which it was rotated at 4°C for 30 minutes. Later 9 mL of PBS/FBS was added to dilute the beads-cells mixture and centrifuged down. The pellet was resuspended in 1 mL PBS/FBS and passed through MACS column after equilibrating the columns with 1 mL PBS/FBS. The cells that were eluted out were all B cells (CD43 negative). They were collected in 10 mL PBS/FBS and centrifuged down. The pellet was resuspended in RPMI 1640 medium supplemented with 10% FBS, 10 mM HEPES, 1 mM Sodium Pyruvate, 2 mM L-Glutamine, 1X Antibiotic Antimycotic and 1X 2-Mercaptoethanol. 500,000 cells/mL cells were seeded per well in a 6- well plate, with 25 µg/ml LPS (Lipopolysaccharide), 5 ng/ml of mouse recombinant IL-4 (Interleukin 4), and 0.5 µg/ml RP105 (or RP/14) in complete RPMI media to activate the B cells and then incubated at 37°C and 5% CO_2 levels.

3.2.2. Cloning

Different constructs (Table 3) were cloned in different ways with PCR (primers in Table 4) and restriction enzymes. For 2x HA-dCas9BLAST, dCas9 was PCR amplified from the original plasmid pGH125_dCas9Blast (Addgene). The forward primer had restriction enzyme BamHI

and 2x HA sequence as an extra flap at the 5' end and reverse primer completely annealed to the dCas9 sequence that contained BsiWI restriction enzyme sequence. To generate 2x HA-dCas9BLAST, original plasmid and the PCR product were digested out using 10 units each of BamHI (NEB) and BsiWI (NEB) and the digested PCR product was ligated to the digested plasmid.

dCas9miniTurbo-Puro/pR26 was cloned in a multi-step process. The first step was to replace Apex from Inducible-Caspex (Addgene) with miniTurbo from 3x HA-miniTurbo-NLS-pCDNA3 (Addgene). To do so, a big sequence, including Apex sequence, from Inducible Caspex was digested out with AscI and NsiI. To put back the original sequences of the plasmid and simultaneously replace Apex with miniTurbo, four PCR products were amplified independently that had overlapping ends with each other. First product was from Inducible Caspex with AscI restriction site at 5' end and an extra 3' end tail that overlapped with the 5' end of second product; second product was from 3x HA-miniTurbo-NLS-pCDNA3 to amplify miniTurbo that had an extra 5' end tail overlapping the first product and 3' end tail that overlapped with third product; third product was from 2x HA-dCas9BLAST to amplify dCas9 with an extra 5' end tail overlapping the second product and 3' end tail that overlapped with fourth product; and finally the fourth product was again from Inducible Caspex with NsiI restriction site and an extra 5' end tail that overlapped with the 3' end of third product. The four products with overlapping regions were mixed and amplified altogether with forward primer of the first product and reverse primer of the fourth. This single PCR product was digested with AscI and NsiI and ligated to the digested Inducible Caspex construct. The next step was to add multi-cloning sites between *Rosa26* homology arms in pR26-CAG-AsiSI/MluI (Addgene) that was used to insert TREG promoter, dCas9, miniTurbo, T2A-GFP and Puromycin (as a single sequence) from the modified Inducible Caspex. Next, SgrAI restriction site was added at 5' end of TREG promoter in modified Inducible Caspex by PCR. Finally TREG promoter, dCas9, miniTurbo, T2A-GFP and Puromycin (as a single sequence) was subcloned into modified pR26-CAG-AsiSI/MluI using 10 units each of SgrAI (NEB) and AsiSI (NEB) restriction enzymes and T4 DNA ligase (NEB) to generate dCas9miniTurbo-Puro/pR26.

To generate pMSCV-U6sgRNA-PGKscfvmT2AGFP plasmid, firstly miniTurbo was cloned into phr-scfvGCN4-sfGFP-GB1-NLS-dWPRE from 3x HA-miniTurbo-NLS-pCDNA3. Then four PCR products were amplified individually with over lapping regions with one another (like described above). First product was from pMSCV-U6sgRNA-PGKPuro2ABFP with AgeI restriction site, second was from modified phr-scfvGCN4-sfGFP-GB1-NLS-dWPRE that contained miniTurbo to amplify scfv-miniTurbo, third was from pMX-235 to amplify GFP with an extra T2A sequence and the fourth product was again from pMSCV-U6sgRNA-PGKPuro2ABFP with PciI restriction site. The four products had overlapping regions and were

mixed and again amplified by PCR with forward primer of the first product and reverse primer of the fourth, into one single PCR product. Later pMSCV-U6sgRNA-PGKscfvmT2AGFP and the PCR product was digested with 10 units each of AgeI (NEB) and PciI (NEB). Finally both the digested products were ligated together with T4 DNA Ligase (NEB).

To generate pMX-ANP32B, ANP32B was PCR amplified from cDNA of *WT* splenocytes with extra sequences containing restriction sites that were to be used for subcloning. The PCR product and pMX-235 were digested and ligated together.

For RIF1 S2138A/D knock-in plasmid, oligos with homology arms and the mutation (Alanine/Aspartic acid) were cloned into TOPO-blunt vector (ThermoFischer Scientific) using the kit's protocol.

3.2.3. Overview of generation of clonal derivatives by CRISPR/Cas9-mediated genome editing

For generating dCas9-miniTurbo expressing CH12 clones, plasmid with gRNA for *Rosa26*, Cas9 and BFP reporter (Cas9-g*Rosa26*-BFP) was electroporated along with knock-in plasmid dCas9miniTurbo-Puro/pR26 that contains *Rosa26* homology arms, dCas9-miniTurbo, T2A-GFP and Puromycin (under Tet-on system) in 1:2 ratio (molar ratio using Promega Biocalculator). BFP positive cells were bulk sorted and incubated in at 37°C and 5% CO_2. After they recovered, they were transiently induced with doxycycline for GFP expression. The GFP positive cells were single sorted and placed back in the incubator for 14 days. Each colony, representing a clone, was split into 3 replica plates; for freezing, maintenance and screening for GFP positive clones by FACS. The selected clones were characterized further by PCR for *WT* allele, Knock-in gene and AIDER gene with one primer outside the homology arm and the other inside the corresponding gene (Table 5). The clones were also expanded and again checked by FACS for GFP expression and by western blot for dCas9 and miniTurbo expression.

For generating RIF1 mutant clonal derivative (S2138A and S2138D), 2-4 guide RNAs were designed, targeting few bp upstream of S2138 in exon 30 using Benchling website. Each guide RNA was cloned into a tandem U6 cassette in pX330-GFP encoding for Cas9. 20µg of gRNA plasmid was electroporated into 2 $x10^6$ CH12 using the Neon Transfection System (ThermoFisher Scientific). GFP-positive cells were bulk sorted and collected in 500 µL of proteinase K buffer (100mM Tris-pH 8, 0,2% SDS, 200mM NaCl, 5mM EDTA) containing with 0.1 mg/ml of proteinase K. The proteinase K lysate was kept at 55^0C overnight following which genomic DNA was isolated (section 3.2.5). PCR was conducted to amplify approximately 500

bp upstream and downstream of sequence that potentially contained the indels. The PCR product was run by gel electrophoresis and the PCR product was extracted (Machery Nagel) and sent for Sanger's sequencing. The files of sequencing results were loaded onto Synthego ICE platform that deconvoluted the data and analysed for Indel score (more the better, at least 70%), Knock-out score (more the better, at least 70%) and R^2 value (at least 0.8). The software recognized the gRNA sequence in the control file and then predicted the PAM sequence. The knock-out score was the percentage of the population in the bulk that had the indel after the PAM and which was not present in the negative control (cells electroporated with gRandom). According to the Synthego ICE analysis, the best gRNA was selected and electroporated to CH12 cells along with knock-in plasmid containing homology arms, mutated Serine residue (Alanine/Aspartic acid) and restriction enzymes BanII (S2138A) and BclI (S2138D). This time GFP-positive cells were single-cell sorted into 96 well plates, and allowed to grow for approximately 14 days, following which they were split into 3 replica plates; for freezing, maintenance and diagnostic digestion analysis to screen positive clones with appropriate enzymes. Based on diagnostic digestion the knock-in positive clones were subjected to further validation with the help of genomic scar analysis and western blot. To determine the genetic scar, the targeted region was amplified by PCR (Table 5) and sent for Sanger's sequencing. The product of successful knock-in (in both alleles) should be clean with single. This was aligned to the wildtype genomic sequence to determine the insertions or deletions introduced. The scheme of Rif1 cDNA sequence was adapted from ENSMBL ENSMUST00000112693.10.

3.2.4. Cell sorting

For single cell sorting, 100ul of media was added to each well in a 96-well plate and for bulk sorting 5 mL was added to each 15 mL falcon tube. Cells were collected 40 hours post electroporation into falcon tube and washed twice with PBS/FBS. The final pellet was resuspended in 500µL of PBS/FBS, poured into FACS tube and taken to FACS Core Facility of MDC for sorting.

3.2.5. Genomic DNA isolation

Genomic DNA was extracted using phenol/chloroform/isoamyl method. For this, cells were pelleted down at 1200rpm for 5 minutes following which they were washed in PBS and centrifuged again. 500µl of proteinase K buffer (100mM Tris-pH 8, 0.2% SDS, 200mM NaCl, 5mM EDTA) was added on top of the pellet along with 5ul of Proteinase K enzyme (Peqlab) and incubated at 55°C for overnight. The following day, the process was started first with

centrifugation of PLG light tube (VWR) at 14000g for 30 seconds. Genomic DNA solution in proteinase K buffer was added on top, to which equal volume of Phenol/Chloroform/Isoamyl alcohol (Roth) was added and rigorously mixed to make a homogenous solution of the aqueous and organic phases. The mix was centrifuged at 14000g at room temperature for 10 minutes. 470µl of the aqueous layer was carefully collected and added to a fresh tube to which again equal volume of Phenol/Chloroform/Isoamyl alcohol was added and mixed thoroughly like in the previous step. The mix was centrifuged at 14000g for 10 minutes at room temperature. 420µl of the aqueous layer was again carefully transferred into a new tube. 3M sodium acetate (pH 5.2), equivalent to $1/10^{th}$ volume of the genomic DNA solution, was added on top. Next, 1µg/µL of glycogen was added and finally 100% ethanol, equivalent to 2.5 times of the final volume, was added and gently inverted several times and placed at -20^0C for 15 minutes. The solution was then centrifuged at 14000g for 30 minutes at 4^0C after which the genomic DNA pellet was visible. The supernatant was carefully aspirated and was washed with 1 mL of 70% ethanol at 14000g for 10 minutes. The washing step was repeated one more time following which the pellet was air dried until it was transparent. 50-100 µL of Tris-EDTA buffer was added to dissolve the pellet and incubated at 55°C for 1 hour and later at room temperature overnight. The concentration was measured using the nano drop machine.

3.2.6. Screening for Knock-in positive clones

Genomic DNA was extracted using the Quick extract solution (Epicenter) and incubated at 65°C for 15 minutes, followed by 68°C for 15 minutes and finally at 98°C for 10 minutes. The targeted region was amplified with one primer annealing outside the homology arms and another one inside. The PCR product was purified with a PCR/Gel purification kit (Machery Nagel) and then it was digested with 10 units of appropriate enzyme overnight. The digested PCR products were run on a 1% agarose gel and positive clones were selected for further validation using genomic scar analysis and western blot.

3.2.7. Genomic scar analysis

After genomic DNA isolation the targeted region was amplified by PCR using Phusion polymerase (ThermoFischer scientific). The PCR product was run on agarose gel and later extracted with gel extraction kit (Machery Nagel). The product were sequenced by Sanger sequencing using the primers that were used for PCR. Clean sequences with single peaks indicated homozygous knock-in. The obtained sequences were compared to the wild type genomic sequence attained from ENSMBL website using the MacVector/Snapgene program.

3.2.8. Immunoblotting

Cell were harvested by centrifuging them at 1200rpm for 5 minutes at 4°C. The pellets were washed with PBS and then snap frozen in liquid nitrogen. RIPA lysis buffer (Sigma-Aldrich) with 1µM DTT, EDTA free protease inhibitor (Sigma-Aldrich) and if required phosphatase inhibitors PhosStop (ThermoFisher Scientific), were used for cell lysis and then incubated for 20 minutes at 4°C. The cell lysate was clarified at 14000g for 10 minutes. Bradford reagent (BioRad) was used to determine protein concentration after which the whole cell extracts were denatured using NuPage loading dye (ThermoFischer Scientific) supplemented with 45 mM DTT and boiled at 72°C for 10 minutes. The lysates were run on pre-cast NuPage 3-8% Tris acetate or 4-12% Bis-Tris gradient gels (ThermoFischer Scientific) at 150V or 200V respectively. Gels were placed together with PVDF (polyvinylidene difluoride, Millipore) membrane for wet-transfer of proteins in Mini Trans-Blot Tank (ThermoFisher Scientific) using transfer buffer (25nM Tris, 192 mM glycine, 20% methanol) at 110 V (constant voltage) for 1.5 hour. The membrane was blocked using either 3% BSA in PBST (1X Phosphate Buffer Saline, 0.1% Tween-20) or 2% skim milk in TBST (1X Tris-Buffered saline, 0.1% Tween-20) for 1 hour, followed by primary antibody (Table 2) incubation either for 1 hour at room temperature or overnight at 4^0C. The membrane was washed 3 times with PBST or TBST for 10 minutes each and then incubated for 1 hour with HRP-conjugated secondary antibody at room temperature. Chemiluminescence solution (PerkinElmer) was added on top of the washed membrane and exposed to films (Amersham hyperfilm ECL, VWR) that were immediately developed using the OPTIMAX 2010 film developer in dark room.

3.2.9. Transfection

For retroviral production, BOSC23 (HEK293T derivative cell lines) were seeded at a density of 100,000/mL in complete DMEM media in a 10cm petri dish. After 24 hours, 6µg of plasmid of interest and 6µg of appropriate viral tropism plasmid were put in a 1.5 mL Eppendorf tube. pECO provides the tropism for murine cells and can be is used for primary B cells and iMEFs. However, CH12 cells, for unknown reason, has modified its surface receptor for viral particles that made only pAMPHO compatible which provides tropism for all mammalian cells. 554 µL of Opti-MEM (Life Technologies) was used to mix the plasmids together with 36 µL Fugene-HD (Promega) that helps transfection of the plasmids into the cells. The total mix of 600 µL was incubated for 10-12 minutes at room temperature and then added to the cells dropwise and then the plate was swirled gently.

For lentiviral production, HEK293T cells were seeded at a density of 300,000 cells/mL in complete DMEM media in a 10cm petri dish. After 24 hours, 12µg of plasmid of interest, 7.5µg

psPAX and 3µg of pMDG.2 (helper plasmids) were added. 600 µL of Opti-MEM (Gibco/Invitrogen) was used to mix the plasmids together with 72 µL Fugene-HD (Promega) that helps transfection of the plasmids into the cells. The entire mixture was incubated for 10-12 minutes at room temperature and then added to the cells dropwise and swirled gently.

3.2.10. Viral transduction

B cells (splenocytes or CH12) or iMEFs were seeded after 24 hours of transfection (section 3.2.9). After 48 hours of transfection, 20mM of HEPES and 10µg/mL of polybrene was added in a 50 mL tube. Viral supernatant from transfected BOSC23/HEK293T was collected with the help of a syringe, added on top of HEPES and polybrene and mixed gently. Fresh DMEM media was added to the BOSC23 cells for second round of transduction. RPMI media from B cells (splenocytes or CH12) was carefully removed and replaced with viral supernatant. Since RPMI media of splenocytes culture contains cytokines, the media from each well of 6-well plate was collected and stored in a 2 mL Eppendorf tube at room temperature. B cells with viral supernatant were spinoculated for 1.5 hour at 2350rpm after which they placed back in the incubator. After 4 hours, viral supernatant was carefully removed and trashed and complete RPMI media was put back in cells (fresh for CH12 and stored for splenocytes). The transduction process was repeated the next day. In case of iMEFs, the viral supernatant was kept for 24 hours and removed only during the second day of transduction when fresh viral supernatant was added. Moreover, iMEFs were not spinoculated.

The transduced cells were used for further experiments like western blot or FACS. For CH12 and iMEFs, depending on which construct was used for transduction, they were selected with antibiotics (2µg/mL Puromycin or 6µg/mL Blasticidin) until they recover completely before setting them up for experiments.

3.2.11. Biotinylation

Cells (BOSC23, CH12 and *Rosa26*$^{dCas9Suntag/+}$ splenocytes) were treated with 500µM of Biotin (Sigma-Aldrich) from a stock concentration of 50mM made in DMSO (dimethylsulfoxide). After 10 minutes, cells were collected and centrifuged down at 1200rpm for 5 minutes at 4^0C. Cells were washed three-four times with ice cold PBS/FBS and centrifuged at 4^0C in order to stop biotinylation reaction. After washing, cells were incubated on ice for 1 hour. Lastly cells were pelleted down and snap frozen with liquid nitrogen and stored at -80^0C until the next step.

3.2.12. Immunoprecipitation and Mass-Spectrometry

For immunoprecipitation of biotinylated proteins, *Rosa26*$^{dCas9Suntag/+}$ splenocytes were activated with 25 µg/ml LPS, 5 ng/ml IL-4, and 0.5 µg/ml RP105, and infected with pMSCV-U6gSµ/gRandom-PGKPscfvmT2AGFP (or gSµ/gRandom) retroviral constructs as described above. At 68-72 hours post-activation, cells were biotinylated, washed and snap frozen as described in section 3.2.11. Cells were lysed with buffer containing 20 mM Tris-HCl, 150mM NaCl, 0.5% NP-40, 1.5mM $MgCl_2$, Complete EDTA-free protease inhibitor cocktail, Phosphatase Inhibitor, 0.5 mM DTT, Pepstatin A, PMSF and Benzonase for 20 minutes. Lysates were clarified by 10 minutes centrifugation at 14000g at 4^0C. Bradford reagent (BioRad) was used to determine protein concentration after which the whole cell extracts were normalized and incubated with anti-Streptavidin magnetic beads (ThermoFisher Scientific) at 4^0C for 4 hours. Beads were washed twice with lysis buffer, once with 1 M KCl, once very briefly with 0.1 M Na2CO3, once very briefly with 2 M urea in 10 mM Tris-HCl (pH 8.0), and twice with lysis buffer without detergent. The biotinylated proteins were eluted out by denaturing the beads using NuPage loading dye (ThermoFisher Scientific) supplemented with 20mM DTT and 2mM biotin and boiled at 72°C for 10 minutes. The beads were proceeded for western blot analysis with anti-Streptavidin-HRP and anti-HA (miniTurbo). For co-IP analysis, western blot was performed with anti-Cas9. For mass-spectrometry, 5% of the beads were taken out for western blot and the remaining were snap frozen and handed over to Selbach lab (Proteome Dynamic lab, MDC).

For immunoprecipitation of RIF1, *Rif1*$^{FH/FH}$ splenocytes were activated with 25 µg/ml LPS, 5 ng/ml of mouse recombinant IL-4, and 0.5 µg/ml RP105. At 72 hours post-activation, cells were irradiated with 10 Gy and left for recovery for 1 hour following which they were collected, washed and snap frozen as described in section 3.2.13. Cells were lysed with buffer comprising 50 mM Tris-HCl, 150mM NaCl, 1% NP-40, MS-SAFE Protease Phosphatase Inhibitor (Sigma-Aldrich), 0.5% Deoxycholate, 0.1% Sodium dodecyl sulfate and Benzonase for 20 minutes. 2-Chloroacetaminde (Sigma-Aldrich) and sodium butyrate (Sigma-Aldrich) were added as inhibitors of sumoylation and acetylation respectively. Lysates were clarified by 10 minutes centrifugation at 14000g at 4^0C. Bradford reagent (BioRad) was used to determine protein concentration after which the whole cell extracts were normalized and incubated with magnetic beads (ThermoFisher Scientific) conjugated with anti-HA at room temperature for 1 hour. Beads were washed twice with lysis buffer with 0.5% NP-40 and twice using lysis buffer without detergent. The proteins were eluted out by denaturing the beads using NuPage loading dye (ThermoFisher Scientific) supplemented with 40mM DTT and boiled at 72°C for 10 minutes. For mass-spectrometry, 5% of the beads were taken out for

western blot analysis using anti-Flag and the remaining were snap frozen and given to Mertins lab (Proteomics facility of MDC).

3.2.13. Rescue of viability assay

RIF1 mutant CH12 clones or CH12 transduced with shBrca1 were counted and seeded at 30,000 cells/mL density and treated with 1μM PARPi (Olaparib, Selleckchem). At 72 hours cells were washed and collected for FACS analysis to determine percentage of viability with 10000-30000 events. iMEFs transduced with pMX-ANP32B were seeded at 50,000 cells/mL, treated with 1μM and 4μM Olaparib and analysed for rescue of viability by FACS at 120 hours. Activated primary B cells were seeded at 500,000 cell/mL density, transduced with pMX-ANP32B and treated with 2μM and 4μM Olaparib. At 72 hours cells were analysed by FACS to determine percentage of viability.

3.2.14. Class switch recombination (CSR) assay

For CSR assay, 50,000 cells/mL CH12 cells were cultured in complete RPMI 1640 complemented with 15 mg/mL αCD40L (BioLegend), 5 ng/ml TGF-β and 5 ng/ml IL-4 to induce the expression of surface IgA. After 48 hours cell suspensions were collected by centrifugation, washed once in PBS/FBS and incubated for 20 minutes at 4^0C on a rotator with PE fluorochrome-conjugated anti-IgA antibodies (Southern Biotech). Stained cells were washed and resuspended in 300-350 μL PBS/FBS. Samples were measured on LSR Fortessa cell analyzer (BD-Biosciences) and 10000-30000 events (of live or of GFP if infected with GFP containing plasmid) were acquired.

For measuring CSR in primary B cells, they were collected at 72 hours and stained with APC-conjugated IgG1 antibody (Southern Biotech). Stained cells were washed and resuspended in 300-350 μL PBS/FBS. Samples were measured on LSR Fortessa cell analyser (BD-Biosciences) and 10000-30000 (of live or of GFP if infected with GFP containing plasmid) events were acquired.

3.2.15. CRISPR/Cas9-mediated CSR

4 guide RNAs against the each Sμ and Sα were designed manually based on number of repeats they target. Each Sμ gRNA was cloned into pX458-GFP and each Sα gRNA was cloned into px330-BFP. Both plasmids have a tandem U6 cassette and encode Cas9. 20μg of gRNA plasmid was electroporated into 2 x10^6 *WT* CH12 using the Neon Transfection System (ThermoFisher Scientific). Control construct was generated by cloning random gRNA

(R) that does not target anywhere in the mouse genome, in both pX458-GFP and px330-BFP. CH12 cells were electroporated with the plasmids and allowed to recover for 12 hours before CSR analysis by FACS. 10000-30000 events of GFP and BFP double positive population was acquired to check for expression of surface IgA.

3.2.16. T7 endonuclease assay

WT CH12 cells electroporated with gRNAs were collected and lysed to extract genomic DNA. Total of 1000bp around the target region was amplified by PCR using Q5 high fidelity polymerase (NEB). The reaction was purified and T7 endonuclease I (NEB) was added for digestion at 37^0C. The reaction was stopped with 0.25M EDTA and purified once more. The products were run on 1% agarose gel and results were observed under UV light.

3.2.17. Genotyping

Mice ear punches were incubated with DirectPCR Ear Lysis reagent (VWR) comprising of 0.1mg/mL of proteinase K (Peqlab) at 55^0C for overnight. Target genes were PCR amplified with HotStarTaq DNA Polymerase (Qiagen). Primers used for *Rosa26*$^{dCas9Suntag/+}$, BALB/c-Tg(CMV-cre)1Cgn/J and *Rosa26*$^{dCas9\text{-}Suntag/+}$ *CMV*$^{Cre/+}$ genotyping listed in Table 5. For cell lines in *in vitro* culture, genomic DNA (gDNA) was extracted from at least $1x10^6$ pelleted cells. Cell pellets were incubated overnight in proteinase K buffer with 0.1 mg/ml of proteinase K diluted at 55^0C and later genomic DNA was extracted with the protocol described in section 3.2.5. Genomic DNA was used to amplify target region with HotStarTaq DNA Polymerase (Qiagen) by PCR. Primers are listed in Table 5.

3.2.18. Immunofluorescence

iMEFs (retrovirally transduced *WT* iMEFs) were seeded on coverslips that were placed into 12-well plates. After 24 hours cells were irradiated with 10 Gy and put back in incubator for 1 hour recovery. Cells were washed with PBS and fixed with 1 mL of 4% paraformaldehyde solution in PBS (Sigma-Aldrich) for 20 min at room temperature. After three quick washes, the samples were permeabilized with 100% chilled methanol for 5 min at room temperature followed by three washes with PBS. Then the coverslips were incubated with blocking solution (5% horse serum in PBS) for 1 hour at room temperature. Cells were stained with rabbit anti-RIF1 or rabbit anti-ANP32B (abcam) for 1 hour at room temperature. Coverslips were washed thrice with PBS and were incubated with fluorochrome-conjugated secondary antibodies goat anti-rabbit Alexa546 (1:500; ThermoFisher Scientific) together with Hoechst stain for nucleus (1:1000) for 1 hour at room temperature. Coverslips were washed three times with PBS and

placed on microscope slides using Prolong Gold Antifade Mountant mounting medium (ThermoFisher Scientific). Images were acquired with Keyence microscope (Zeiss). Foci analysis was done with automated counting software from Keyance (BZ-X800) and mean fluorescence intensity was analysed by ImageJ software (NIH).

3.2.19. Colony formation assay

To determine cell survival following replication-induced DSBs, iMEFs (*WT1* iMEFs, *WT2* iMEFs, *53bp1*$^{-/-}$ iMEFs and *Brca1*$^{\Delta 11/\Delta 11}$ iMEFs) were plated in 60 mm dishes, with three technical replicates. Following 24 hours, cells were treated with 0.5 μM of PARPi, which was also replenished after 7 days. iMEFs were cultured in PARPi containing media for a total of 14 days. On the day of colony formation assay processing, media was aspirated from the plates and colonies were subsequently fixed with 15% acetic acid in methanol for 5 minutes, followed by staining with 0.5% Crystal Violet (Sigma-Aldrich) in 1:1 methanol/water (v/v) for 30 minutes. The plates were washed thrice with PBS. 10% SDS solution was used to dissolve the crystal violet retained in the cells and 1 mL was used to quantify the mean absorbance with spectrophotometer (Eppendorf).

3.2.20. Intra-cellular staining of Cas9

Cells were collected and washed once with PBS. The pellet was resuspended in 50 μL of PBS and added in a well of 96-well plate. 100 μL of fixation medium (Reagent A; Abcam) was added on top, mixed thoroughly and incubated in dark for 15 minutes at room temperature. Cells were washed with 100 μL PBS and the pellet was resuspended in 100 μL of permeabilization medium (Reagent B; Abcam). 2 μL of antibody was added on top for staining and the mix was incubated in dark for 30 minutes at room temperature. Cells were washed thrice with 200 μL of PBS and the final pellet was resuspended in chilled flow buffer (PBS, 2% FBS, 5μM EDTA) for FACS acquisition.

4. RESULTS

4.1. PART I: Generation of a dCas9 expressing B cell model system to identify DSB factors at *Igh* locus during CSR

4.1.1. CRISPR-mediated targeted chromatin purification of the *Igh* locus DNA elements using 2xHA dCas9Blast construct.

In order to identify proteins and RNA species interacting with the *Igh* locus during CSR, I planned to perform targeted chromatin purification of both S regions and the 3'RR (Figure 9A). To do so, I used the murine B cell lymphoma cell line, CH12, as model system[84], with a CRISPR-Cas9 based approach for targeted chromatin isolation[121-122]. CH12 are highly proliferative B cells that can be induced to express AID and undergo CSR to IgA *in vitro* with high efficiency. Since CH12 cells lack the ability to get transfected, I transduced them with a lentiviral plasmid from Addgene called pGH125_dCas9Blast. This way only the dCas9 expressing cells can be selected with Blasticidine (Figure 9F). The selected CH12 cells would be further subjected to another lentiviral system from Addgene named lenti-GuidePuro for gRNAs expression (Figure 9F).

In order to implement co-immunoprecipitation experiments, I added a tag at the 5' end of dCas9 in pGH125_dCas9Blast. Since there was no unique restriction enzyme anywhere within the dCas9 in the plasmid, I amplified the entire dcas9 using a forward primer that carried an extra 2x HA tag sequence and a restriction enzyme (Figure 9B). I digested out the original dCas9 and ligated the PCR product, 2xHA-dCas9, back to the vector. The new plasmid was then called 2x HA-dCas9BLAST and I verified it by diagnostic digestion with BsiWI and BamHI (Figure 9C) and Sanger's sequencing (data not shown). I proceeded to transfect the plasmid in HEK293T cells to validate the expression of dCas9 protein by western blot (Figure 9D). I also validated the plasmid lenti-GuidePuro by transducing CH12 cells with lenti-GuidePuro viral particles, produced by HEK293T cells (Figure 9F) and treating them with or without 2μg/ml Puromycin. I analysed viability with FACS using the Forward scatter (FSC) and Side scatter plot (SSC) that had already been established in our lab as an efficient read-out for cellular viability. The infected cells were viable after puromycin treatment for 48 hours in contrast to the uninfected ones, that proved successful integration of the plasmid (Figure 9E). Finally, I set up the experiment to generate stable CH12 cells expressing 2x HA-dCas9BLAST. However, none of the cells expressed dCas9 even after Blasticidine selection (data not shown). This observation could suggest that since dCas9 is a large protein or due to an alternative unknown reason, viral transduction is not an efficient approach to generate CH12

cells stably expressing the protein. It prompted me to change the system for pulling-down *Igh* locus.

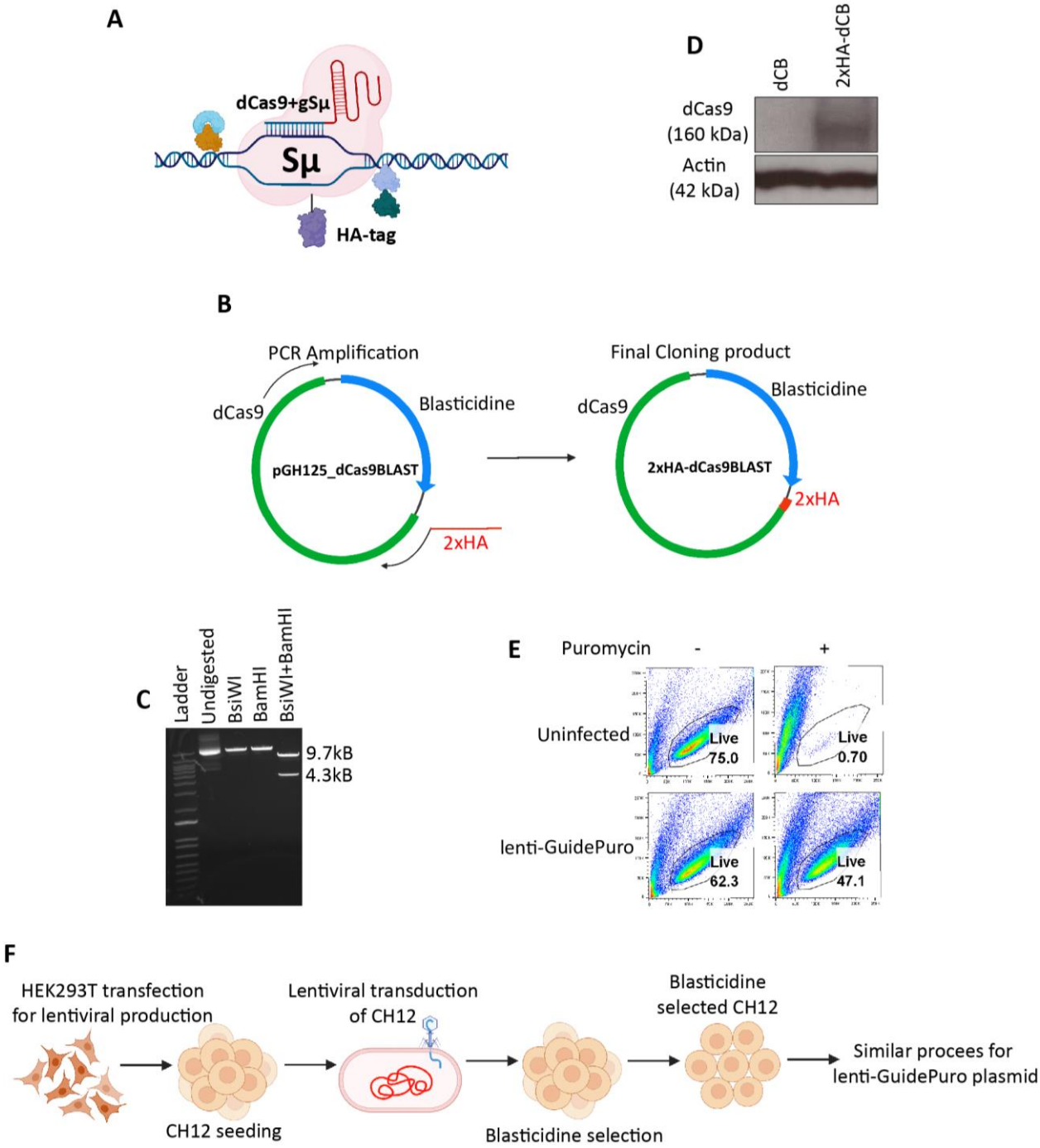

Figure 9. CRISPR-mediated targeted chromatin purification of the *Igh* locus using 2xHA-dCas9Blast construct. (A) Schematic representation of dCas9 targeting Sμ region of the *Igh* locus. (B) Schematic representation of the cloning strategy to generate 2xHA-dCas9Blast construct from pGH125_dCas9Blast. Blast, Blasticidine. (C) Diagnostic digestion of 2xHA-dCas9Blast with BsiWI and BamHI. (D) Western blot analysis of dcas9 with anti-HA in pGH125_dCas9Blast (dCB) and 2xHA-dCas9Blast (2xHA-dCB) expressing HEK293T cells. (E) Representative FACS plot for viability (gated

population indicates live population) in CH12 either uninfected or lenti-GuidePuro plasmid infected, treated with and without Puromycin. X-axis is SSC and Y-axis is FSC. (F) Schematic representation of experimental set up to establish stably expressing 2x HA-dCas9BLAST and lenti-GuidePuro CH12 cells by lentiviral transduction.

4.1.2. Coupling CRISPR and proximity labelling using dCas9miniTurbo-Puro/pR26 construct for *Igh* locus purification.

One of the major challenges for a single locus-purification approach is the need to maximize the amount of pulled-down material. To do so, I coupled the use of the CH12 with a CRISPR-TurboID based approach for targeted chromatin isolation (Figure 10A). dCas9-TurboID-mediated chromatin isolation uses nuclease-deficient Cas9 protein (dCas9) fused to a mutated form of Biotin ligase (miniTurbo), to label proteins within a 10 nm radius of a specific targeted genomic sequence (Figure 10A). In the presence of biotin, miniTurbo catalyses the formation of biotin-5′-AMP anhydride, which disperses out to biotinylate proximal proteins on nucleophilic residues[121-122]. Biotinylation process by dCas9-TurboID will considerably increase the pull-down efficiency of single loci. This approach will be able to identify proteins as well as protein-associated RNAs that could be sequestered for mass-spectrometry and RNA-sequencing respectively.

Since transduction of dCas9 plasmid in CH12 cells was not possible, I proceeded to knock-in CRISPR-TurboID system in its *Rosa26* locus that will stably express the proteins and help me to bypass the limitation projected by viral transduction. *Rosa26* is a locus in mouse genome that is constitutively transcribed without the expression of any protein, making it a very useful site for transgene integration[126]. Moreover, the system is transiently induced under the Tet-on system for minimizing off-target biotinylation. The Tet-On system is dependent on Reverse Tetracycline Controlled Transactivator (rtTA) that recognizes Tetracycline Response Element (TRE) sequences and suppresses it. Exogenous presence of tetracycline or its analogue doxycycline binds to rtTA after which it releases the suppression from TRE promotor[127]. In order to do this I cloned dCas9miniTurbo-Puro/pR26 construct through a multi-step cloning process. I used Inducible Caspex (Addgene) to clone Tet-on system, 2x HA-dCas9BLAST to clone dCas9 and 3x HA-miniTurbo-NLS-pCDNA3 (Addgene) to clone miniTurbo, all into pR26-CAG-AsiSI/MluI backbone that contains the *Rosa26* homology arms for the knock-in (Figure 10B). To verify the sequence of the new construct I digested it with unique restriction enzymes AsiSI and MluI (Figure 10C) and also analysed it by Sanger's sequencing (data not shown).

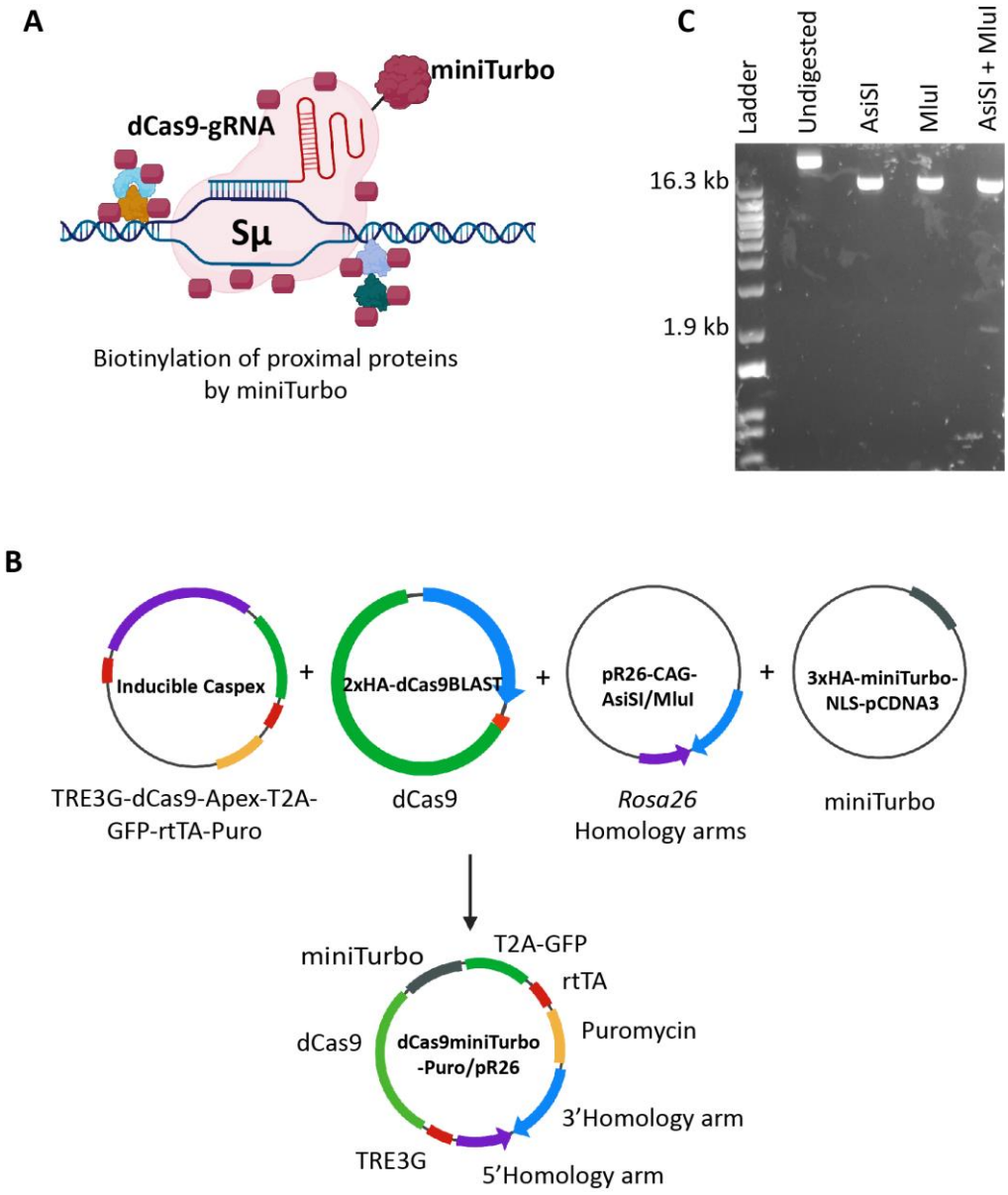

Figure 10. Coupling CRISPR and proximity labelling using dCas9miniTurbo-Puro/pR26 construct for *Igh* locus purification. (A) Schematic representation of proximity labelling with CRISPR/cas9 system. (B) Schematic representation of the constructs used to generate the final vector dCas9miniTurbo-Puro/pR26 with the Tet-on system from Inducible Caspex in pR26-CAG-AsiSI/MluI backbone through a multi-step cloning process. (C) Diagnostic digestion of dCas9miniTurbo-Puro/pR26 with AsiSI and MluI.

4.1.3. dCas9miniTurbo-Puro/pR26 construct encodes a functional dCas9miniTurbo fusion protein.

To test the dCas9miniTurbo-Puro/pR26 construct, I transfected it in BOSC23 cells (HEK293 derivative cell lines) and determined the inducibility, expression and activity of the

dCas9miniTurbo fusion protein (Figure 11A). I observed a substantial increase in GFP upon doxycycline treatment, confirming the activity of the Tet-on inducible system (Figure 11B). This feature is particularly crucial to minimize the background signal in the mass-spectrometry detection step. dCas9 expression under Tet-on system was confirmed by western blot analysis (Figure 11C). Similarly western blot analysis with anti-Streptavidin confirmed that under doxycycline induction and in the presence of biotin, miniTurbo biotinylates its proximal proteins (Figure 11D).

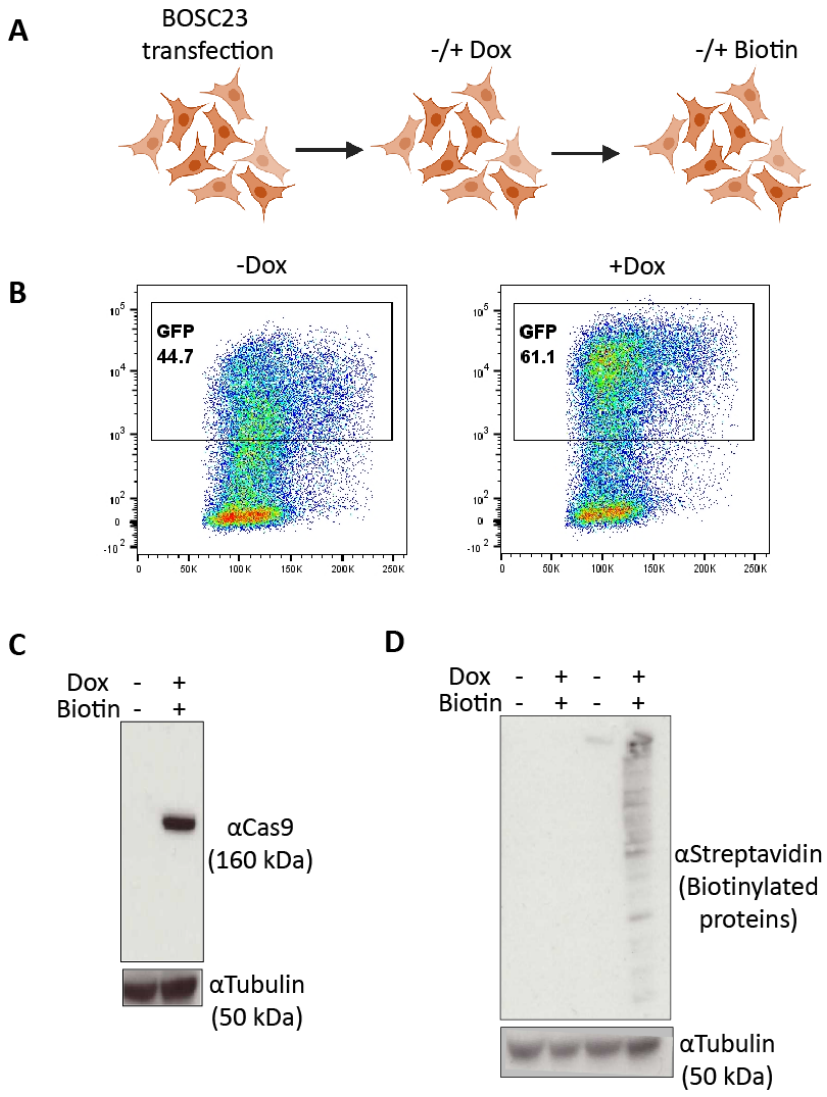

Figure 11. dCas9miniTurbo-Puro/pR26 construct encodes a functional dCas9miniTurbo fusion protein. (A) Schematic representation of experimental set up to validate the expression of dCas9miniTurbo-Puro/pR26 construct. (B) Representative FACS plots showing GFP expression after transient transcfection of the construct in BOSC23 cells, and with and without Dox treatment. Gated population indicates GFP positive population. (C-D) Western blot analysis of dCas9 with anti-Cas9 (C) and biotinylated proteins with anti-Streptavidin (D) alongwith Tubulin loading controls. Dox, doxycycline.

4.1.4. Generation of dCas9miniTurbo-Puro/pR26 knock-in CH12 cell lines.

To generate the knock-in CH12 cell lines, I co-electroporated the dCas9miniTurbo-Puro/pR26 construct and the plasmid Cas9-g*Rosa26*-BFP (Addgene) that encodes *WT* Cas9 and a gRNA against *Rosa26* locus, in *WT* CH12, *Zmynd8*$^{-/-}$ CH12 and *AIDER* CH12. *AIDER* CH12 cell lines were generated by knock-in of the AIDER construct into the *Rosa26* locus of *Aicda*$^{-/-}$ CH12 cells. Treatment of *AIDER* CH12 cells with the cytokines cocktail will lead to induction of GLTα (GLTμ is constitutive) without break formation since these cells are knock-out for AID, and the constitutively expressed AIDER is retained into the cytoplasm. Since AID is fused to ER (estrogen receptor), only upon 4-Hydroxytamoxifen (4-HT) addition, AIDER will translocate into the nucleus to induce breaks at the S regions that will then be repaired by NHEJ[128]. This approach allows considerable synchronization of the CSR events and greatly facilitate experimental scale-up. Moreover, this will also allow for using cells untreated for 4-HT to be used to retrieve pre-break dynamics at the locus, before AID target is accomplished. Thus, this is a great model system to comprehensively get a full visualization of *Igh* locus during the entire course of CSR and not just DSB repair. In case of *Zmynd8*$^{-/-}$ CH12, given the described role of ZMYND8 in modulating the activity of the 3'RR[50], ZMYND8-deficient cells can be employed for both validation and exploratory purposes. After electroporation of the constructs, BFP positive cells were then sorted in bulk, and the population was enriched for dCas9miniTurbo-Puro/pR26 knock-in cells under puromycin selection. However, single cell sorting after puromycin selection did not yield any dCas9-expressing clones (data not shown). Therefore, I adopted an alternative approach, and transiently induced the TRE3G promoter and single cell sorted only the GFP positive cells that were possibly the clones expressing dCas9-miniTurbo (Figure 12A and B). Some GFP positive clones were selected for further characterization to validate the knock-in as described further below.

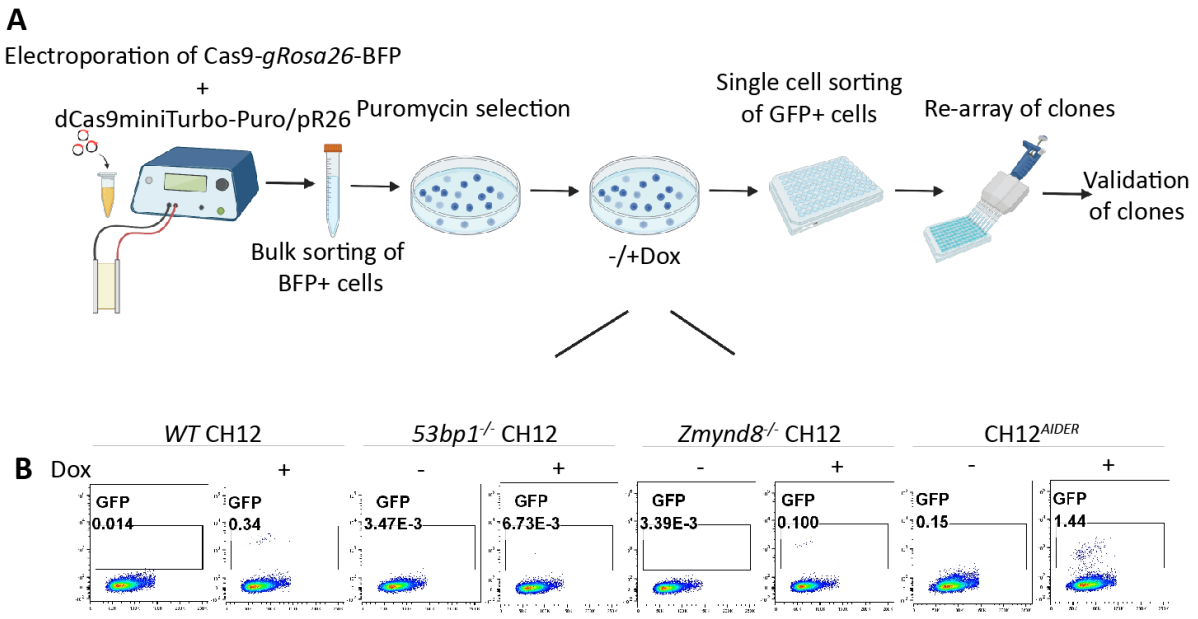

Figure 12. Generation of dCas9miniTurbo-Puro/pR26 knock-in CH12 cell lines. (A) Schematic representation of CRISPR/Cas9 knock-in strategy for generation and selection of knock-in clonal derivatives. (B) Representative FACS plots of puromycin-selected knock-in CH12 cell lines of different genotypes in bulk with and without Dox induction. Gated population indicates GFP positive population. Dox, doxycycline.

4.1.5. Genotypic validation of dCas9miniTurbo-Puro/pR26 knock-in CH12 clonal derivatives.

The GFP positive CH12 cell lines were first validated at the genomic level by amplifying the TRE3G promoter and N-terminus of the dCas9 coding sequence with forward primer outside the 5' *Rosa26* homology arm (Fwd) (Figure 13A and B). In order to verify if the knock-in is homozygous, I also amplified the *WT* allele with both the primers outside the homology arms (Fwd, Rev2) (Figure 13A). Four of the five *WT* clones had the knock-in only in one of the *Rosa26* allele whereas *Zmynd8*$^{-/-}$ CH12 had homozygous knock-in in all the five clones that were selected for validation (Figure 13B). Moreover, apart from one *AIDER* CH12 clone, the rest four clones still maintained the AIDER knock-in (verified with one primer outside homology arm and once inside AIDER transgene), suggesting that in these four clones one allele has a successful dCas9miniTurbo-Puro knock-in and the other continues to have the AIDER knock-in (Figure 13C).

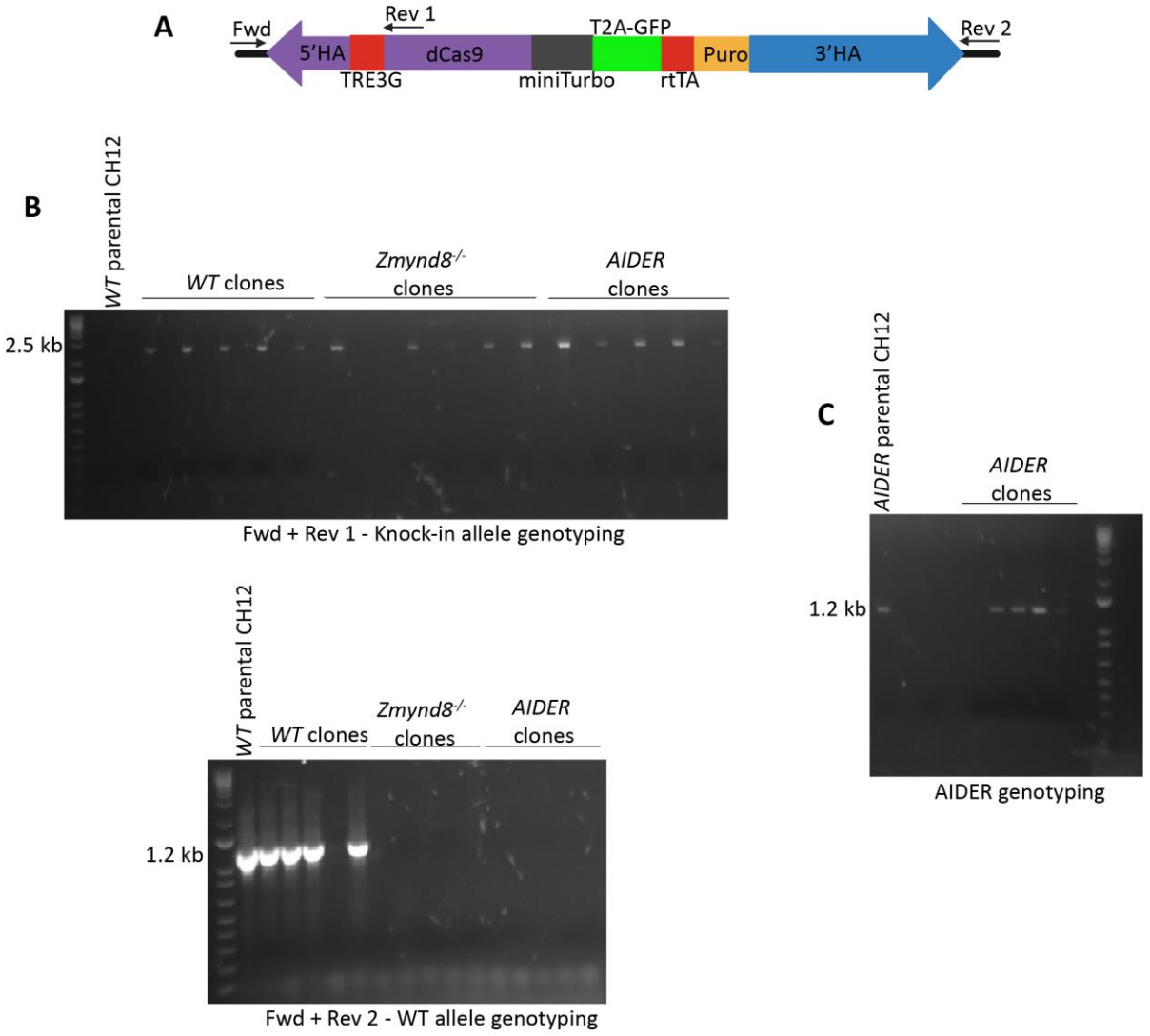

Figure 13. Genotypic validation of dCas9miniTurbo-Puro/pR26 knock-in CH12 clonal derivatives. (A) Schematic representation of the genotyping strategy. To verify the knock-in, TRE3G promoter and N-terminus of dCas9 coding sequence were amplified with forward primer outside the 5' *Rosa26* homology arm and reverse primer inside the transgene (B,C) Genotyping results of selected knock-in clones. The parental *WT/AIDER* CH12 cell line was used as a negative control. gDNA, genomic DNA. Fwd, forward. Rev, reverse.

4.1.6. Validation of GFP in dCas9miniTurbo-Puro/pR26 knock-in CH12 clonal derivatives.

I continued to verify the expression of GFP upon doxycycline induction in the selected knock-in clones (Figure 14A). I also performed a kinetics experiment and monitored GFP expression at various time points under doxycycline treatment. GFP was already detectable after approximately 10 hours (depicted as 10 h) post induction (Figure 14B). *AIDER* CH12 clones

seemed to be losing GFP at 48 hours. Nonetheless, since the GFP is fused to a T2A sequence, its expression analysis suggests successful knock-in.

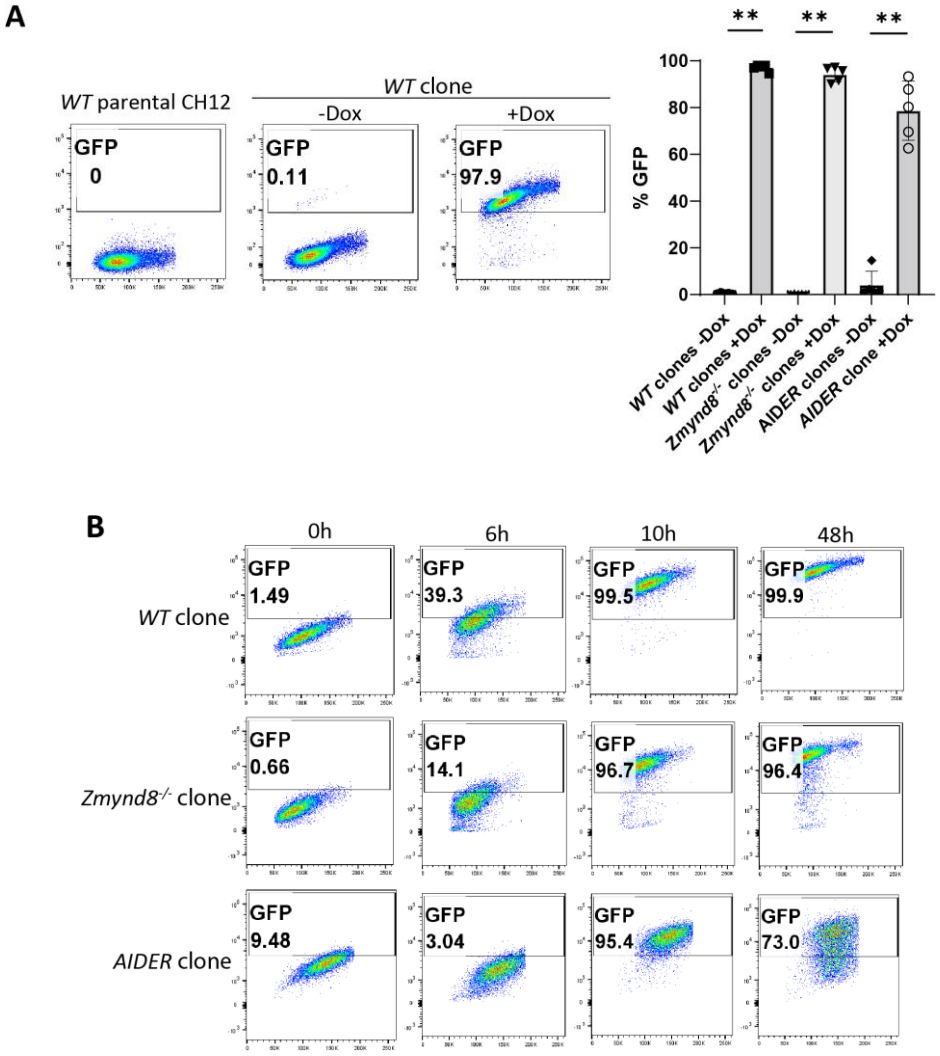

Figure 14. Validation of GFP in dCas9miniTurbo-Puro/pR26 knock-in CH12 clonal derivatives. (A) Left: Representative FACS plot of one clone per genotype (*WT*, *Zmynd8*$^{-/-}$ and *AIDER* clones) showing GFP expression with and without Dox induction (-/+Dox). Gated population indicates GFP positive population. Right: Summary graph for the selected knock-in clones of each genotype. Mann Whitney test was employed for statistical analysis. **= p value<=0.01. (B) Representative FACS plots showing GFP expression at 0 h, 6 h,10 h and 48 h of Dox treatment in one clone per knock-in *WT*, *Zmynd8*$^{-/-}$ and *AIDER* to verify the kinetics of TRE3G promoter activity. Gated population indicates GFP positive population. Dox, doxycycline.

4.1.7. Validation of miniTurbo in dCas9miniTurbo-Puro/pR26 knock-in CH12 clonal derivatives.

I next tested the activity of miniTurbo following addition of doxycycline and biotin. Although, I confirmed the successful construct integration at the *Rosa26* locus and inducible GFP expression, I did not detect any biotinylation signal in western blot analysis with anti-Streptavidin (Figure 15A and Figure 14B). Interestingly I also observed high basal level of biotinylation in *WT* parental CH12 without biotin treatment. To assess whether dCas9miniTurbo fusion protein was expressed at levels below the detection limit of western blot analysis, I performed intracellular staining for biotinylation with APC-conjugated anti-Streptavidin and quantified with flow cytometry.

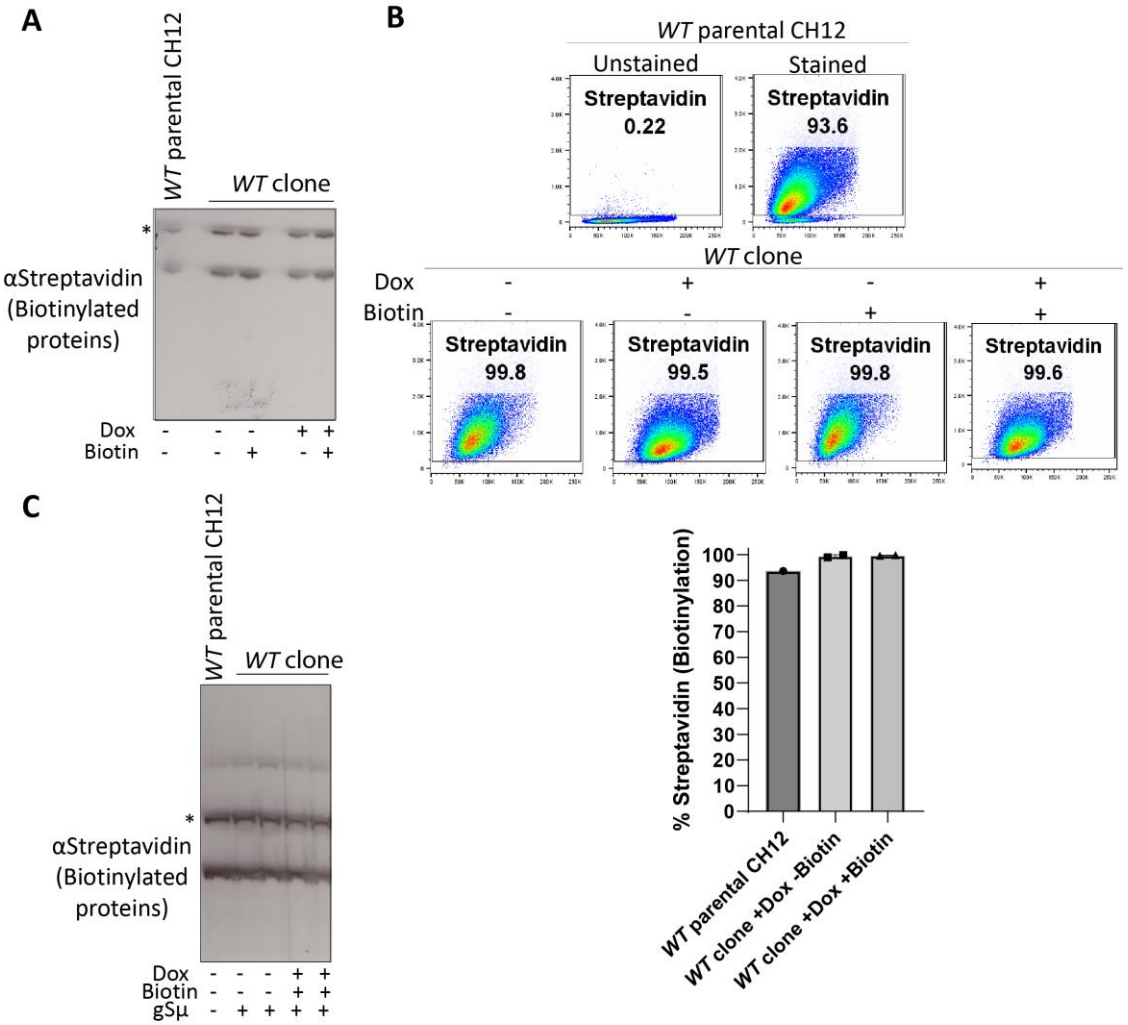

Figure 15. Validation of miniTurbo in dCas9miniTurbo-Puro/pR26 knock-in CH12 clonal derivatives. (A) Western blot analysis of biotinylation with anti-Streptavidin in a knock-in *WT* CH12 clone. *WT* parental CH12 was used as a negative control for background levels of biotinylation in the

CH12 cell line. Unspecific bands (asterisk) depict equal loading. (B) Top: Representative FACS plots of Streptavidin intracellular staining in *WT* parental CH12 cells and *WT* clones. Gated population indicates Streptavidin positive population. Bottom: Graphical representation of two *WT* clones for % Streptavidin (Biotinylation) that denotes percentage of cells having biotinylated proteins. (C) Western blot analysis of biotinylated proteins in a *WT* knock-in clone infected with a gRNA against Sμ (gSμ) and treated with or without Dox and biotin. The parental *WT* CH12 was used as a negative control for background levels of biotinylation in the CH12 cell line. Unspecific bands (asterisk) depict equal loading. Dox, doxycycline.

However, there was no increase of biotinylation from the basal level, which was already too high to give a dynamic range of difference (Figure 15B). Finally, I considered the possibility that gRNA-mediated targeting of putatively low levels of dCas9miniTurbo expressed from one allele could concentrate the protein and increase its detection by assessing the levels of biotinlyation after doxycycline induction. I again found no evidence of miniTurbo activity (Figure 15C).

4.1.8. Validation of dCas9 in dCas9miniTurbo-Puro/pR26 knock-in CH12 clonal derivatives.

Finally, I tested for the expression of dCas9 in the knock-in clones. I wanted to address the question whether dCas9miniTurbo fusion protein was rapidly degraded upon induction. Western blot analysis at different time points after doxycycline treatment showed no presence of dcas9, even though I had observed the expression of GFP after 10 hours of the treatment (Figure 16A and 14B). Moreover, I could observe dCas9 protein expression after transient transfection of a dCas9-expression plasmid in BOSC23 cells that confirms the ability of the antibody to detect dCas9 and not just *WT* Cas9 (Figure 16A).

Once more, to assess whether dCas9miniTurbo fusion protein was expressed at levels below the detection limit of western blot analysis, I optimized a protocol for intracellular staining of dCas9 for FACS analysis. Since I had to perform the experiment in several clones and the original intracellular staining required the use of large amount of the antibody (1:50 dilution), I titrated it in *WT* CH12 electroporated with a *WT* Cas9 expression plasmid known as px458 (Figure 16B). I chose to use 1:250 dilution to proceed with the actual experiment. However, I did not detect dCas9 expression in any of the knock-in cell lines (Figure 16C). Following the same line of miniTurbo assessment, I considered if gRNA-mediated targeting of putatively low levels of dCas9miniTurbo could concentrate the dCas9 and increase its detection by intracellular staining after doxycycline induction. Also in this case, I found no evidence of

dCas9 protein (Figure 16D). In conclusion, all clones I selected based on genomic DNA analysis, puromycin enrichment, and inducible GFP expression, failed to express the dCas9miniTurbo fusion protein, which was an essential requirement for my initially proposed project.

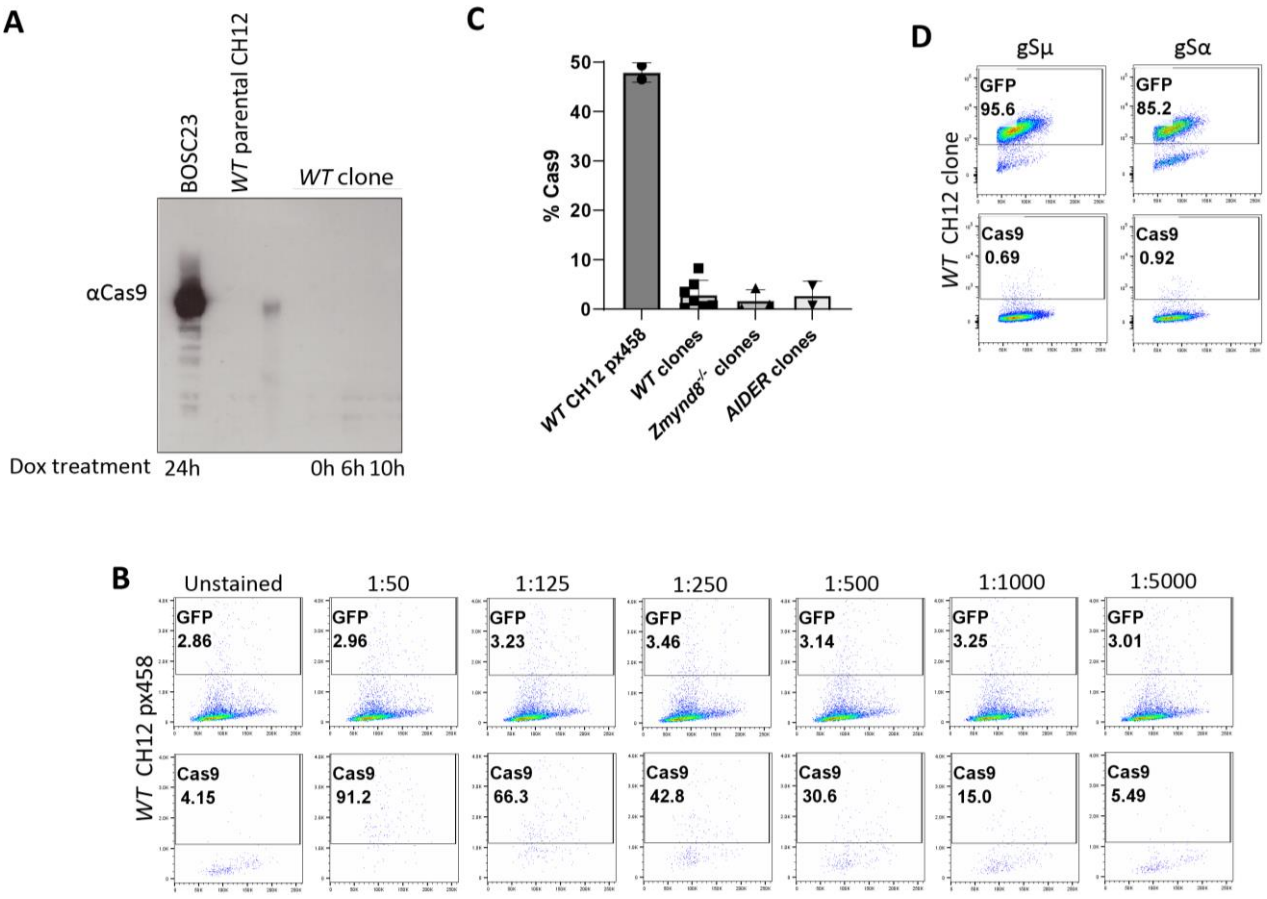

Figure 16. Validation of dCas9 in dCas9miniTurbo-Puro/pR26 knock-in CH12 clonal derivatives. (A) Western blot analysis of dCas9 with anti-Cas9 in a knock-in *WT* CH12 clone. BOSC23 cells transfected with the same plasmid and induced with Dox was included as positive control. (B) Representative FACS plots of titration of intracellular staining of anti-Cas9 antibody in *WT* CH12 px458 (*WT* parental CH12 cells electroporated with px458-T2A-GFP plasmid). Gated population on top indicates GFP positive population, from which Cas9 positive population was plotted and gated. (C) Graphical representation of intracellular Cas9 staining in knock-in *WT* CH12, *Zmynd8*$^{-/-}$ and *AIDER* clones. *WT* CH12 px458 was used as a positive control for Cas9 expression and detection. (D) Representative FACS plots of intracellular Cas9 in a *WT* knock-in clone infected with a gRNA against Sμ (gSμ) and gSα and treated with Dox. Gated population on top indicates GFP positive population, from which Cas9 positive population was derived and gated. Dox, doxycycline.

4.1.9. Generation of lenti-GuideBlast plasmid to deliver gRNA.

While I was generating and validating the clones, I was also establishing a system to deliver gRNA to the dCas9miniTurbo knocked-in cells. Earlier I would have used lenti-GuidePuro, with Puromycin as the selection marker, for gRNA expression in CH12 cells that were supposed to be transduced with 2x HA-dCas9BLAST vector. However, since I changed my approach and the CH12 cells were knocked-in with a plasmid already containing Puromycin gene, I had to tweak the gRNA plasmid with another selection marker. In order to do that I replaced Puromycin in lenti-GuidePuro with Blasticidine using PCR and restriction digestion.

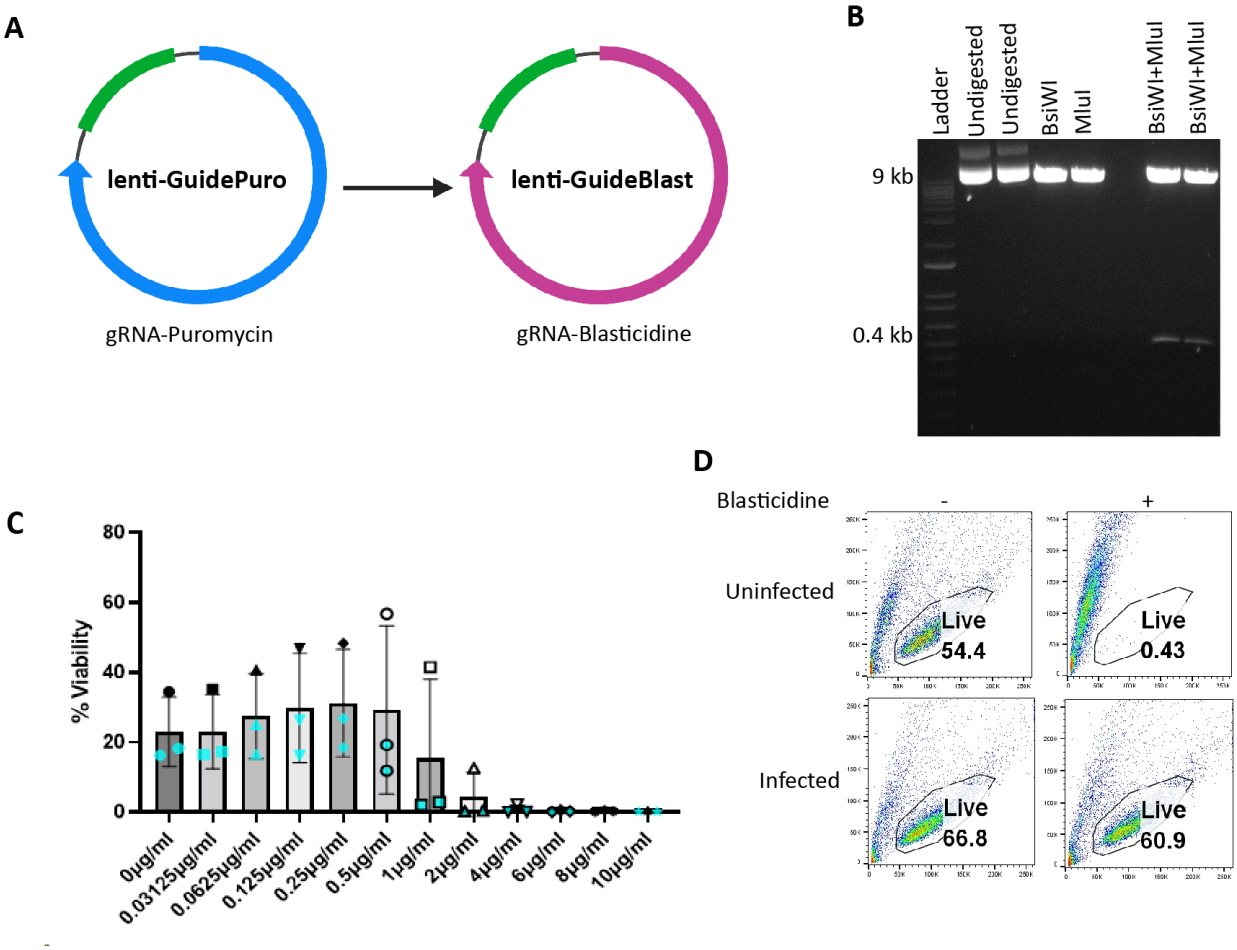

Figure 17. Generation of lenti-GuideBlast plasmid to deliver gRNA. (A) Schematic representation of the cloning strategy to generate lenti-GuideBlast construct from lenti-GuidePuro plasmid purchased from Addgene. (B) Diagnostic digestion of lenti-GuideBlast with BsiWI and MluI. (C) Summary graph of Blasticidine kill curve performed on either *WT* CH12 (black) and two of its clonal derivatives (blue). The graph represents %Viability based on FACs data. (D) Representative FACS plots of blasticidine-selected lenti-GuideBlast infected CH12 cells. Gated population indicates live population. Blast, Blasticidine. Puro, Puromycin.

I called the new construct lenti-GuideBlast (Figure 17A). I verified lenti-GuideBlast with diagnostic digestion (Figure 17B) and Sanger's sequencing (data not shown). I validated the expression of lenti-GuideBlast by transducing it in *WT* CH12 and testing the efficiency of the Blasticidine gene. I checked for viability using FACS with or without 6µg/ml Blasticidine treatment after 48 h. The infected cells were viable in contrast to the uninfected ones that proved successful integration of the plasmid (Figure 17D). The concentration of the Blasticidine was chosen based on a kill curve experiment I performed on *WT* CH12 and two of its clonal derivatives (Figure 17C). Therefore, the plasmid can be used in CH12 cells for gRNA expression.

4.1.10. Selection and validation of gRNAs for targeted *Igh* locus purification.

S regions are highly repetitive in nature, and the use of classical assays like T7 endonuclease assay and Sanger's sequencing to assess for gRNA targeting efficiency is not feasible. However, its repetitive nature provide the advantage of considerably increasing the pull-down efficiency since one gRNA will bind to several regions within the corresponding S region. I employed CRISPR/Cas9-mediated CSR to indirectly assess the targeting efficiency of gRNAs against the S regions[129]. I designed gRNAs for both Sµ and Sα and cloned them in either px458 or px330 that contain Cas9 and tandem gRNA cassette (Section 3.2.15). I employed previously described gRNAs in *Ramachandran et. al., Cell Reports, 2016*, that are efficiently targeting the 5' of Sµ and 3' of Sα as controls (referred here as SµCtrl and SαCtrl). I cannot use any of the control gRNAs described in the publication mentioned above for *Igh* locus purification since they do not target repetitive sequences at both Sµ and Sα. The ones I designed and cloned (four gRNAs each for Sµ and Sα) bind to several repetitive sequences within the specific S region. Moreover, these gRNAs bind throughout the respective S region sequence and not just at its 5' or 3' end. This feature reduces the possibility of pulling-down the recombined Sµ-Sα of the unproductive *Igh* locus allele in CH12[87]. Unactivated *WT* CH12 cells were co-electroporated with SµCtrl with one gRNA that I designed against Sα, and similarly SαCtrl with one gRNA against Sµ. I used CSR (%IgA) levels as read-out for targeting proficiency (Figure 18A). A gRNA (Random gRNA, R) that does not target any sequence in mouse genome was co-electroporated with SµCtrl and SαCtrl as negative controls for targeting. With this method I was able to verify gRNAs Sµ1, Sµ2, Sµ3 and Sµ4 as well as Sα1, Sα2, Sα3 and Sα4 (Figure 18B). I selected Sµ1 and Sα2 for *Igh* locus precipitation since they displayed maximum switch to IgA and target the maximum repetitive sequences in the corresponding S regions. In order to verify if all the gRNAs I had designed are targeting any other S regions non-specifically, I simultaneously had checked for IgG2b level since its

stimulation condition is the same as IgA. None of the gRNAs displayed switch to IgG2b (Figure 18C, representative FACS plot only with Sμ1 and Sα2).

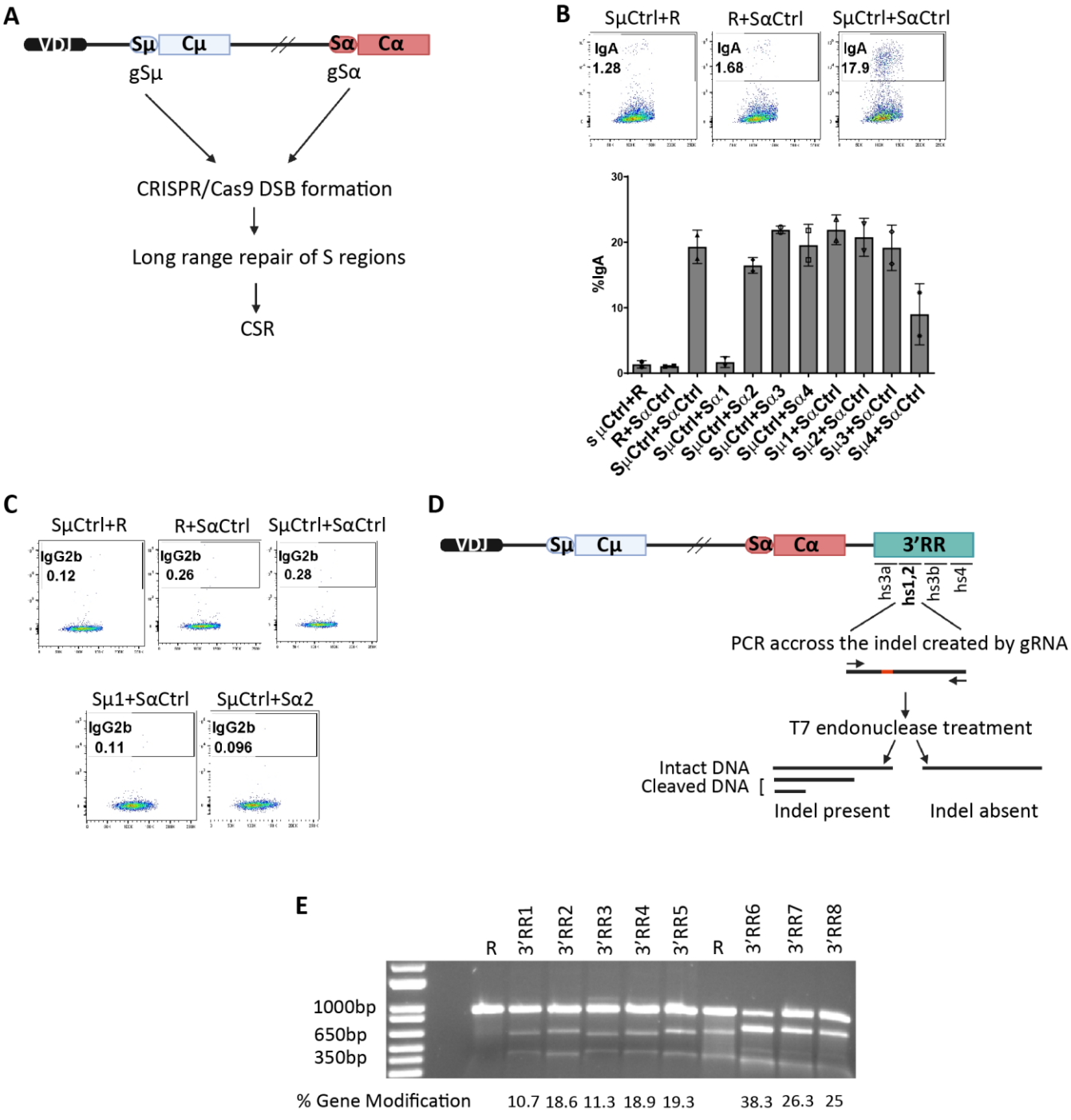

Figure 18. Selection and validation of gRNAs for targeted *Igh* locus purification. (A) Schematic representation depicting CRISPR/Cas9-induced CSR assay. (B) Top: Representative FACS plots depicting %IgA in unactivated *WT* CH12 electroporated with control gRNAs, either Random (R) or against Sμ and Sα used in *Ramacharndran et. al. Cell Reports, 2016*. Gated population indicates IgA

positive population. Bottom right: Graphs summarizing CRISPR/Cas9-mediated CSR for two independent experiments. (C) %IgG2b in unactivated WT CH12 electroporated with control gRNAs, Random (R), Sμ and Sα used in *Ramacharndran et. al. Cell Reports, 2016* with Sμ1 and Sα2 gRNAs that I had selected for *Igh* locus pull-down. Gated population indicates IgG2b positive population. (D) Schematic representation of T7 endonuclease assay. (E) Gel image of T7 endonuclease assay for 3'RR gRNAs. % Gene modification was calculated with the Image J software.

Next, we designed gRNAs targeting regions withing the 3'RR super enhancer of the *Igh* locus. 3'RR has 4 core transcriptional enhancer regions namely hs3a, hs1,2, hs3b and hs4[50]. We designed gRNAs specifically for hs1,2 and hs3b core enhancer regions since our lab found RNA Polymerase II to be significantly increased at these two sites in ZMYND8-deficient primary B cell[50]. I started with testing the gRNAs for hs1,2 and to do so I electroporated them in *WT* CH12. In this case, I assessed targeting efficiency by using T7 endonuclease method. The assay is based on the principle that T7 endonuclease can cleave any dsDNA that contains indel/mismatch (Figure 18D). Quantification of percent gene modification by T7 endonuclease was calculated using Image J software that showed none of the gRNAs were sufficiently efficient (Figure 18E). However, it is difficult to extrapolate quantification of T7 assay with gRNA efficiency.

4.1.11. Primary B cells (Splenocytes) as the new model system from dCas9 expressing mice.

We purchased Rosa26-LSL-dCas9 mice (*Gt(ROSA)26Sor*$^{tm1(CAG\text{-}dCas9\text{-}SunTag)Khk}$) mice from the Jacksons laboratory. This mouse has dCas9-P2A-BFP fused to Suntag and preceded by a loxP-STOP-loxP (LSL) cassette at the *Rosa26* locus, all under a CAG promoter (Figure 19A). This mouse has been previously used as the component of a CRISPRa system[130], but has never been tested for locus-specific pull-down.

In order to remove the STOP cassette, I first bred Rosa26-LSL-dCas9 mice with BALB/c-Tg(CMV-cre)1Cgn/J mice, which express Cre recombinase under the cytomegalovirus promoter that is active in almost all tissues (Figure 19B)[131]. The F1 generation, which was heterozygous for both alleles (*Rosa26*$^{dCas9\text{-}Suntag/+}$ *CMV*$^{Cre/+}$), was further bred with C57BL6/J mice to ensure germline transmission of the deleted allele and to breed out Cre (*Rosa26*$^{dCas9\text{-}Suntag/+}$, Figure 19B). The presence of a single copy of dCas9-Suntag in the heterozygous configuration will contribute to reduce excess accumulation at dCas9-Suntag at S region as well as off-target regions. The mice were always genotyped for the Suntag gene and presence or absence of the STOP cassette and Cre at every breeding step (data not shown). I isolated

splenocytes from *Rosa26*$^{dCas9\text{-}Suntag/+}$ and validated the presence of dCas9 at the protein level by western blot (Figure 19C). I also checked for BFP protein (was not checked originally by the lab which generated the mice) and assessed the level of isotype switching with FACS (Figure 19D). The mice expressed dCas9 and BFP and switched to IgG1 at *WT* level.

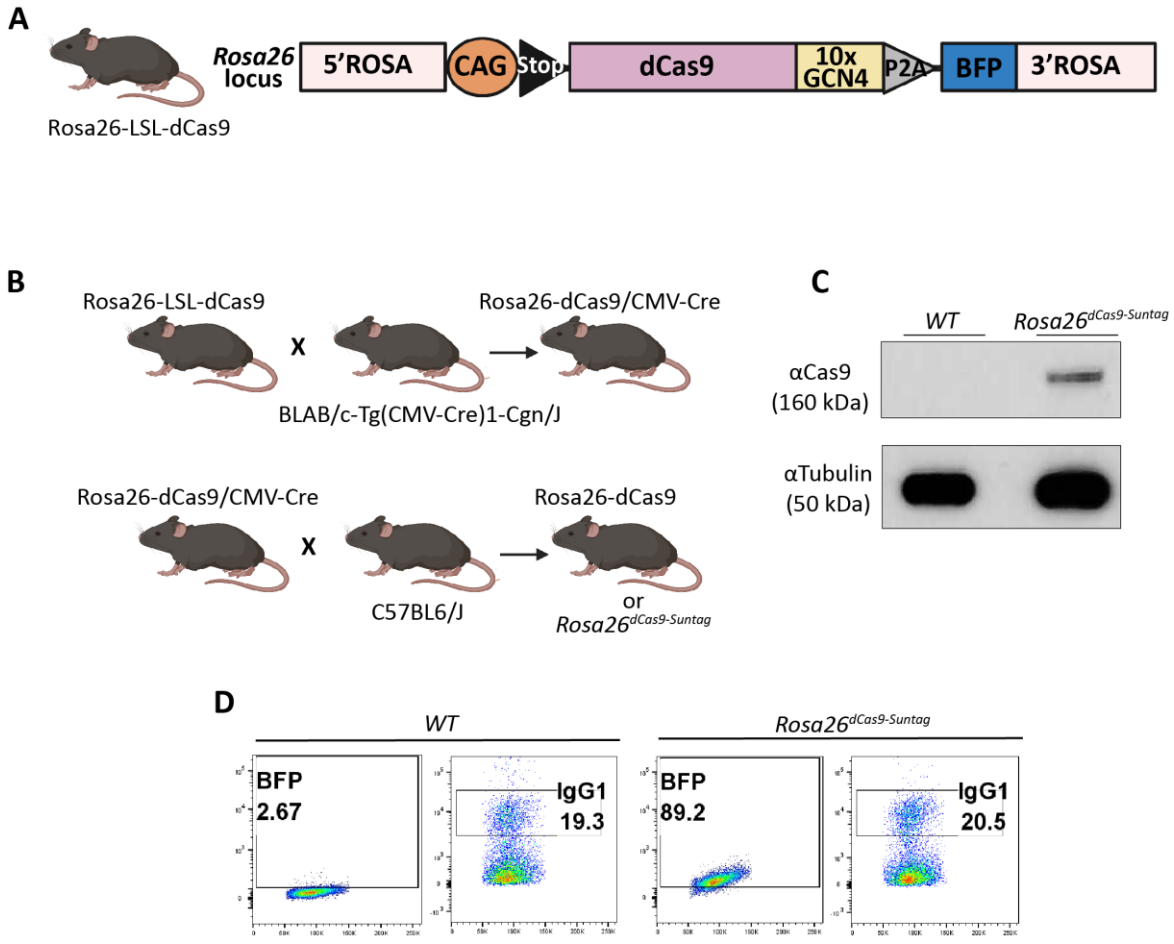

Figure 19. Primary B cells (Splenocytes) as the new model system from dCas9 expressing mice. (A) Schematic representation of the *Rosa26* locus of Rosa26-LSL-dCas9 mice (*Gt(ROSA)26Sor*$^{tm1(CAG\text{-}dCas9\text{-}SunTag)Khk}$) purchased from Jackson's laboratories. (B) Breeding scheme of Rosa26-LSL-dCas9 mice with BALB/c-Tg(CMV-cre)1Cgn/J mice and later C57BL6/J mice to generate Rosa26-dCas9 or *Rosa26*$^{dCas9\text{-}Suntag/+}$. (C) Validation of *Rosa26*$^{dCas9\text{-}Suntag/+}$ mice by Western blot analysis to assess the expression of dCas9 with anti-Cas9 along with loading control Tubulin. (D) Validation of *Rosa26*$^{dCas9\text{-}Suntag/+}$ mice by FACS to assess the expression of BFP and switch to IgG1 after stimulation for 72 h with LPS, IL-4 and RP/14. Gated populations indicate BFP and IgG1 positive populations.

4.1.12. pMSCV-U6sgRNA-PGKscfvmT2AGFP construct bypasses double retroviral transduction complexity.

I generated the retroviral construct pMSCV-U6sgRNA-PGKscfvmT2AGFP, which contains the gRNA cassette, single-chain-variable-fragment ((scfv); for GCN4-peptide) fused to HA-tagged miniTurbo and T2A-GFP reporter, through a multi-step cloning process (Figure 20A). I used several plasmids, 3x HA-miniTurbo-NLS-pCDNA3, phr-scfvGCN4-sfGFP-GB1-NLS-dWPRE and pMX-235 to clone miniTurbo, scfvGCN4 and GFP respectively. I subcloned them in the backbone of pMSCV-U6sgRNA-PGKPuro2ABFP, after removing its Puromycin and BFP sequence, by PCR and restriction digestion. I validated the final plasmid by diagnostic digestion (Figure 20B) and Sanger's sequencing (data not shown).

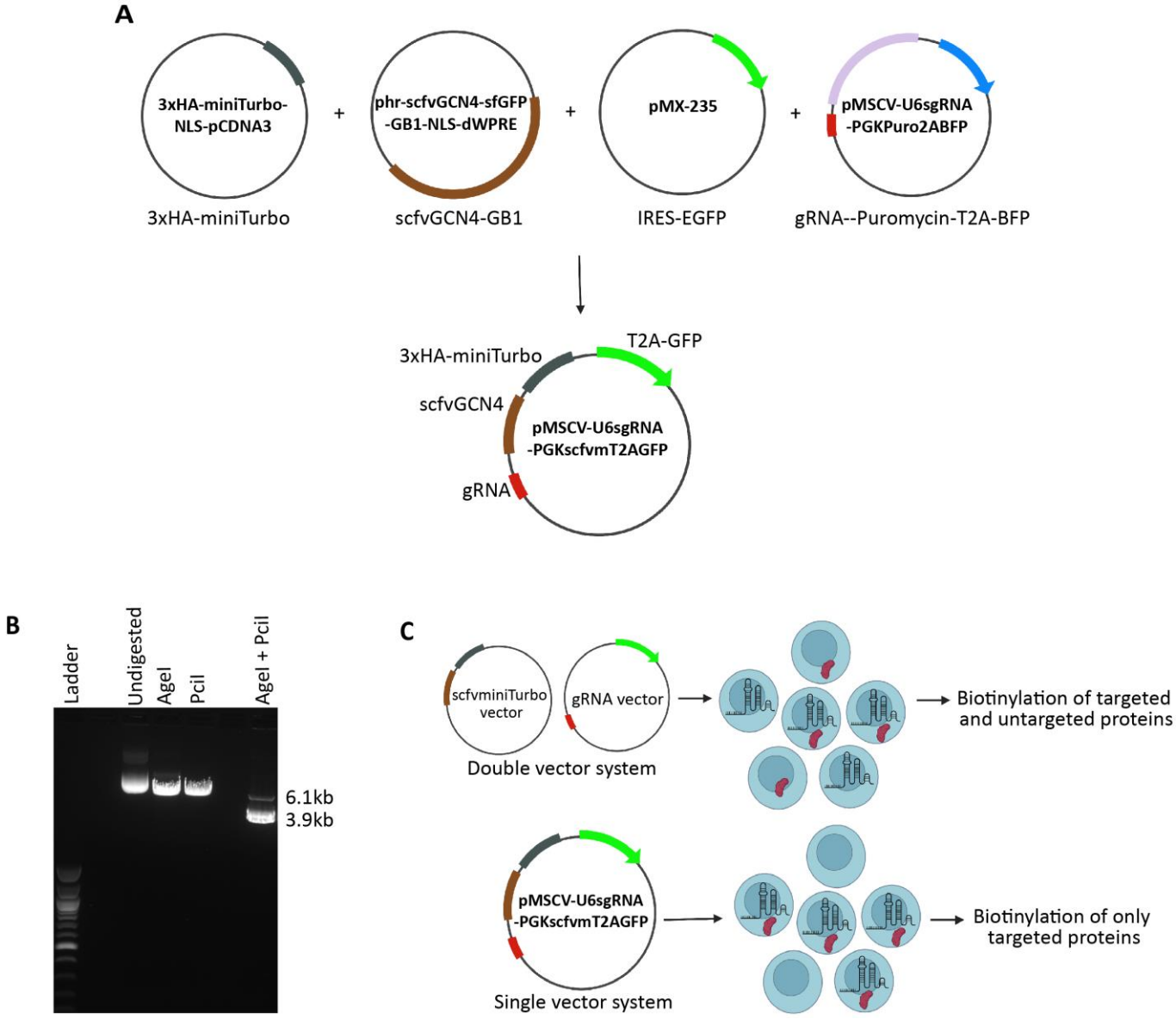

Figure 20. pMSCV-U6sgRNA-PGKscfvmT2AGFP construct bypasses double retroviral transduction complexity. (A) Schematic representation of the constructs used to clone pMSCV-

U6sgRNA-PGKPscfvmT2AGFP plasmid in pMSCV-U6sgRNA-PGKPuro2ABFP backbone through a multi-step cloning process in . (B) Diagnostic digestion of pMSCV-U6sgRNA-PGKPscfvmT2AGFP plasmid with AgeI and PciI. (C) Schematic representation of advantage of single vector system over double vector system.

I had cloned a few more plasmids before to use for transduction in splenocytes and observed through the process that delivering two plasmids, one for scfv-miniTurbo and another for gRNA, might reduce the efficiency of transduction. Moreover, it can also add another level of complexity of FACS sorting the double positive cells since not every cell would receive both the vectors. Therefore, I cloned both scfv-miniTurbo and gRNA into one plasmid i.e. pMSCV-U6sgRNA-PGKscfvmT2AGFP, that could bypass the above difficulties (Figure 20C).

4.1.13. pMSCV-U6sgRNA-PGKscfvmT2AGFP construct encodes a functional miniTurbo fusion protein.

In order to verify the functionality of the genes in the construct, I transfected it in BOSC23 cells. I used the original backbone vector pMSCV-U6sgRNA-PGKPuro2ABFP as a control. I performed FACS analysis and observed that BOSC23 got robustly transfected with pMSCV-U6sgRNA-PGKscfvmT2AGFP and was expressing GFP (Figure 21). Therefore, I proceeded to validate the vector in splenotcytes.

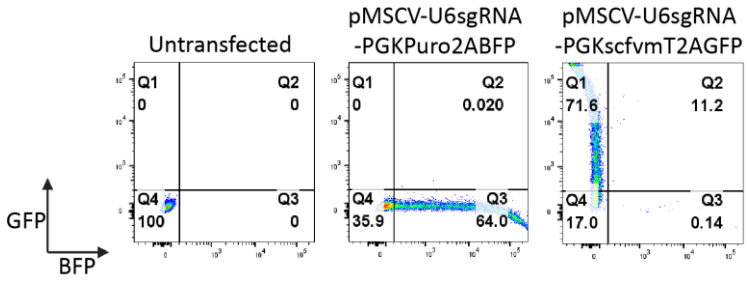

Figure 21. pMSCV-U6sgRNA-PGKscfvmT2AGFP construct encodes a functional miniTurbo fusion protein. FACS plots of transfected BOSC23 with original plasmid pMSCV-U6sgRNA-PGKPuro2ABFP and cloned plasmid pMSCV-U6sgRNA-PGKscfvmT2AGFP.

4.1.14. Validation of new model system *Rosa26*$^{dCas9\text{-}Suntag/+}$ mice for *Igh* locus precipitation.

Rosa26$^{dCas9\text{-}Suntag/+}$ expresses Suntag that consists of a 10 peptide array of GCN4-derived peptide epitopes that bind with high affinity to scfv introduced separately by plasmid pMSCV-U6sgRNA-PGKscfvmT2AGFP. Scfv consists of variable regions of one heavy and light chain connected by a linker for efficient folding[130]. Thereby the dCas9-Suntag and scfv-miniTurbo can form a complex together. The plasmid also expresses sgRNA that will target dCas9-Suntag/scfv- miniTurbo complex at the locus of interest such as Sμ (Figure 22A). To validate the model system, I isolated splenocytes from *Rosa26*$^{dCas9\text{-}Suntag/+}$ and *WT* mice and activated them with specific cytokines that induce CSR to IgG1 isotype[50,93]. I transduced activated splenocytes with pMSCV-U6gSμ-PGKscfvmT2AGFP (also referred to as gSμ from here on) retroviral particles produced by BOSC23.

As a control, I used pMSCV-U6gRandom-PGKscfvmT2AGFP (also referred to as gRandom from here on) that does not target anywhere in the mouse genome. I found that the viral transduction of these newly generated constructs is extremely efficient (Figure 22B). I verified that scfv-miniTurbo is robustly binding to dCas9-Suntag by Streptavidin-mediated immunoprecipation (IP) followed by western blot analysis by anti-Streptavidin (IP), anti-Cas9 (dCas9; co-IP) and anti-HA (miniTurbo; IP) (Figure 22C). Finally, I verified if CSR to IgG1 is affected in the splenocytes. I observed that splenocytes from *Rosa26*$^{dCas9\text{-}Suntag/+}$ infected with gSμ show a minor decrease in CSR compared to gRandom which might be due to the presence of dCas9 at Sμ (Figure 22D), although this analysis doesn't directly confirm if dCas9-Suntag/scfv-miniTurbo complex is being targeted at the Sμ region. Nevertheless, the formation of the complex and biotinylation of proximal proteins, including dCas9 is confirmed by IP validating that with an efficient gRNA, the model system can be used for locus specific pull-down experiments.

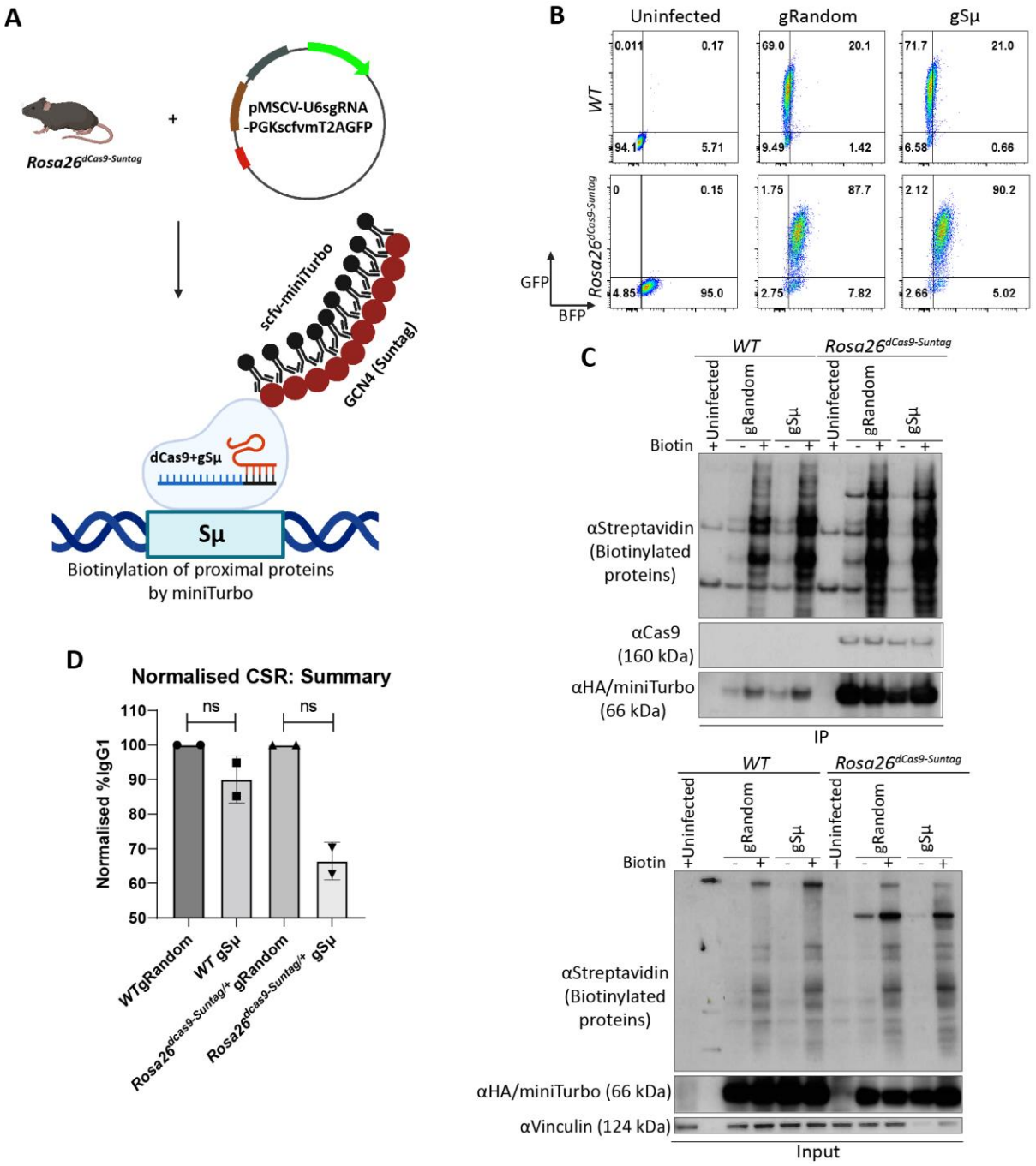

Figure 22. Validation of new model system *Rosa26*$^{dCas9\text{-}Suntag/+}$ mice for *Igh* locus precipitation. (A) Scheme of working principle of pMSCV-U6gSμ-PGKscfvmT2AGFP (or gSμ) plasmid in *Rosa26*$^{dCas9\text{-}Suntag/+}$ mice after its viral transduction. mt: miniTurbo. (B) FACS plot of viral transduction efficiency of gSμ/gRandom plasmids in isolated splenocytes from *WT* mice and *Rosa26*$^{dCas9\text{-}Suntag/+}$ mice. (C) Western blot analysis of immunoprecipitated biotinylated proteins in gSμ/gRandom transduced *WT* and *Rosa26*$^{dCas9\text{-}Suntag/+}$ splenocytes blotted with anti-Streptavidin and co-immunoprecipitated dCas9 and miniTurbo proteins blotted with anti-Cas9 and anti-HA respectively (miniTurbo). (D) Summary graph of CSR to IgG1 in *WT* and *Rosa26*$^{dCas9\text{-}Suntag/+}$ splenocytes transduced with gSμ/gRandom at 68 h post activation with LPS, IL-4 and RP/14.

4.1.15. Pilot mass-spectrometry.

I proceeded to set up a pilot experiment for mass-spectrometry. I isolated splenocytes from three *Rosa26*$^{dCas9\text{-}Suntag/+}$ mice that served as three biological replicates. I transduced them with the viral supernatant of pMSCV-U6sgRNA-PGKscfvmT2AGFP (gSμ/gRandom) generated from BOSC23 cells. The infected splenocytes were treated with or without biotin and collected for Streptavidin-based IP (Figure 23A). The samples for given for mass-spectrometry analysis

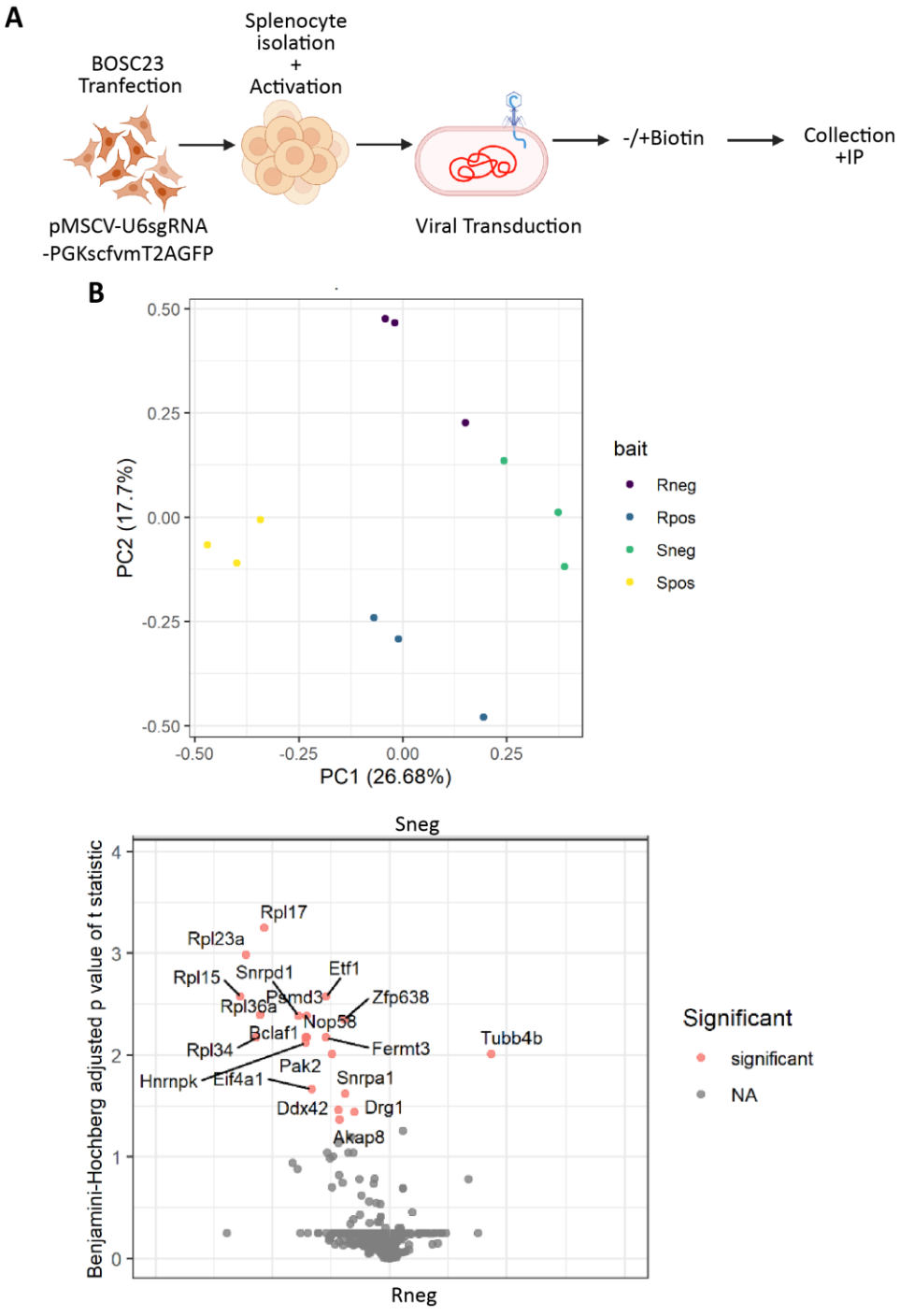

Figure 23. Pilot mass-spectrometry. (A) Schematic representation of transduction of splenocytes with gSμ/gRandom plasmid (B) Top: PCA analysis of mass-spectrometry data. Bottom: Volcano plot of Sneg (Primary B cells transduced with gSμ without exogenous Biotin) versus Rneg data (Primary B cells transduced with gRandom without exogenous Biotin).

to Selbach lab, MDC. PCA analysis show that the biological replicates for each gRandom (-/+Biotin) and gSμ (-/+Biotin) group together. Although, gSμ with biotin treatment (Spos) grouped closer to gRandom with biotin treatment (Rpos) (Figure 23B). Similarly gSμ without biotin treatment (Sneg) grouped closer to gRandom without biotin treatment (Rneg) (Figure 23B). Since cells have endogenous biotin, Sneg versus Rneg could also generate useful information. However, no known CSR proteins were enriched in Spos versus Rpos or Sneg versus Rneg and thus the data from the mass-spectrometry analysis was inconclusive.

4.2. PART II: ANP32B does not modulate 53BP1 during DSB end-protection

4.2.1. Generation of ANP32B overexpressing cells.

ANP32B was identified as a protein associating specifically with 53BP1[28A] mutant (28 Serine-Threonine residues mutated to Alanine) in a SILAC-based mass-spectrometry study[91]. The protein was identified with 5 unique peptides and a PEP value of 1.39×10^{-17}. ANP32B is a pro-proliferation protein that promotes G1/S phase progression[132-133]. However, there is no evidence about a potential involvement and precise role of this protein in DSB repair.

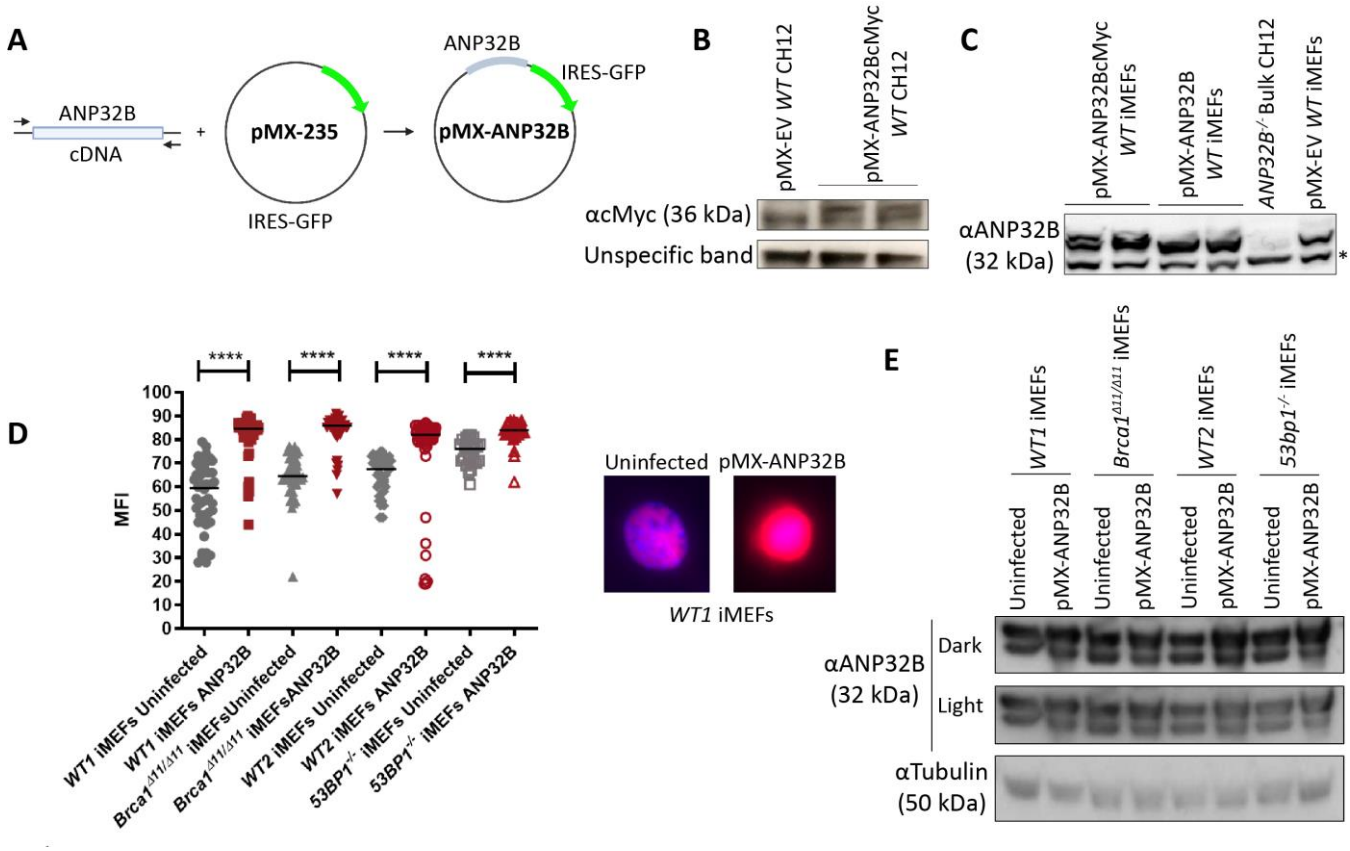

Figure 24. Generation of ANP32B overexpressing cells. (A) Schematic representation of cloning of ANP32B in pMX-235 (or pMX-EV). (B) Western blot analysis of ANP32B (pMX-ANP32BcMyc) overexpression in *WT* CH12 with anti-cMyc. Unspecific bands denote equal loading. (C) Western blot analysis of ANP32B overexpression (pMX-ANP32B and pMX-ANP32BcMyc) in *WT* iMEFs. Bulk *Anp32b*$^{-/-}$ CH12 were included as negative control of ANP32B expression. EV, empty vector. Non-specific band (indicated by asterisk) denotes equal loading. (D) Immunofluorescence analysis of ANP32B overexpression (pMX-ANP32BcMyc) with anti-ANP32B in different genotypes of iMEFs along with representative image of *WT1* iMEFs. Mann-Whitney test was employed for statistical analysis. ****= p value<=0.0001. (E) Western blot analysis ANP32B overexpression assessment in different genotypes of iMEFs with anti-ANP32B. MFI, Mean Fluorescence Intensity.

My hypothesis involved ANP32B as negative regulator of 53BP1 during DSB and to do so I overexpressed the protein in various cell types and performed different kinds of experiments to prove it. I first amplified the gene with and without cMyc-tag from mouse splenocyte cDNA and cloned it into pMX-235 (or pMX-empty vector or pMX-EV) plasmid that contains IRES-GFP and Puromycin for gating and selection purpose respectively (Figure 24A). The final constructs were either pMX-ANP32B or pMX-ANP32BcMyc. I generated CH12 overexpressing ANP32B using the plasmid with the retroviral experimental set-up and verified the expression by western blot (Figure 24B). I also overexpressed ANP32B in *WT* immortalized murine embryonic fibroblasts (iMEFs) where I could select the cells with Puromycin and generated iMEFs stably expressing the protein (Figure 24C). For another set of experiments, I also generated ANP32B overexpressing iMEFs in different genotypes (*WT1, Brca1*$^{\Delta 11/\Delta 11}$*, WT2, 53bp1*$^{-/-}$), which I verified by western blot and immunofluorescence (Figure 24D and E). I proceeded to use all these model systems to test my hypotheses.

4.2.2. ANP32B is dispensable for the regulation of 53BP1 activity during CSR.

I assessed whether ANP32B has a negative impact on 53BP1's interaction with its phospho-dependent partner RIF1 during CSR. To do so, I overexpressed ANP32B in both *WT* CH12 and splenocytes isolated from *WT* mice, and monitored CSR efficiency by gating on GFP that indicates transduction efficiency. I found that ANP32B overexpression did not reduce CSR in both the model system (Figure 25A and B). In parallel, I deleted ANP32B in *WT* CH12 in bulk by CRISPR-Cas9 gene editing and observed that CSR does not increase in the absence of the protein (Figure 25C). Next, I assessed directly whether ANP32B competes with RIF1 for binding to 53BP1. To do so, I determined RIF1 recruitment to sites of DNA DSBs after ANP32B overexpression *via* ionizing radiation foci formation (IRIF). RIF1 IRIF is dependent on 53BP1 phosphorylation by ATM at N-terminal S/TQ sites, and mutagenesis of these residues abrogates RIF1 interaction with 53BP1 and foci formation[93]. I employed iMEFs for foci analysis in place of B cells, as we have already established robust protocols for high-throughput automated foci quantification with this model system in the lab. *WT* iMEFs overexpressing ANP32B did not display decreased RIF1 foci formation following IR-induced DNA damage, which is indicative of unaffected recruitment of RIF1 to DSBs (Figure 25D). Altogether, these data indicate that ANP32B does not have an antagonistic relationship with the 53BP1 phospho-dependent partner RIF1, and it is dispensable for the regulation of 53BP1 activity during CSR.

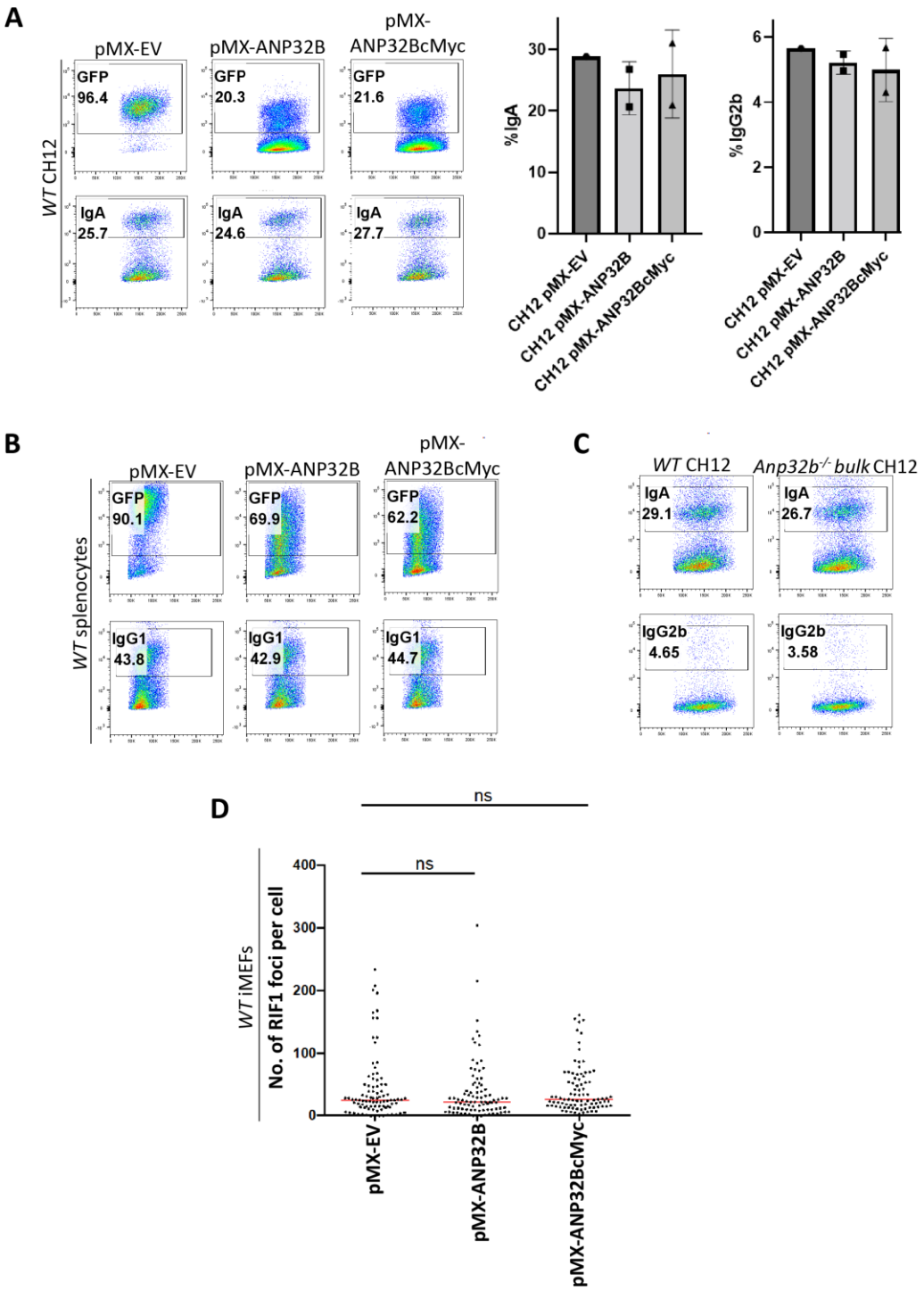

Figure 25. ANP32B is dispensable for the regulation of 53BP1 activity during CSR. (A) Left: Representative FACS plot showing transduction efficiency (%GFP) and CSR (%IgA) in *WT* CH12 infected with empty vector (EV) and ANP32B constructs (either untagged or cMyc-tagged) 48 h after stimulation with TGFβ, IL-4, and anti-CD40. Gated population on top indicates GFP positive population, from which IgA positive population was plotted and gated. Right: Graph summarizing results for ANP32B infections with two independent plasmids with and without tag. (B) Representative FACS plots showing transduction efficiency (%GFP) and CSR (%IgG1) in *WT*

splenocytes infected with either EV or constructs encoding ANP32B and stimulated for 96 h with LPS, IL-4 and RP/14. Gated population on top indicates GFP positive population, from which IgG1 positive population was plotted and gated. (C) Left: Representative FACS plots showing CSR to IgA after somatic targeting of ANP32B in bulk *WT* CH12 (*Anp32b*$^{-/-}$ *bulk*) cells by CRISPR-Cas9. Gated population indicates IgA positive population. (D) Number of RIF1 foci per cell in *WT* iMEFs overexpressing ANP32B. Mann-Whitney test was employed for statistical analysis. ns= non-significant (p value>=0.05).

4.2.3. ANP32B is dispensable for re-wiring of HR in the absence of BRCA1.

Next, I assessed whether the interaction between ANP32B and unphosphorylated 53BP1 might protect cells from PARPi-induced synthetic lethality in the absence of BRCA1, either by inhibiting the interaction of PTIP with S25 or by inhibiting the binding of Mob domain interactors (Figure 5)[99-100]. To test this hypothesis, I overexpressed ANP32B in *WT* and *Brca1*$^{\Delta 11/\Delta 11}$ iMEFs, which express an hypomorph-BRCA1 mutant deficient for HR[85], and measured cell viability with and without PARPi treatment. The concentration of PARPi to use to treat iMEFs was chosen by a kill curve experiment, on the basis of which I used 1µg/ml and 4µg/ml (Figure 26A). I did not find any difference in viability observed between *Brca1*$^{\Delta 11/\Delta 11}$ iMEFs infected with empty vector (EV) and *Brca1*$^{\Delta 11/\Delta 11}$ iMEFs overexpressing ANP32B (Figure 26B). I obtained similar results when performing the same experiment in *Brca1*$^{f/f}$ *Cd19*$^{cre/+}$ and *Cd19*$^{+/+}$ primary B cells (Figure 26C). In parallel I also performed colony formation assay (CFA) with PARPi in two different kinds of *WT* iMEFs (*WT1, WT2*), *Brca1*$^{\Delta 11/\Delta 11}$ iMEFs and also included *53bp1*$^{-/-}$ iMEFs as another negative control similar to *WT* condition. I again observed that *Brca1*$^{\Delta 11/\Delta 11}$ iMEFs transduced with pMX-ANP32B did not gain viability under PARPi treatment (Figure 26D). However, I observed that both the uninfected *WT* iMEFs were sensitive to PARPi in this assay, which could be due to PARPi treatment to very low number of cells seeded. Interestingly the sensitivity was lost in *WT* iMEFs (*WT1, WT2*) upon pMX-ANP32B transduction. Nonetheless, I concluded that ANP32B does not have an antagonistic role with PTIP or Mob domain interacting proteins, and does not modulate 53BP1's ability to promote genome instability and cell death in the absence of BRCA1.

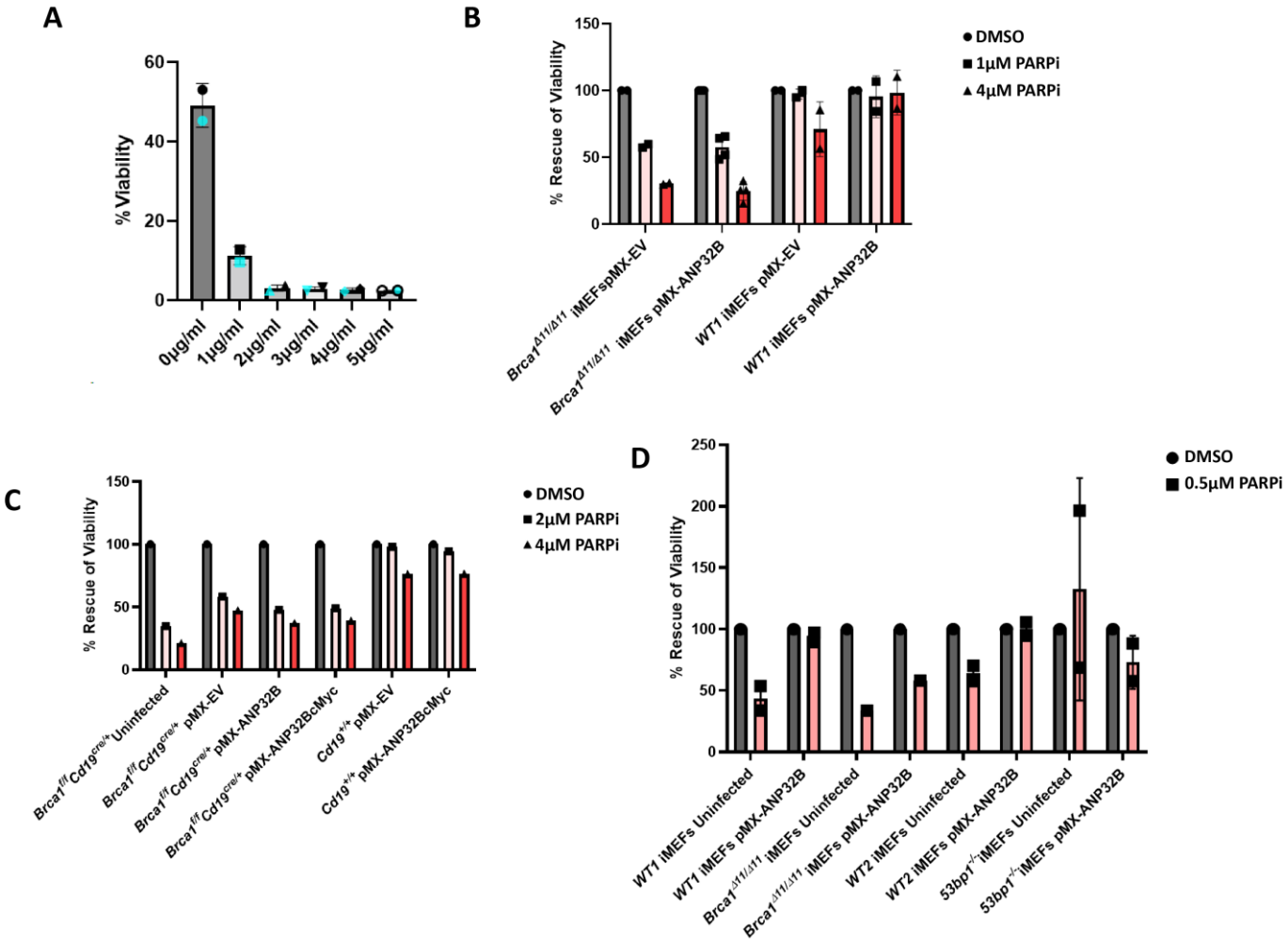

Figure 26. ANP32B is dispensable for re-wiring of HR in the absence of BRCA1. (A) Kill curve assay in either *WT* (black) or *53bp1-/-* (blue) iMEFs (B) Summary graph of two independent rescue of viability assays in *Brca1*$^{\Delta 11/\Delta 11}$ and *WT* iMEFs overexpressing ANP32B and treated for 5 days with 1µM and 4µM of PARPi using FACS. All samples were normalized to our vehicle control DMSO. (C) Graphical representation rescue of viability assay in *Brca1*$^{f/f}$ *Cd19*$^{cre/+}$ and *Cd19*$^{+/+}$ primary B cells overexpressing ANP32B and treated for 36h with 2µM and 4µM of PARPi using FACS. All samples were normalized to our vehicle control DMSO. (D) Summary graph of two independent rescue of viability experiments with 0.5µM PARPi using colony formation assay, in two different *WT* iMEFs (*WT1, WT2*), *Brca1*$^{\Delta 11/\Delta 11}$ iMEFs and *53bp1*$^{-/-}$ iMEFs, overexpressing ANP32B, on day 10. All samples were normalized to our vehicle control DMSO.

4.3. PART III: Dissection of RIF1 post-translational regulation during DSB end protection

4.3.1. Identification of serine phospho-sites in mouse RIF1 post IR.

I first defined the cell type-based model system to use by assessing the level of RIF1 protein expression in CH12, activated splenocytes and iMEFs. To do so, I carried out western blot analysis for RIF1 (and Flag-tag for Rif1$^{FH/FH}$ mice), and observed that both CH12 and splenocytes express considerably more RIF1 than iMEFs (Figure 27A). Optimization of IP proved that HA-based pull-down is more efficient than Flag since there was lesser amount of residual RIF1 remaining in the supernatant after removal of the precipitated protein (Figure 27B). Thus, I proceeded to work with splenocytes from Rif1$^{FH/FH}$ mice (RIF1 tagged with Flag and 2xHA) for immunoprecipitating RIF1 using HA tag.

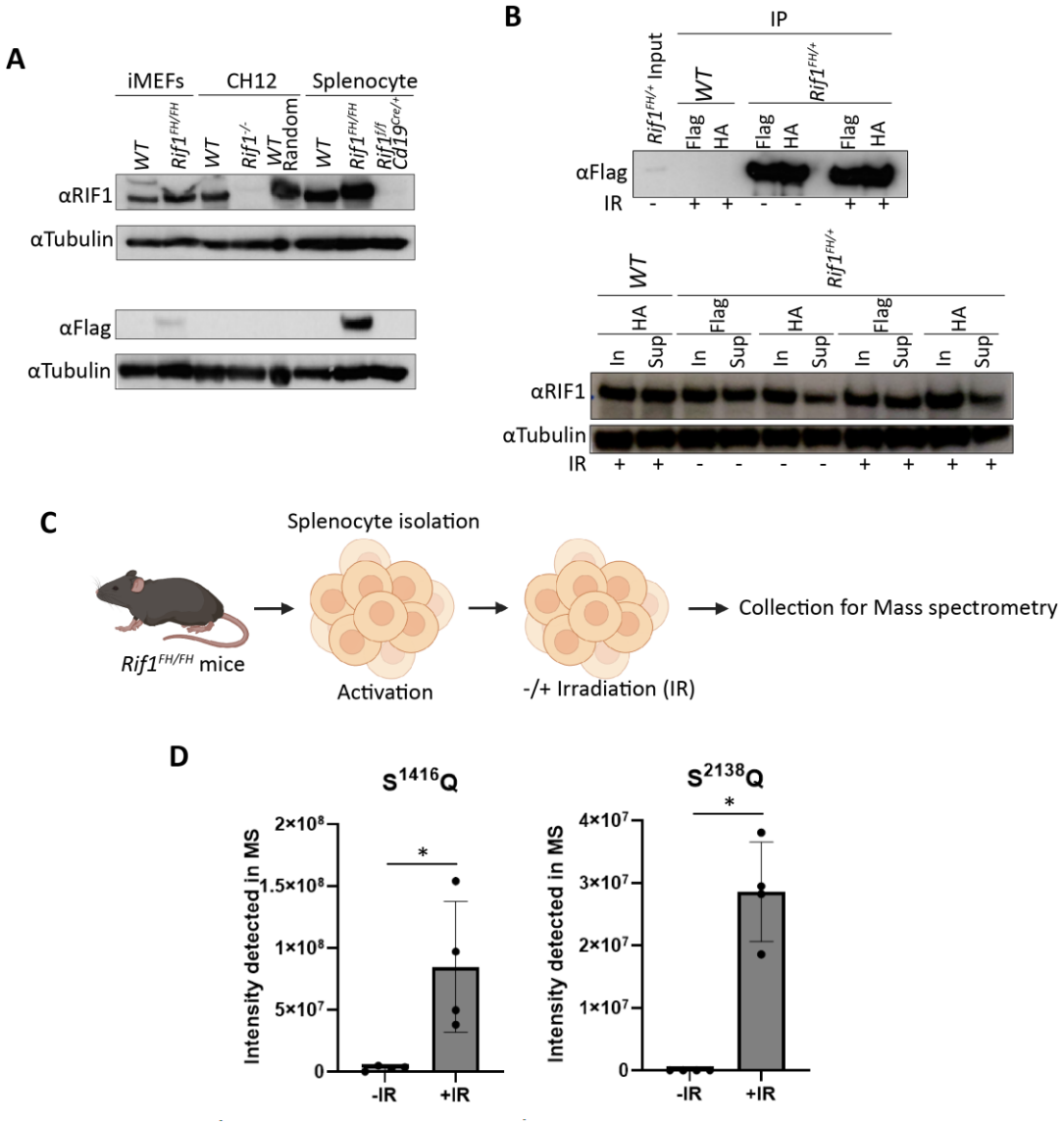

Figure 27. Identification of serine phospho-sites in mouse RIF1 post IR. (A) Western blot analysis with αRIF1 and αFlag in *WT* iMEFs, *Rif1*$^{FH/FH}$ iMEFs, *WT* CH12, *Rif1*$^{-/-}$ CH12 clone, CH12 clone electroporated with a gRandom (*WT* Random), *WT* splenocytes, *Rif1*$^{FH/FH}$ splenocytes and *Rif1*$^{f/f}$ *CD19*$^{Cre/+}$ splenocytes. (B) Optimisation of pull-down with anti-HA and anti-Flag and western blot using IP, Input (In) and Supernatant (Sup) samples. (C) Schematic representation of experimental set-up of the MS for identification of phosphosites and analysis of the identified phosphosites. (D) Graphical representation of phospho-sites RIF1 S^{1416}Q and S^{2138}Q identified post IR by MS in four biological replicates. Mann-Whitney test was employed for statistical analysis. *= p value<=0.05. In, Input. Sup, Supernatant.

In collaboration with Mertins lab, MDC, we employed label- free mass-spectrometry strategy (LC-MS/MS: liquid chromatography-tandem mass-spectrometry) to detect the presence of different PTMs like phosphorylation, acetylation and sumoylation (Figure 27C)[134-135]. Analysis revealed phosphorylation to be the predominant PTM in the protein under IR condition, with the majority of phospho-residues being serines. Among all motifs, S^{1416}Q and S^{2138}Q were the only conserved SQ sites (consensus of ATM/ATR) that were found to be reproducibly phosphorylated in all the four biological replicates (Figure 27D). S^{1416}Q was also identified as part of a cluster (S^{1387}Q, S^{1416}Q, and S^{1528}Q) in another independent mass-spectrometry analysis in our lab. This cluster has recently been established in our lab to be dispensable for end-protection, but instead regulates replication fork protection during replication stress[85]. Therefore, I proceeded to test only S^{2138}Q, if it regulates RIF1-mediated DSB end-protection function.

4.3.2. Generation of S^{2138}Q CH12 cell lines.

RIF1 is a large protein made of almost 2426 amino acids in mammalian cells (Figure 4A). As described earlier, RIF1 has highly conserved N-terminus HEAT repeats domain followed by the poorly conserved IDR. The CTD is divided into 3 regions (I, II, III), each bearing different functions, from which CTD-I contains the SILK-RVxF motif. The sequence location of SILK-RVxF in yeast is within N-terminus, but shifted to the C-terminal end in higher eukaryotes during evolution[85,115] (Figure 28A).

To asses end-protection function of S^{2138}Q I chose toxic-NHEJ repair and CSR as the functional read outs and thereby I used BRCA1 mutant CH12 cells (*Brca1*$^{mut/mut}$) that have the exon 11 deleted making them deficient for HR repair but proficient in CSR[85]. I employed CRISPR/Cas9 knock-in at exon 30 of RIF1 to generate *Brca1*$^{mut/mut}$ *Rif1*^{S2138A} (serine to alanine; phospho-mutant) and *Brca1*$^{mut/mut}$ *Rif1*^{S2138D} (serine to aspartic acid; phospho-mimic) (Figure 28B). Since aspartic acid is a negatively charged amino acid that resembles the negative

charge of serine post-phosphorylation, the mutation is assumed to mimic phosphorylation condition[85]. However, other protein changes like conformational modification might not be recapitulated with this mutation.

For CRISPR/Cas9 knock-in for CH12 clonal generation, I electroporated homologous directed repair (HDR) donor plasmid containing the mutations, restriction sites for clone verification and the homology arms (cloned into a TOPO vector) along with a Cas9-gRNA plasmid with GFP reporter gene (px458) and single cell sorted the GFP positive cells (Figure 28C). As controls I generated clones that were electroporated with gRandom that doesn't target anywhere in the mouse genome. I characterized the clones by Sanger's sequencing and western blot analysis (Figure 28D and E). Based on the results I chose two *Brca1*$^{mut/mut}$ random clones, four *Brca1*$^{mut/mut}$ *Rif1*^{S2138A} clones and three *Brca1*$^{mut/mut}$ *Rif1*^{S2138D} clones (Figure 28E).

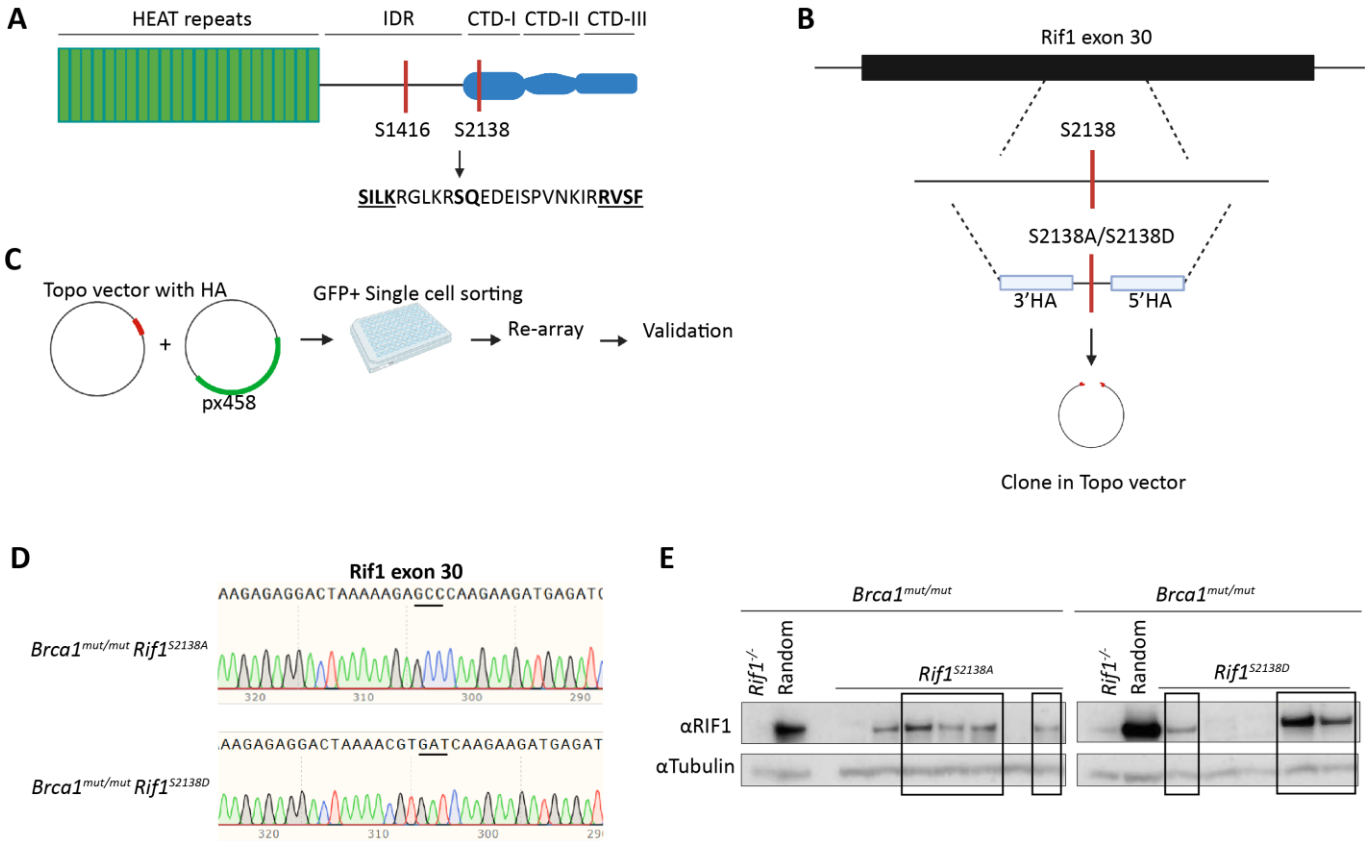

Figure 28. Generation of S^{2138}Q CH12 cell line. (A) Scheme of RIF1 protein structure and positions of serine 1416 and 2138. (B) Schematic representation of CRIPR/Cas9 knock-in to generate serine to alanine (phospho-mutant) and serine to aspartic acid (phospho-mimic) in *Brca1*$^{mut/mut}$ CH12. (C) Schematic representation of experimental set up to generate and validate the knock-in in *Brca1*$^{mut/mut}$ CH12. (D) Representative image of sequence analysis of one clone of each *Brca1*$^{mut/mut}$ *Rif1*^{S2138A} and *Brca1*$^{mut/mut}$ *Rif1*^{S2138D}. (E) Western blot analysis of the CRISPR/Cas9 knock-in clones for RIF1 protein with anti-RIF1

and tubulin was the loading control. The clones selected/marked in the western blot are the ones with which experiments were further conducted.

4.3.3. S^{2138}Q is dispensable for end-protection during NHEJ repair.

WT and *Brca1*$^{mut/mut}$ CH12 cells can switch to IgA and IgG2b isotypes under the same activation condition. I observed that *Brca1*$^{mut/mut}$ *Rif1*^{S2138A} and *Brca1*$^{mut/mut}$ *Rif1*^{S2138D} are proficient for CSR to both the isotypes (Figure 29A). I also observed that just like the *Brca1*$^{mut/mut}$ random clones and parental *Brca1*$^{mut/mut}$, *Brca1*$^{mut/mut}$ *Rif1*^{S2138A} and *Brca1*$^{mut/mut}$ *Rif1*^{S2138D} undergo toxic-NHEJ repair rendering them to have no rescue of viability upon PARPi treatment (Figure 29B). *Brca1*$^{mut/mut}$ *Rif1*$^{-/-}$ was our positive control for these experiments. Therefore, I concluded that S^{2138}Q is dispensable for end-protection function.

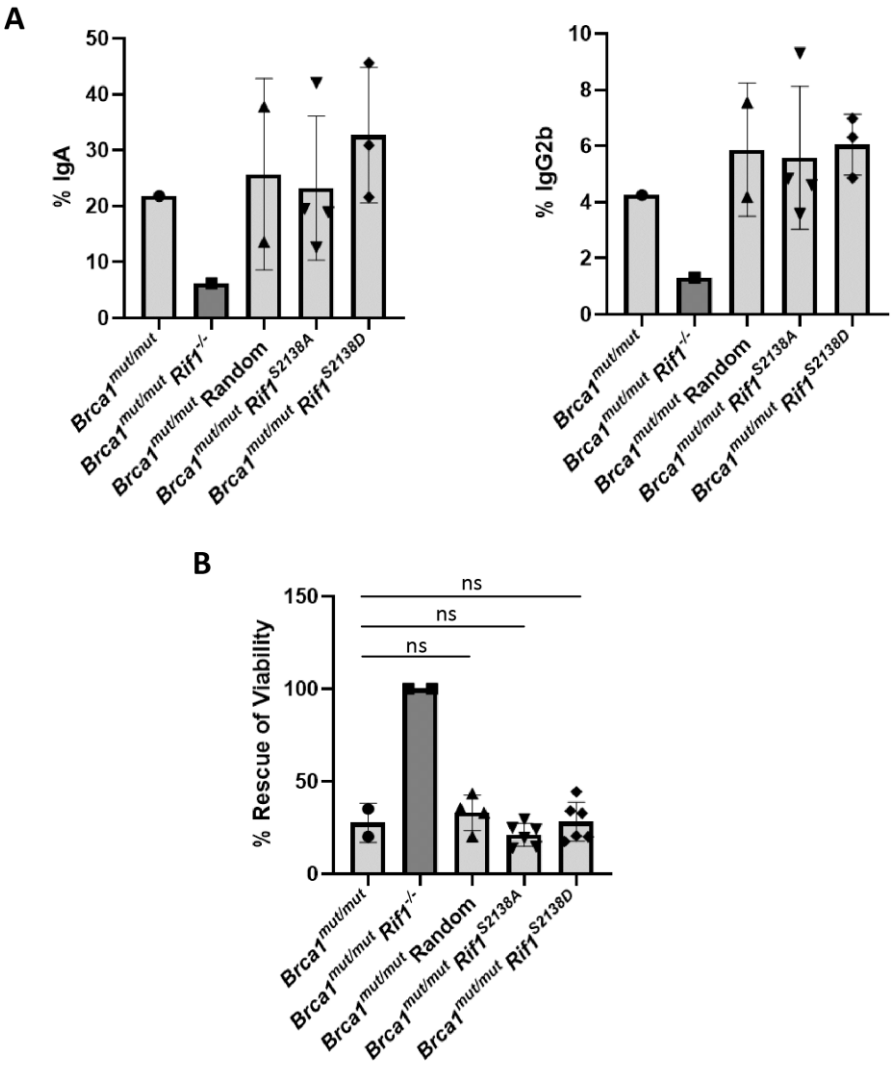

Figure 29. S^{2138}Q is dispensable for end-protection during NHEJ repair. (A) Graph of CSR to IgA and IgG2b in *Brca1*$^{mut/mut}$ *Rif1*^{S2138A} and *Brca1*$^{mut/mut}$ *Rif1*^{S2138D} clones. (B) Summary graph of two

independent rescue of viability experiments in *Brca1*$^{mut/mut}$ *Rif1*^{S2138A} and *Brca1*$^{mut/mut}$ *Rif1*^{S2138D} clones. Mann-Whitney test was employed for statistical analysis. ns= non-significant (p value>=0.05).

4.3.4. Clones with truncated RIF1 protein show separation of function in end-protection.

During the process of validation of the *Brca1*$^{mut/mut}$ *Rif1*^{S2138A} and *Brca1*$^{mut/mut}$ *Rif1*^{S2138D} clones, I came across two clones (named as *Brca1*$^{mut/mut}$ A1 and *Brca1*$^{mut/mut}$ B3) that underwent erroneous HDR during knock-in resulting in frame-shift mutation and generation of premature termination codon thereby deleting the entire RIF1 C-terminal region (Figure 30A and B).

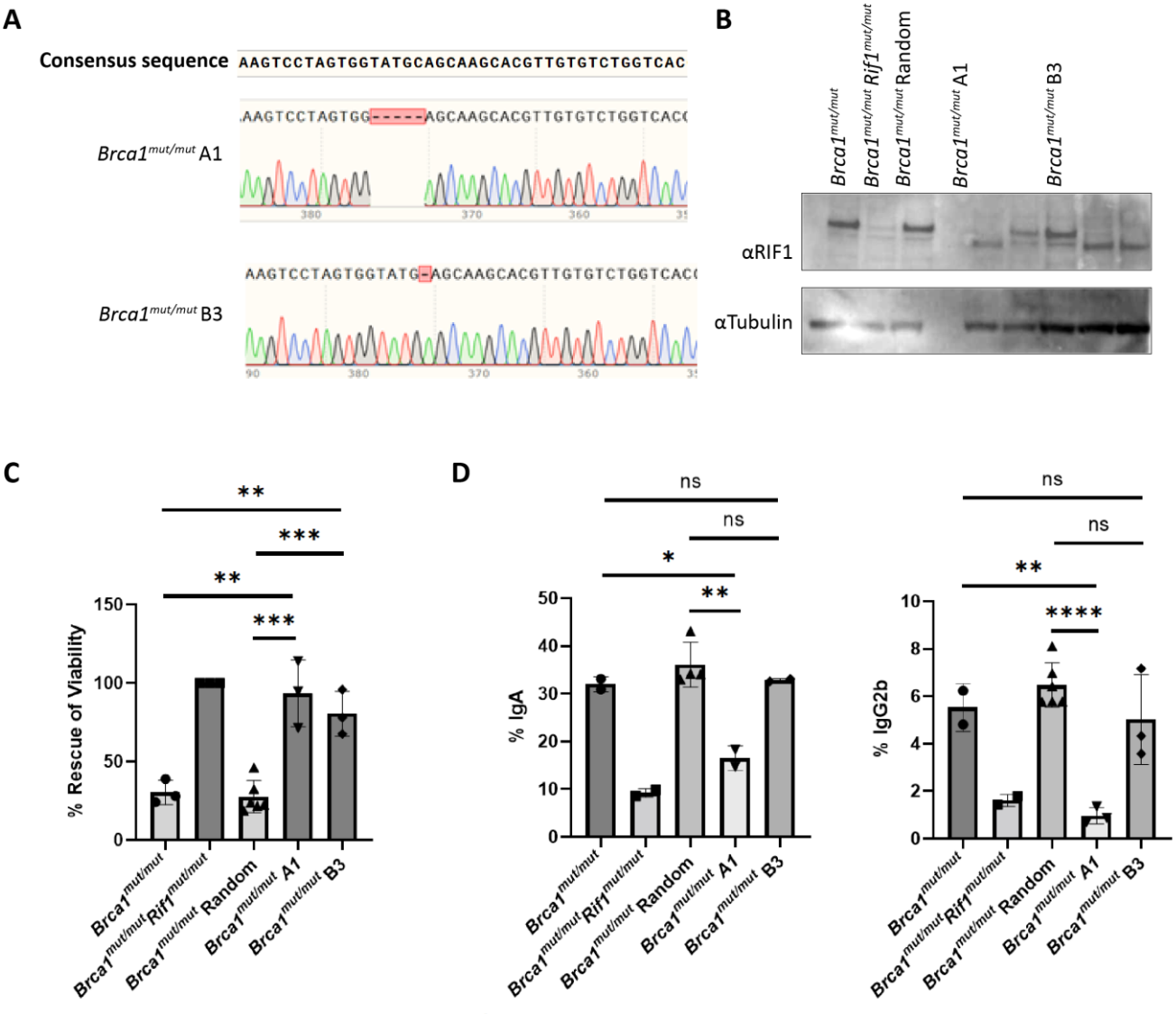

Figure 30. Clones with truncated RIF1 protein show separation of function in end-protection. (A) Sequence of two clones (A1 and B3) with truncated RIF1 protein. (B) Western blot analysis of RIF protein in A1 and B3 clones. (C) Summary graph of three independent rescue of viability experiments in the clones. Student t test statistical analysis has been implemented. (D) Summary graph of CSR to IgA (two independent experiments) and IgG2b (three independent experiments) in the clones. Student

t test statistical analysis has been implemented. ns= non-significant (p value>=0.05). ****= p value<=0.0001. ***= p value<=0.001. **= p value<=0.01. *= p value<=0.05.

As a control I used a *Brca1*$^{mut/mut}$ *Rif1*$^{mut/mut}$ clone that has in-frame deletion in both the alleles at the HEAT repeats of RIF1 due to which damage-induced foci formation is abrogated making it defective for end-protection function[113]. Both *Brca1*$^{mut/mut}$ A1 and *Brca1*$^{mut/mut}$ B3 clones display partial rescue of viability upon PARPi treatment when compared to *Brca1*$^{mut/mut}$ *Rif1*$^{mut/mut}$, confirming HR re-wiring (Figure 30C). However, the clone *Brca1*$^{mut/mut}$ B3 can switch at almost *WT* levels to IgA and IgG2b (Figure 30D).

4.3.5. Trace amount of RIF1 promotes robust end-protection during CSR and replication associated DSBs caused by PARPi.

Mutation of three dileucine motifs to alanine in 53BP1 (53BP1^{3LA}) is deficient in RIF1 recruitment but is proficient in recruiting the further downstream end-protection factor Sheildin[110]. This mutation also does not affect CSR. It was suggested that this phenotype could be due trace amount of RIF1 still being recruited at the damage, although in *Setiaputra et. al., Molecular Cell, 2022*, results were more inclined towards the other hypothesis that 53BP1 can regulate Shieldin function independently of RIF1. Since in spite of having similar frame-shift mutation the clones display different phenotype, I did not exclude the possibility that in the clone B3 somehow the PCR primers were unable to bind to the second allele that could be still expressing trace levels of *WT* RIF1. I hypothesised that in clone B3 this trace amount of RIF1 was promoting CSR which is a single locus event, but failed to promote end-protection during genome wide replication associated DSBs caused by PARPi.

Our former PhD student had generated CH12 clones that has NLS-3xHA knocked-in upstream of RIF1 N-terminus. The *NLS-3xHA-Rif1* clones express considerably low amount of RIF1 compared to WT and *Brca1*$^{mut/mut}$ (Figure 31A). The clones can switch robustly, which confirmed that trace amount of RIF1 can promote robust CSR (Figure 31B).

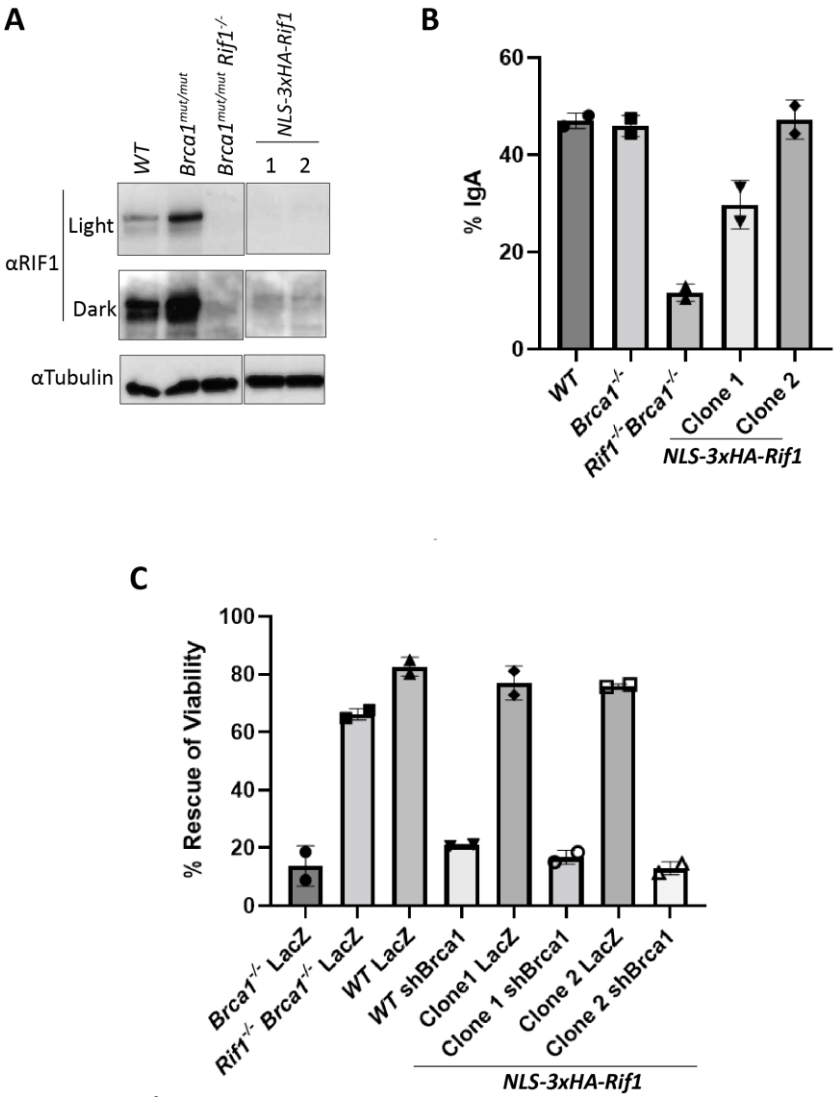

Figure 31. Trace amount of RIF1 can promote robust end-protection during CSR and replication associated DSBs caused by PARPi. (A) Western blot analysis of RIF1 in two *NLS-3xHA-Rif1* knock-in clones. (B) Summary graph of two independent experiments of CSR to IgA of the *NLS-3xHA-Rif1* knock-in clones. (C) Summary graph of two independent infections followed by rescue of viability assays in *NLS-3xHA-Rif1* knock-in clones.

I used these clones to test my hypothesis. I virally transduced them with shBrca1, selected them with puromycin and then treated them with PARPi to observe rescue of viability. The clones display *Brca1*$^{mut/mut}$ type phenotype and not *Brca1*$^{mut/mut}$ *Rif1*$^{-/-}$ upon PARPi treatment, thereby dismissing my hypothesis (Figure 31C). I used *WT* parental CH12 as a control to confirm the efficiency of the shBrca1. I concluded that trace amount of RIF1 is sufficient to promote end-protection at genome wide DSBs.

5. DISCUSSION

PART I

Rosa26$^{dCas9\text{-}Suntag/+}$ mice was originally generated for CRISPRa or CRISPRi[130]. I expanded the application of the mice to study DNA-Protein-RNA interactions by coupling its CRISPR/Cas9 system with proximity labelling, a system that has not been established for B cells yet. Since *Rosa26*$^{dCas9\text{-}Suntag/+}$ expresses dCas9 in every somatic cell, the approach can be implemented for isolating any genomic locus in order to discover local chromatin factors that regulate gene expression or DNA-associated reactions. I specifically developed this approach for purifying *Igh* locus proteins and RNAs that support the repair of programmed DSBs during isotype switching. However, *Rosa26*$^{dCas9\text{-}Suntag/+}$ mice also enables us to break-down every step of CSR that will subsequently determine how it is temporally controlled over the course of the entire process. By implementing genotypes like *Aicda*$^{-/-}$ (knock-out of AID protein), *53bp1*$^{-/-}$, etc, that are mice deficient of key determinants functioning at different phases of CSR, we will establish novel interacting partners or regulators. Activation of *Aicda*$^{-/-}$ *Rosa26*$^{dCas9\text{-}Suntag/+}$ primary B cells will only induce proliferation and initiate GLT and thereby will reveal novel pre-break regulators at S regions[125]. *53bp1*$^{-/-}$ *Rosa26*$^{dCas9\text{-}Suntag/+}$ splenocytes will have GLT and AID-induced DSBs, but will not be able to switch due to lack of end-protection promoted by 53BP1-RIF1-Sheildin-CST axis and other repair independent functions of 53BP1[91-98]. These mice will provide information about additional proteins involved in repair of CSR DSBs that the 53BP1-RIF1-Sheildin-CST axis might be interacting with. Besides, we can also gain more information about A-EJ proteins and its interplay with NHEJ to inhibit extensive resection at break sites and thereby unproductive CSR[54]. Therefore, the model system can be extended to explore various other dynamic elements of CSR reaction.

5.1. CH12 as a model system for *Igh* locus precipitation

CH12 is a very advantageous model system to study CSR in B cells. Under specific stimulus conditions, the cells can switch from IgM to IgA[84-85,93]. CH12 is the only *in vitro* B cell culture that is known to undergo CSR. The cell line makes it even more useful and interesting to study the *Igh* locus since our lab has also generated modified CH12 clones like *Aicda*$^{-/-}$, *53bp1*$^{-/-}$ etc. AID deaminates S regions that are processed into DSBs and 53BP1 imparts the repair component of the DSBs. Thus, these proteins promote very important but distinct functions during CSR reaction. Additionally, *AIDER* CH12 is a great tool to synchronize formation of CSR breaks and effectively study pre-break and post-break dynamics at the locus during CSR. Despite all these benefits, my work showed that CH12 could not serve as the model system for this project with the major drawback being expression of dCas9 in the generated cell lines.

5.1.1. CH12 and Cas9

One of the biggest challenges of the project was to generate dCas9 expressing B cells either retrovirally or by CRISPR/Cas9 knock-in. Previously in our lab, fellow colleagues attempted to generate Cas9-expressing stable CH12 cells, but the cells were not surviving after transduction. However, nucleofection of Cas9 constructs (like electroporation of px458) that allow for transient expression of the protein doesn't kill the cells. B cells are not capable of getting stably transfected and thus, retroviral or lentiviral mode of gene transfer became the primary method for stable gene expression. Lentiviral particles have a packaging limit of 10kb. Insert from 5' LTR to 3' LTR can be up to maximum 10kb for an efficient ransduction[136]. LTR or long terminal repeats are sequences that support the integration of the cDNA of the gene of interest into the host genome. LTR flank both 5' and 3' ends of the gene to be inserted in the plasmid[136]. dCas9 with T2A Blasticidine and 2x HA tags in 2xHA dCas9-BLAST make up to 4.8 kb in size. In theory, the insert is within the packaging limit, but nonetheless, CH12 cells failed to express dCas9. It seemed that Blasticidine was being expressed, since after the viral transduction of the plasmid and followed by Blasticidine selection, the cells were viable (data not shown). Blasticidine is preceded by T2A , a sequence that cleaves the two proteins it connects during translation (dCas9 and Blasticidine in this case). If there is a frame shift mutation then the T2A or even the Blasticindine sequence will be hindered and therefore not get expressed. It is possible that the dCas9 sequence mutated under unknown reasons causing in-frame deletions that lead to the failure of its expression without effecting the expression of T2A-Blasticidine, even though the plasmid transduced was thoroughly verified by diagnostic digestion and Sanger's sequencing. Therefore, I changed my approach of transgene expression in CH12. I selected CRISPR/Cas9 knock in method coupled with proximity labeling using miniTurbo from TurboID system[121-122]. I generated a plasmid with the insert dCas9, miniTurbo, T2A-GFP and Puromycin that was be knocked-in into the *Rosa26* locus. In this case, dCas9-miniTurbo fusion proteins along with T2A-GFP are under the TRE3G promoter, and Puromycin under the rTtA promoter also known as the Tet-on system[127]. Three clonal derivates of CH12 were chosen for the knock-in, *WT*, *AIDER* and *Zmynd8*$^{-/-}$. The genotyping proved that the insert is successfully integrated at the *Rosa26* locus, albeit the sequencing of the entire construct inside the cells was not performed. Instead I verified the protein expression, which showed the expression of GFP only under doxycycline treatment. This suggests that the Tet-on system and T2A-GFP is functional in all the tested clones (5 clones of each CH12 clonal derivatives), albeit I could not see the expression of dCas9 and miniTurbo in any of them. It is quite unlikely that again an in-frame mutation occurred in all the 15 clones, even though I cannot completely dismiss this possibility. This possibility can be ruled out by sequencing the clones for dCas9 and miniTurbo. Furthermore,

in dCas9 western blots, I observed that the knocked-in CH12 clones had smaller bands that were absent in parental CH12 cells (Figure 16A). Hence, it is also likely that splicing sites were generated that lead to expression of smaller spliced and non-functional protein products.

5.1.2. CH12 vs Splenocytes for *Igh* locus precipitation

With the inability to produce Cas9/dCas9-expressing CH12 cells, I considered *Igh* locus pull-down in primary B cells from mice that express dCas9. However, CH12 still provides some major advantages over primary B cells due to which it was my initial choice of model system in the project. Apart from being highly proliferative and possessing the ability to class switch, *WT* CH12 cells provide the opportunity for using its unstimulated state as a negative control for mass-spectrometry of the *Igh* locus. After isolation, primary B cells need to be activated not only for CSR but also for culturing purpose. The unstimulated state or naïve B cells might not be an efficient negative control because they are all at G0 cell cycle stage unlike stimulated cells, which are highly proliferative and a large proportion of the population in culture are in S/G2 phase[91]. Thereby CSR is not the only physiological difference between naïve and activated splenocytes.

Originally I had planned to implement *AIDER* CH12 for *Igh* locus purification, which can be stimulated to initiate GLT without AID targeting at S regions for DSB induction. Only upon treatment with 4-HT, AIDER translocates into the nucleus to induce the breaks in a synchronized manner. AID-mediated breaks are the only physiological difference between the two conditions and therefore, these cell lines represented a great model system for determining both pre- and post- break events at *Igh* locus. In primary B cells of *Rosa26*$^{dCas9\text{-}Suntag/+}$, pre-break role of CSR proteins cannot be investigated. For developing the same conditions as *AIDER* CH12 for the primary B cells, we considered to cross *AIDER* mice with *Rosa26*$^{dCas9\text{-}Suntag/+}$. We enquired with several labs, but none of them still maintained a live colony in their mouse facility. Purchasing the *AIDER* mice sperm for rederivation, and then breeding with *Rosa26*$^{dCas9\text{-}Suntag/+}$ would have taken several months. Alternatively, I crossed *Rosa26*$^{dCas9\text{-}Suntag/+}$ with *Aicda*$^{-/-}$ mice to generate *Rosa26*$^{dCas9\text{-}Suntag/+}$ *Aicda*$^{-/-}$, which if employed against *Rosa26*$^{dCas9\text{-}Suntag/+}$ will also decipher S region pre-break elements. I have also generated *53bp1*$^{-/-}$ *Rosa26*$^{dCas9\text{-}Suntag/+}$ parallely. I will implement these mice in my upcoming mass-spectrometry experiments that will allow me to dissect CSR and uncover novel factors.

5.1.3 Alternative approaches to use CH12 for *Igh* locus precipitation

Nuclease dead Cas9 (dCas9) from *Streptococcus Pyogenes* was not possible to express stably in CH12 cells. Even though the dCas9 insert in the lentiviral construct was within the packaging limit, it still is a large foreign protein to express. To this end, a smaller Cas protein CasΦ, a 70kDa Cas protein from huge bacteriophages might be useful due to its compact size[137]. Additionally, methods that don't rely on CRISPR could also serve as an alternative. One such technique is PiCh (proteomics of isolated chromatin segments) that uses probes tagged with desthiobiotin to target and precipitate a gene of interest. This strategy is the reverse of ChIP, whereby we can retrieve information about proteins interacting with the target chromatin[138].

5.1.4 Endogenous biotinylation in CH12

While characterizing CH12 cells for miniTurbo expression and function, I observed that the cells exhibit atleast three heavily biotinylated proteins (Figure 15A). Assuming that, by coupling any of the alternate methods mentioned above (Section 5.1.3) with proximity labeling, the *Igh* locus is successfully pulled-down in CH12, the possibility of precipitating a large quantity of the internal biotinylated proteins must be taken into consideration. Massive endogenous biotinylation might skew mass-spectrometry peptide detection if the amount of proteins biotinylated by exogenous biotin at a single locus is very low. This possibility yet again renders CH12 in disadvantage compared to primary B cells. Though there is also some endogenous biotinylation in primary B cells, but significantly lower than CH12.

5.2. Mass-spectrometry of *Igh* locus proteins in *Rosa26*$^{dCas9\text{-}Suntag/+}$ splenocytes: Outlook

The pilot mass-spectrometry analysis did not reveal any known CSR proteins, including key DSB repair factors. It is highly possible that biotinylation and/or IP conditions need to be enhanced. To test the best biotinylation condition, a kinetics of the reaction could be set up in *Rosa26*$^{dCas9\text{-}Suntag/+}$ primary B cells transduced with pMSCV-U6sgRNA-PGKscfvmT2AGFP with different concentrations of exogenous biotin treatment. Furthermore, retroviral transduction of the plasmid generates several copy number of the proteins that might exceed the ratio of dCas9-Suntag expressed in *Rosa26*$^{dCas9\text{-}Suntag/+}$ primary B cells. Excess scfv-miniTurbo that doesn't form complex with dCas9-Suntag, might be dispersed all over inside the cells biotinylating any protein that comes to its proximity. Thus, it could be advantageous to increase the amount of dCas9 in the cells by implementing homozygous *Rosa26*$^{dCas9\text{-}Suntag/dCas9\text{-}Suntag}$ splenocytes that will express dCas9 from both the alleles instead of one.

Moreover, the proteins involved in CSR are mostly bound to the chromatin (53BP1, RIF1 etc)[139]. Biotinylated cytoplasmic or nuclear proteins might have hindered in the detection of small amount of Sμ bound repair proteins, due to which I can also implement chromatin fractionation to eliminate the background biotinylated proteins and enrich only the ones that are chromatin bound. These enriched chromatin bound proteins when analysed by mass-spectrometry will increase the chance of identifying *bona fide* Sμ interactome factors.

PART II

ANP32B was identified as an interactor of 53BP1^{28A}, the unphosphorylated analogue of the 53BP1^{91}. A few factors have been established over the years that restrict the function of 53BP1 as a pro-NHEJ protein. Specifically, TIRR is a *bona fide* partner of unphosphorylated 53BP1 that was hypothesized to limit excess 53BP1 loading on chromatin in order to prevent its hyperactivity[89]. Altogether, ANP32B was a promising candidate in the SILAC analysis that could also potentially limit 53BP1 regulation during DSB repair. However, I proved that ANP32B does not participate in DSB repair.

5.3. Relationship between ANP32B and 53BP1

I established that ANP32B has no effect on the association of Rif1, PTIP or Mob domain interactors with 53BP1 and in their ability to modulate 53BP1 functions during CSR or repair of DNA replication-associated DSBs in BRCA1-deficient cells. The other potential role of ANP32B could be modulation of 53BP1-dependent activation of p53 transcriptional programs. 53BP1 possesses a BRCA1 C-terminus (BRCT) domain and an oligomerization domain (Oligo) that are important to support its interaction with p53 and the ability of 53BP1 to activate p53 transcriptional program and G1 arrest/apoptosis following DNA damage. Removal of any of these domains allows cells to escape the G1/S cell cycle checkpoint and G1 arrest due to the inability to fully activate the p53 program. This is a functionally independent role of 53BP1 from DNA end-protection[90]. In a SILAC-based pull-down for 53BP1 phospho-dependent interactors, we found ANP32B as an interactor of 53BP1 that specifically associates with the 28A phospho-mutant (mutation of all 28 S-T/Q sites to Alanine; 53BP1^{28A}) suggesting that it interacts only with unphosphorylated 53BP1^{91}. Since ANP32B is a pro-proliferation protein that promotes G1/S phase progression and also has been described to form a transcriptional repressive complex with p53 in hematopoietic stem cells, we cannot exclude the possibility that the protein negatively regulates p53 and thereby G1/S check point through 53BP1[132-133,140]. Moreover, some of my results also indicated the same hypothesis.

Brca1$^{\Delta 11/\Delta 11}$ iMEFs transduced with pMX-EV and pMX-ANP32B and treated with PARPi did not show any difference in rescue of viability by both FACS and colony formation assay. For FACS I had used *WT* iMEFs, also infected with pMX-EV and pMX-ANP32B. As expected, *WT* cells expressing empty vector (pMX-EV) and overexpressing ANP32B did not show any difference in viability when treated with 1μM PARPi. Interestingly with 4μM PARPi, *WT* cells expressing pMX-EV were sensitive, and this sensitivity was lost on ANP32B overexpression (Figure 26B). Similarly, for the colony formation assay, I used *WT1* iMEFs and *WT2* iMEFs as controls, all infected with pMX-ANP32B. I observed that untransduced *WT* iMEFs (*WT1, WT2*) were sensitive to PARPi in this assay. This phenotype could be due to the effect of PARPi treatment on very low number of cells that were seeded for this assay. However, I again observed that the sensitivity was lost in both *WT* iMEFs on pMX-ANP32B transduction (Figure 26D). I hypothesise that chronic amount of DSBs generated by replication stress with high PARPi concentration in *WT* iMEFs initiated checkpoint signalling through 53BP1 and p53 cascade. When ANP32B is overexpressed, the interaction between 53BP1 and p53 was antagonised and therefore it inhibited checkpoint activation thus promoting cell proliferation. It is already known that loss of 53BP1 or p53 increases the incidence of tumor development. Furthermore, loss of ANP32B has been correlated to slower proliferation even after oncogenic immortalization[132]. Additionally, ANP32B is highly expressed in chronic myelogenous leukemia (CML) and its deletion augments p53 activity in leukemic stem cells in CML model[140]. Thereby 53BP1-ANP32B-p53 signalling axis could provide cellular homeostasis, making 53BP1 at the crossroad of the interplay between cell growth and cell death (Figure 32B). It is also interesting to note that during germinal centre reaction, p53 expression is supressed that indicates checkpoint inactivation to support completion of CSR[76]. Moreover, according to ImmGen database, germinal centre cells display high expression of ANP32B. Hence, it is possible that ANP32B plays a role in advancing from G1/S checkpoint after CSR reaction is completed (Figure 32A). If this balance is mediated through 53BP1, then his function will add to yet another role of 53BP1 during CSR in B cells apart from end-protection, maintaining break order and orientation (inversion:deletion) ratio[102-103].

In *WT* condition, Nutlin-3, an inhibitor of MDM2 (mouse double minute 2; an essential negative regulator of p53) induces accumulation of p53 and therefore cell cycle arrest/apoptosis[141]. If overexpression of ANP32B can release the cells from cell cycle arrest

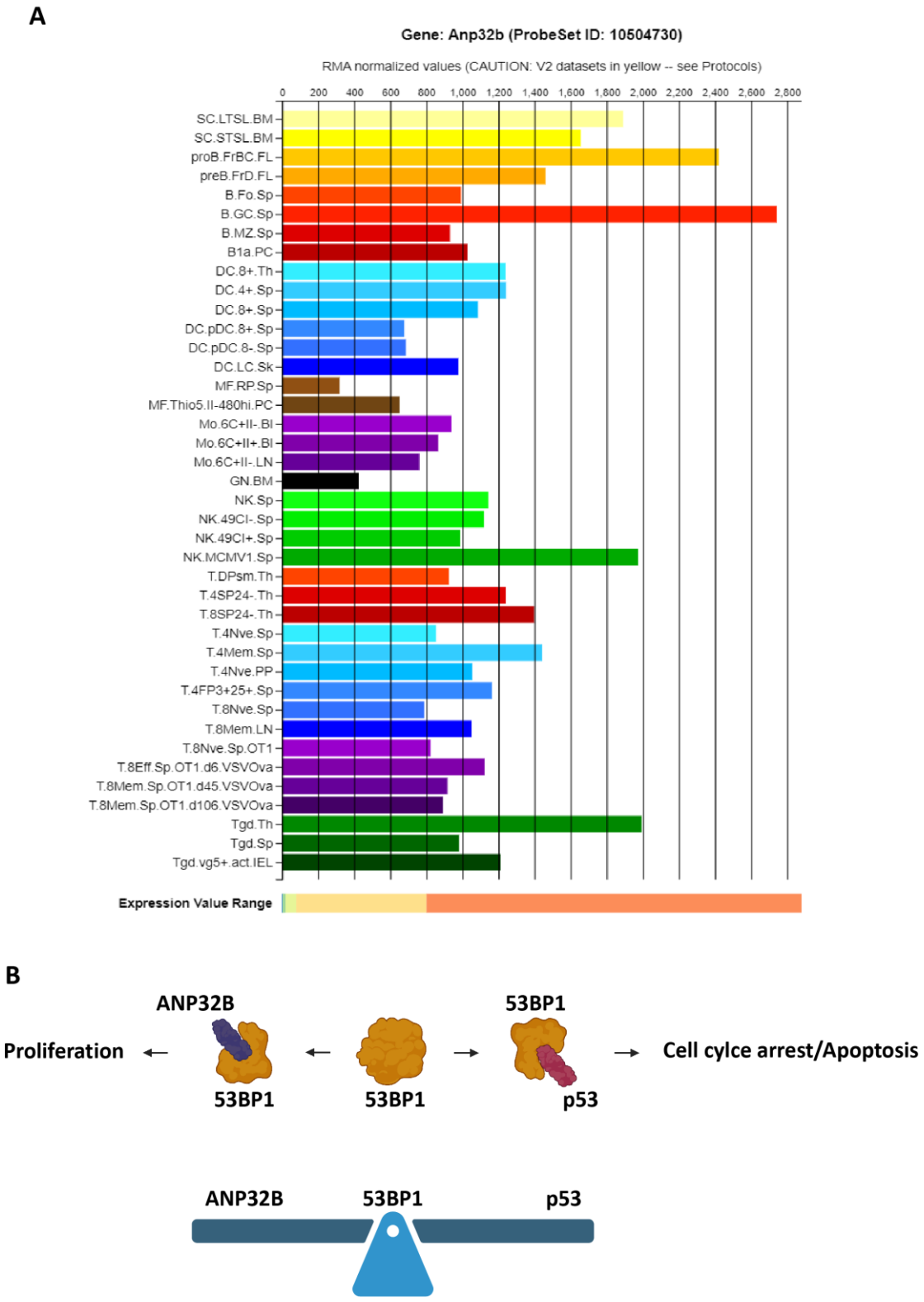

Figure 32. Relationship between ANP32B and 53BP1. (A) ImmGen database of microarray of ANP32B (http://rstats.immgen.org/Skyline_microarray/skyline.html) representing B.GC.Sp. (B cells in germinal center of spleen) with highest expression. **B)** Working model to explain coordination of proliferation and apoptosis mediated through 53BP1 *via* ANP32B and p53 respectively. This could provide cellular homeostasis.

and display viability in the presence of Nutlin-3, then it could suggest the possibility of direct or indirect ANP32B and p53 interaction. 53BP1-depleted ANP32B overexpressing cells if doesn't exhibit a difference in cell viability under Nutlin-3 treatment from the ones expressing only the endogenous ANP32B, can indicate relationship of 53BP1-ANP32B-p53. In parallel to this notion, I had observed that *53bp1*$^{-/-}$ iMEFs transduced with both pMX-EV and pMX-ANP32B did not show a difference in sensitivity to PARPi in the colony formation assay (Figure 26D). Most importantly, the cells should have *WT* p53 and not mutated or deleted, which is usually the foundation of immortalized cell lines. Therefore, presence of *WT* p53 in the iMEFs I had used needs to be verified before I proceed to verify this hypothesis[142]. Primary MEFs would be the ideal cells for such experiments to rule out p53 mutation or deletion.

PART III

RIF1 is a pro-NHEJ factor that together with 53BP1 is indispensable for DSB repair during CSR and toxic-NHEJ. However, post-translational regulation of RIF1 is yet to be elucidated. To this end I performed a mass-spectrometry study and found serine 2138 of the protein to be phosphorylated with significantly high intensity values upon IR. On further assessment, I found the PTM to have no repair function.

5.5. Phospho-regulation of RIF1 through S2138

RIF1 has several S-T/Q sites that are consensus sites for ATM/ATR phosphorylation. I ~~had~~ performed a mass-spectrometry experiment with activated and irradiated primary B cells isolated from Rif1$^{FH/FH}$ mice (RIF1 tagged with Flag and 2xHA) in order to visualize a PTM map of RIF1 post-DSBs. Only S2138 was detected to be phosphorylated in all four biological replicates with high intensities (Figure 27C). However, the phospho-site did not display any implication in DNA end-protection and CSR (Figure 29A and B). Additionally, through an independent mass-spectrometry study, our lab had previously established that phosphorylation of a cluster of three S-T/Q sites at IDR (S1387, S1416 and S1528) is consensus of ATM/ATR and were identified after irradiation in activated primary B cells are also dispensable for DNA end-protection and CSR. Phosphorylation of the cluster recruited RIF1 to stalled replication forks to protect them from degradation following replication stress from hydroxyurea treatment in CH12 cells[85]. It was possible that similar to S1387, S1416 and S1528, S2138 is also phosphorylated under replication stress. Notably, S1416 was detected with high abundance simultaneously to S2138 in the mass-spectrometry experiment that I conducted (Figure 27C). Moreover, S2138 phospho-site is located in between RVxF-SILK

motif. The domain is responsible for recruiting PP1 to protect stalled replication forks[115]. However, I did not investigate if S2138 has a role in replication fork-protection since *Moiseeva et. al., PNAS, 2019* had already that the SQ motif is not required for PP1 binding in the human ortholog[143].

5.6 Role of RIF1 in toxic-NHEJ

Brca1$^{mut/mut}$ B3 clone underwent erroneous homology directed repair during knock-in at RIF1 exon 30, thus resulting in frame shift mutation and generation of premature termination codon thereby deleting the entire RIF1 C-terminal region (Fig. 30A-C). *Brca1*$^{mut/mut}$ B3 clone displays partial rescue of viability upon PARPi treatment, confirming HR re-wiring. However, it can switch at almost *WT* levels to IgA and IgG2b, the reason of which remains unclear. Moreover, another clone *Brca1*$^{mut/mut}$ A1 also underwent similar frame-shift mutation and behaves like *Rif1*$^{-/-}$ displaying partial rescue of viability and defective CSR. The difference in behaviour of the two clones is puzzling (Figure 30D and E).

Recently it was reported by *Setiaputra et. al., Molecular Cell, 2022*, that 53BP1^{7A} mutant (mutation of 7 S-T/Q sites to Alanine at the Pro domain) is able to recruit RIF1, as opposed to the previously established observation that the mutant abrogates RIF1 association[93,110]. However, 53BP1^{7A} is unable to recruit the Sheildin complex. Another mutant was developed named 53BP1^{3LA} recruits Shieldin at DSBs without the recruitment of RIF1. This study argues against the recently established theory of a linear 53BP1-RIF1-Shieldin axis[110]. In line of these observations, it is possible that *Brca1*$^{mut/mut}$ B3 clone is functionally very similar to 53BP1^{7A} and 53BP1^{3LA}, thus depicting a non-linear 53BP1-RIF1-Shieldin correlation. The clone can still recruit Sheildin to promote CSR and partial formation of chromosomal radials that might not be sufficiently toxic for the cells.

Additionally, the above study also discussed the likelihood of trace amount of Shieldin or RIF1 being recruited at the damage sites in the mutants 53BP1^{7A} and 53BP1^{3LA}, respectively. Another independent study from the same lab (Durocher lab: *Escribano-Díaz et. al., Molecular Cell, 2013*) also showed that reduced levels of RIF1 protein in B cells can still facilitate CSR, albeit not as proficiently as *WT* condition[113]. It is possible that one of the allele in *Brca1*$^{mut/mut}$ B3 clone expresses trace levels of RIF1 that possesses end-protection function, but somehow the PCR primers were unable to amplify it. Western blot of the clone display a faint *WT* RIF1 protein band (Figure 30B). The trace amount of RIF1 probably supports CSR that occurs at a single locus, but might not be sufficient to repair genome-wide DSBs generated by PARPi. However, the experiment I performed to test this hypothesis demonstrated that even very low amount of RIF1, expressed in *NLS-3xHA-Rif1* clones, can protect genome-wide DNA break

ends (Figure 31A and C). Although, it is difficult to estimate exactly how much RIF1 turnover is required by a cell to regulate its functions during DSB repair. As a preliminary step to determine if modest DNA end-protection activity is present in *Brca1*$^{mut/mut}$ B3 clone, analysis of metaphase spreads will verify the existence of radials that might not be abundant enough to induce cell death.

Cell death by toxic-NHEJ is primarily due to the formation of chromosomal radials, which are the result of joining of two or more chromosomal ends in the absence of DSBs end resection and HR[99]. Radial formation is due to various processes like DNA end-protection mediated by 53BP1 and its interaction partners RIF1, Sheildin and CST, interaction of PTIP with 53BP1 through an unknown mechanism and by chromosomal mobility through 53BP1 Mob domain, with the latter two having no function in CSR[93,99-100]. Thus, DSB end-protection is not the only determinant of toxic-NHEJ during replication-induced DSBs. Thus, another possibility is that, like 53BP1, RIF1 mediates toxic-NHEJ with multiple mechanisms/activities to generate chromosomal radials.

5.7 Significance of RIF1 C-Terminus in DNA end-protection

RIF1 C-terminal end is dispensable for RIF1 foci formation at DSBs, but is crucial for blocking BRCA1 accumulation in G1 cell cycle phase[113]. Inhibition of BRCA1 foci formation indicates protection of DNA ends, even though it is an ancillary read-out. Multiple assays like CSR and rescue of viability along with analysis of chromosomal radials under PARPi treatment are more direct functional read-outs to demonstrate end-protection. *Brca1*$^{mut/mut}$ A1 clone has a frame-shift mutation, which causes a premature termination codon that eliminates the entire C-terminal domain of RIF1. The clone exhibits abrogation of CSR and partial rescue of viability, which could strongly suggest the importance of C-terminus in DNA end-protection.

6. REFERENCES

1) Lindahl, T., & Nyberg, B. (1972). Rate of Depurination of Native Deoxyribonucleic Acid. *Biochemistry*. https://doi.org/10.1021/bi00769a018
2) Lindahl T. (1993). Instability and decay of the primary structure of DNA. *Nature*.
3) Barnes, D. E., & Lindahl, T. (2004). Repair and genetic consequences of endogenous DNA base damage in mammalian cells. In *Annual Review of Genetics*. https://doi.org/10.1146/annurev.genet.38.072902.092448
4) Jackson, S. P., & Bartek, J. (2009). The DNA-damage response in human biology and disease. In *Nature*. https://doi.org/10.1038/nature08467
5) Friedberg, E. C. (2008). A brief history of the DNA repair field. *Cell Research*, *18*(1), 3–7. https://doi.org/10.1038/cr.2007.113
6) Oster, S., & Aqeilan, R. I. (2020). Programmed DNA Damage and Physiological DSBs: Mapping, Biological Significance and Perturbations in Disease States. *Cells*, *9*(8). https://doi.org/10.3390/cells9081870
7) Chaudhuri, J., & Alt, F. W. (2004). Class-switch recombination: Interplay of transcription, DNA deamination and DNA repair. In *Nature Reviews Immunology*. https://doi.org/10.1038/nri1395
8) Pan-Hammarström, Q., Zhao, Y., & Hammarström, L. (2007). Class Switch Recombination: A Comparison Between Mouse and Human. In *Advances in Immunology*. https://doi.org/10.1016/S0065-2776(06)93001-6
9) Blackford, A. N., & Jackson, S. P. (2017). ATM, ATR, and DNA-PK: The Trinity at the Heart of the DNA Damage Response. In *Molecular Cell*. https://doi.org/10.1016/j.molcel.2017.05.015
10) Burma, S., Chen, B. P., Murphy, M., Kurimasa, A., & Chen, D. J. (2001). ATM Phosphorylates Histone H2AX in Response to DNA Double-strand Breaks. *Journal of Biological Chemistry*. https://doi.org/10.1074/jbc.C100466200
11) Hustedt, N., & Durocher, D. (2017). The control of DNA repair by the cell cycle. In *Nature Cell Biology*. https://doi.org/10.1038/ncb3452
12) Panchakshari, R. A., Zhang, X., Kumar, V., Du, Z., Wei, P. C., Kao, J., Dong, J., & Alt, F. W. (2018). DNA double-strand break response factors influence end-joining features of IgH class switch and general translocation junctions. *Proceedings of the National Academy of Sciences of the United States of America*. https://doi.org/10.1073/pnas.1719988115
13) Dunnick, W., Hertz, G. Z., Scappino, L., & Gritzmacher, C. (1993). DNA sequences at immunoglobulin switch region recombination sites. *Nucleic Acids Research*. https://doi.org/10.1093/nar/21.3.365

14) Yan, C. T., Boboila, C., Souza, E. K., Franco, S., Hickernell, T. R., Murphy, M., Gumaste, S., Geyer, M., Zarrin, A. A., Manis, J. P., Rajewsky, K., & Alt, F. W. (2007). IgH class switching and translocations use a robust non-classical end-joining pathway. *Nature*. https://doi.org/10.1038/nature06020

15) Boboila, C., Yan, C., Wesemann, D. R., Jankovic, M., Wang, J. H., Manis, J., Nussenzweig, A., Nussenzweig, M., & Alt, F. W. (2010). Alternative end-joining catalyzes class switch recombination in the absence of both Ku70 and DNA ligase. *Journal of Experimental Medicine*. https://doi.org/10.1084/jem.20092449

16) Chang, H. H. Y., Pannunzio, N. R., Adachi, N., & Lieber, M. R. (2017). Non-homologous DNA end joining and alternative pathways to double-strand break repair. In *Nature Reviews Molecular Cell Biology*. https://doi.org/10.1038/nrm.2017.48

17) Pannunzio, N. R., Watanabe, G., & Lieber, M. R. (2018). Nonhomologous DNA end-joining for repair of DNA double-strand breaks. In *Journal of Biological Chemistry*. https://doi.org/10.1074/jbc.TM117.000374

18) Bebenek, K., Pedersen, L. C., & Kunkel, T. A. (2014). Structure-function studies of DNA polymerase λ. *Biochemistry*. https://doi.org/10.1021/bi4017236

19) Moon, A. F., Pryor, J. M., Ramsden, D. A., Kunkel, T. A., Bebenek, K., & Pedersen, L. C. (2014). Sustained active site rigidity during synthesis by human DNA polymerase μ. *Nature Structural and Molecular Biology*. https://doi.org/10.1038/nsmb.2766

20) Wright, W. D., Shah, S. S., & Heyer, W. D. (2018). Homologous recombination and the repair of DNA double-strand breaks. In *Journal of Biological Chemistry*. https://doi.org/10.1074/jbc.TM118.000372

21) Symington, L. S. (2016). Mechanism and regulation of DNA end resection in eukaryotes. In *Critical Reviews in Biochemistry and Molecular Biology*. https://doi.org/10.3109/10409238.2016.1172552

22) Oh, J., & Symington, L. S. (2018). Role of the Mre11 complex in preserving genome integrity. In *Genes*. https://doi.org/10.3390/genes9120589

23) Hiom, K. (2001). Recombination: Homologous recombination branches out. In *Current Biology*. https://doi.org/10.1016/S0960-9822(01)00138-5

24) Krejci, L., Altmannova, V., Spirek, M., & Zhao, X. (2012). Homologous recombination and its regulation. In *Nucleic Acids Research*. https://doi.org/10.1093/nar/gks270

25) Zhao, W., Steinfeld, J. B., Liang, F., Chen, X., Maranon, D. G., Jian Ma, C., Kwon, Y., Rao, T., Wang, W., Sheng, C., Song, X., Deng, Y., Jimenez-Sainz, J., Lu, L., Jensen, R. B., Xiong, Y., Kupfer, G. M., Wiese, C., Greene, E. C., & Sung, P. (2017). BRCA1-BARD1 promotes RAD51-mediated homologous DNA pairing. *Nature*. https://doi.org/10.1038/nature24060

26) West, S. C., Blanco, M. G., Chan, Y. W., Matos, J., Sarbajna, S., & Wyatt, H. D. M. (2016). Resolution of recombination intermediates: Mechanisms and regulation. *Cold Spring Harbor Symposia on Quantitative Biology*. https://doi.org/10.1101/sqb.2015.80.027649

27) Sfeir, A., & Symington, L. S. (2015). Microhomology-Mediated End Joining: A Back-up Survival Mechanism or Dedicated Pathway? In *Trends in Biochemical Sciences*. https://doi.org/10.1016/j.tibs.2015.08.006

28) Sallmyr, A., & Tomkinson, A. E. (2018). Repair of DNA double-strand breaks by mammalian alternative end-joining pathways. In *Journal of Biological Chemistry*. https://doi.org/10.1074/jbc.TM117.000375

29) Wood, R. D., & Doublié, S. (2016). DNA polymerase θ (POLQ), double-strand break repair, and cancer. In *DNA Repair*. https://doi.org/10.1016/j.dnarep.2016.05.003

30) Mateos-Gomez, P. A., Gong, F., Nair, N., Miller, K. M., Lazzerini-Denchi, E., & Sfeir, A. (2015). Mammalian polymerase θ promotes alternative NHEJ and suppresses recombination. *Nature*. https://doi.org/10.1038/nature14157

31) Ceccaldi, R., Liu, J. C., Amunugama, R., Hajdu, I., Primack, B., Petalcorin, M. I. R., O'Connor, K. W., Konstantinopoulos, P. A., Elledge, S. J., Boulton, S. J., Yusufzai, T., & D'Andrea, A. D. (2015). Homologous-recombination-deficient tumours are dependent on Polθ -mediated repair. *Nature*, *518*(7538), 258–262. https://doi.org/10.1038/nature14184

32) Tomkinson, A. E., & Sallmyr, A. (2013). Structure and function of the DNA ligases encoded by the mammalian LIG3 gene. In *Gene*. https://doi.org/10.1016/j.gene.2013.08.061

33) Dutta, A., Eckelmann, B., Adhikari, S., Ahmed, K. M., Sengupta, S., Pandey, A., Hegde, P. M., Tsai, M. S., Tainer, J. A., Weinfeld, M., Hegde, M. L., & Mitra, S. (2017). Microhomology-mediated end joining is activated in irradiated human cells due to phosphorylation-dependent formation of the XRCC1 repair complex. *Nucleic Acids Research*. https://doi.org/10.1093/nar/gkw1262

34) Della-Maria, J., Zhou, Y., Tsai, M. S., Kuhnlein, J., Carney, J. P., Paull, T. T., & Tomkinson, A. E. (2011). Human Mre11/human Rad50/Nbs1 and DNA ligase IIIα/XRCC1 protein complexes act together in an alternative nonhomologous end joining pathway. *Journal of Biological Chemistry*. https://doi.org/10.1074/jbc.M111.274159

35) Simsek, D., Brunet, E., Wong, S. Y. W., Katyal, S., Gao, Y., McKinnon, P. J., Lou, J., Zhang, L., Li, J., Rebar, E. J., Gregory, P. D., Holmes, M. C., & Jasin, M. (2011). DNA ligase III promotes alternative nonhomologous end-joining during chromosomal

translocation formation. *PLoS Genetics*. https://doi.org/10.1371/journal.pgen.1002080

36) Masani, S., Han, L., Meek, K., & Yu, K. (2016). Redundant function of DNA ligase 1 and 3 in alternative end-joining during immunoglobulin class switch recombination. *Proceedings of the National Academy of Sciences of the United States of America*. https://doi.org/10.1073/pnas.1521630113
37) Arakawa, H., Bednar, T., Wang, M., Paul, K., Mladenov, E., Bencsik-Theilen, A. A., & Iliakis, G. (2012). Functional redundancy between DNA ligases i and III in DNA replication in vertebrate cells. *Nucleic Acids Research*. https://doi.org/10.1093/nar/gkr1024
38) Bhargava, R., Onyango, D. O., & Stark, J. M. (2016). Regulation of Single-Strand Annealing and its Role in Genome Maintenance. In *Trends in Genetics*. https://doi.org/10.1016/j.tig.2016.06.007
39) Saha, T., Sundaravinayagam, D., & Di Virgilio, M. (2021). Charting a DNA Repair Roadmap for Immunoglobulin Class Switch Recombination. In *Trends in Biochemical Sciences*. https://doi.org/10.1016/j.tibs.2020.10.005
40) Schroeder, H. W., & Cavacini, L. (2010). Structure and function of immunoglobulins. *Journal of Allergy and Clinical Immunology*. https://doi.org/10.1016/j.jaci.2009.09.046
41) NORMAN, P. (1995). Immunobiology: The immune system in health and disease. *Journal of Allergy and Clinical Immunology*. https://doi.org/10.1016/s0091-6749(95)70025-0
42) Bassing, C. H., Swat, W., & Alt, F. W. (2002). The mechanism and regulation of chromosomal V(D)J recombination. In *Cell*. https://doi.org/10.1016/S0092-8674(02)00675-X
43) de la Morena, M. T. (2016). Clinical Phenotypes of Hyper-IgM Syndromes. *Journal of Allergy and Clinical Immunology: In Practice*. https://doi.org/10.1016/j.jaip.2016.09.013
44) Durandy, A., Kracker, S., & Fischer, A. (2013). Primary antibody deficiencies. *Nature Reviews Immunology*, *13*(7), 519–533. https://doi.org/10.1038/nri3466
45) Teng, G., & Schatz, D. G. (2015). Regulation and Evolution of the RAG Recombinase. In *Advances in Immunology*. https://doi.org/10.1016/bs.ai.2015.07.002
46) Chaudhuri, J., & Alt, F. W. (2004). Class-switch recombination: Interplay of transcription, DNA deamination and DNA repair. In *Nature Reviews Immunology*. https://doi.org/10.1038/nri1395
47) Pavri, R., & Nussenzweig, M. C. (2011). AID targeting in antibody diversity. In *Advances in Immunology*. https://doi.org/10.1016/B978-0-12-387663-8.00005-3

48) Methot, S. P., & Di Noia, J. M. (2017). Molecular Mechanisms of Somatic Hypermutation and Class Switch Recombination. In *Advances in Immunology*. https://doi.org/10.1016/bs.ai.2016.11.002

49) Boboila, C., Alt, F. W., & Schwer, B. (2012). Classical and Alternative End-Joining Pathways for Repair of Lymphocyte-Specific and General DNA Double-Strand Breaks. In *Advances in Immunology*. https://doi.org/10.1016/B978-0-12-394300-2.00001-6

50) Delgado-Benito, V., Rosen, D. B., Wang, Q., Gazumyan, A., Pai, J. A., Oliveira, T. Y., Sundaravinayagam, D., Zhang, W., Andreani, M., Keller, L., Kieffer-Kwon, K. R., Pękowska, A., Jung, S., Driesner, M., Subbotin, R. I., Casellas, R., Chait, B. T., Nussenzweig, M. C., & Di Virgilio, M. (2018). The Chromatin Reader ZMYND8 Regulates Igh Enhancers to Promote Immunoglobulin Class Switch Recombination. *Molecular Cell*. https://doi.org/10.1016/j.molcel.2018.08.042

51) Cortizas, E. M., Zahn, A., Hajjar, M. E., Patenaude, A.-M., Di Noia, J. M., & Verdun, R. E. (2013). Alternative End-Joining and Classical Nonhomologous End-Joining Pathways Repair Different Types of Double-Strand Breaks during Class-Switch Recombination. *The Journal of Immunology*. https://doi.org/10.4049/jimmunol.1301300

52) Lee-Theilen, M., Matthews, A. J., Kelly, D., Zheng, S., & Chaudhuri, J. (2011). CtIP promotes microhomology-mediated alternative end joining during class-switch recombination. *Nature Structural and Molecular Biology*. https://doi.org/10.1038/nsmb.1942

53) Bothmer, A., Rommel, P. C., Gazumyan, A., Polato, F., Reczek, C. R., Muellenbeck, M. F., Schaetzlein, S., Edelmann, W., Chen, P. L., Brosh, R. M., Casellas, R., Ludwig, T., Baer, R., Nussenzweig, A., Nussenzweig, M. C., & Robbiani, D. F. (2013). Mechanism of DNA resection during intrachromosomal recombination and immunoglobulin class switching. *Journal of Experimental Medicine*. https://doi.org/10.1084/jem.20121975

54) Shukla, V., Halabelian, L., Balagere, S., Samaniego-Castruita, D., Feldman, D. E., Arrowsmith, C. H., Rao, A., & Aravind, L. (2020). HMCES Functions in the Alternative End-Joining Pathway of the DNA DSB Repair during Class Switch Recombination in B Cells. *Molecular Cell*. https://doi.org/10.1016/j.molcel.2019.10.031

55) Saintamand, A., Rouaud, P., Saad, F., Rios, G., Cogné, M., & Denizot, Y. (2015). Elucidation of IgH 3′ region regulatory role during class switch recombination via germline deletion. *Nature Communications*. https://doi.org/10.1038/ncomms8084

56) Muramatsu, M., Sankaranand, V. S., Anant, S., Sugai, M., Kinoshita, K., Davidson, N. O., & Honjo, T. (1999). Specific expression of activation-induced cytidine deaminase

(AID), a novel member of the RNA-editing deaminase family in germinal center B cells. *Journal of Biological Chemistry*. https://doi.org/10.1074/jbc.274.26.18470

57) Nina Papavasiliou, F., & Schatz, D. G. (2002). The activation-induced deaminase functions in a postcleavage step of the somatic hypermutation process. *Journal of Experimental Medicine*. https://doi.org/10.1084/jem.20011858

58) Chaudhuri, J., Basu, U., Zarrin, A., Yan, C., Franco, S., Perlot, T., Vuong, B., Wang, J., Phan, R. T., Datta, A., Manis, J., & Alt, F. W. (2007). Evolution of the Immunoglobulin Heavy Chain Class Switch Recombination Mechanism. In *Advances in Immunology*. https://doi.org/10.1016/S0065-2776(06)94006-1

59) Jeevan-Raj, B. P., Robert, I., Heyer, V., Page, A., Wang, J. H., Cammas, F., Alt, F. W., Losson, R., & Reina-San-Martin, B. (2011). Epigenetic tethering of AID to the donor switch region during immunoglobulin class switch recombination. *Journal of Experimental Medicine*. https://doi.org/10.1084/jem.20110118

60) Pavri, R., Gazumyan, A., Jankovic, M., Di Virgilio, M., Klein, I., Ansarah-Sobrinho, C., Resch, W., Yamane, A., San-Martin, B. R., Barreto, V., Nieland, T. J., Root, D. E., Casellas, R., & Nussenzweig, M. C. (2010). Activation-induced cytidine deaminase targets DNA at sites of RNA polymerase II stalling by interaction with Spt5. *Cell*. https://doi.org/10.1016/j.cell.2010.09.017

61) Zheng, S., Vuong, B. Q., Vaidyanathan, B., Lin, J. Y., Huang, F. T., & Chaudhuri, J. (2015). Non-coding RNA Generated following Lariat Debranching Mediates Targeting of AID to DNA. *Cell*. https://doi.org/10.1016/j.cell.2015.03.020

62) Schrader, C. E., Guikema, J. E. J., Linehan, E. K., Selsing, E., & Stavnezer, J. (2007). Activation-Induced Cytidine Deaminase-Dependent DNA Breaks in Class Switch Recombination Occur during G1 Phase of the Cell Cycle and Depend upon Mismatch Repair. *The Journal of Immunology*. https://doi.org/10.4049/jimmunol.179.9.6064

63) Wiedemann, E. M., Peycheva, M., & Pavri, R. (2016). DNA Replication Origins in Immunoglobulin Switch Regions Regulate Class Switch Recombination in an R-Loop-Dependent Manner. *Cell Reports*. https://doi.org/10.1016/j.celrep.2016.11.041

64) Petersen, S., Casellas, R., Reina-San-Martin, B., Chen, H. T., Difilippantonio, M. J., Wilson, P. C., Hanitsch, L., Celeste, A., Muramatsu, M., Pilch, D. R., Redon, C., Ried, T., Bonner, W. M., Honjo, T., Nussenzweig, M. C., & Nussenzweig, A. (2001). AID is required to initiate Nbs1/γ-H2AX focus formation and mutations at sites of class switching. *Nature*. https://doi.org/10.1038/414660a

65) Wang, Q., Kieffer-Kwon, K. R., Oliveira, T. Y., Mayer, C. T., Yao, K., Pai, J., Cao, Z., Dose, M., Casellas, R., Jankovic, M., Nussenzweig, M. C., & Robbiani, D. F. (2017). The cell cycle restricts activation-induced cytidine deaminase activity to early G1.

Journal of Experimental Medicine, *214*(1), 49–58. https://doi.org/10.1084/jem.20161649

66) Soulas-Sprauel, P., Le Guyader, G., Rivera-Munoz, P., Abramowski, V., Olivier-Martin, C., Goujet-Zalc, C., Charneau, P., & De Villartay, J. P. (2007). Role for DNA repair factor XRCC4 in immunoglobulin class switch recombination. *Journal of Experimental Medicine*. https://doi.org/10.1084/jem.20070255

67) Boboila, C., Jankovic, M., Yan, C. T., Wang, J. H., Wesemann, D. R., Zhang, T., Fazeli, A., Feldman, L., Nussenzweig, A., Nussenzweig, M., & Alt, F. W. (2010). Alternative end-joining catalyzes robust IgH locus deletions and translocations in the combined absence of ligase 4 and Ku70. *Proceedings of the National Academy of Sciences of the United States of America*. https://doi.org/10.1073/pnas.0915067107

68) Franco, S., Murphy, M. M., Li, G., Borjeson, T., Boboila, C., & Alt, F. W. (2008). DNA-PKcs and Artemis function in the end-joining phase of immunoglobulin heavy chain class switch recombination. *Journal of Experimental Medicine*. https://doi.org/10.1084/jem.20080044

69) Liu, X., Wang, X. S., Lee, B. J., Wu-Baer, F. K., Lin, X., Shao, Z., Estes, V. M., Gautier, J., Baer, R., & Zha, S. (2019). CtIP is essential for early B cell proliferation and development in mice. *Journal of Experimental Medicine*. https://doi.org/10.1084/jem.20181139

70) Yousefzadeh, M. J., Wyatt, D. W., Takata, K. ichi, Mu, Y., Hensley, S. C., Tomida, J., Bylund, G. O., Doublié, S., Johansson, E., Ramsden, D. A., McBride, K. M., & Wood, R. D. (2014). Mechanism of Suppression of Chromosomal Instability by DNA Polymerase POLQ. *PLoS Genetics*. https://doi.org/10.1371/journal.pgen.1004654

71) Li, Y., Gao, X., & Wang, J. Y. (2011). Comparison of two POLQ mutants reveals that a polymerase-inactive POLQ retains significant functionin tolerance to etoposide and γ-irradiation in mouse B cells. *Genes to Cells*. https://doi.org/10.1111/j.1365-2443.2011.01550.x

72) Robert, I., Dantzer, F., & Reina-San-Martin, B. (2009). Parp1 facilitates alternative NHEJ, whereas Parp2 suppresses IgH/c-myc translocations during immunoglobulin class switch recombination. *Journal of Experimental Medicine*. https://doi.org/10.1084/jem.20082468

73) Hasham, M. G., Donghia, N. M., Coffey, E., Maynard, J., Snow, K. J., Ames, J., Wilpan, R. Y., He, Y., King, B. L., & Mills, K. D. (2010). Widespread genomic breaks generated by activation-induced cytidine deaminase are prevented by homologous recombination. *Nature Immunology*. https://doi.org/10.1038/ni.1909

74) Hasham, M. G., Snow, K. J., Donghia, N. M., Branca, J. A., Lessard, M. D., Stavnezer, J., Shopland, L. S., & Mills, K. D. (2012). Activation-Induced Cytidine Deaminase-

Initiated Off-Target DNA Breaks Are Detected and Resolved during S Phase. *The Journal of Immunology*. https://doi.org/10.4049/jimmunol.1200414

75) Yamane, A., Robbiani, D. F., Resch, W., Bothmer, A., Nakahashi, H., Oliveira, T., Rommel, P. C., Brown, E. J., Nussenzweig, A., Nussenzweig, M. C., & Casellas, R. (2013). RPA Accumulation during Class Switch Recombination Represents 5'-3' DNA-End Resection during the S-G2/M Phase of the Cell Cycle. *Cell Reports*. https://doi.org/10.1016/j.celrep.2012.12.006

76) Phan, R. T., & Dalla-Favera, R. (2004). The BCL6 proto-oncogene suppresses p53 expression in germinal-centre B cells. *Nature*. https://doi.org/10.1038/nature03147

77) Zan, H., Tat, C., Qiu, Z., Taylor, J. R., Guerrero, J. A., Shen, T., & Casali, P. (2017). Rad52 competes with Ku70/Ku86 for binding to S-region DSB ends to modulate antibody class-switch DNA recombination. *Nature Communications*. https://doi.org/10.1038/ncomms14244

78) Eccleston, J., Yan, C., Yuan, K., Alt, F. W., & Selsing, E. (2011). Mismatch Repair Proteins MSH2, MLH1, and EXO1 Are Important for Class-Switch Recombination Events Occurring in B Cells That Lack Nonhomologous End Joining. *The Journal of Immunology*. https://doi.org/10.4049/jimmunol.1003104

79) Cortizas, E. M., Zahn, A., Hajjar, M. E., Patenaude, A.-M., Di Noia, J. M., & Verdun, R. E. (2013). Alternative End-Joining and Classical Nonhomologous End-Joining Pathways Repair Different Types of Double-Strand Breaks during Class-Switch Recombination. *The Journal of Immunology*. https://doi.org/10.4049/jimmunol.1301300

80) Ling, A. K., So, C. C., Le, M. X., Chen, A. Y., Hung, L., & Martin, A. (2018). Double-stranded DNA break polarity skews repair pathway choice during intrachromosomal and interchromosomal recombination. *Proceedings of the National Academy of Sciences of the United States of America*. https://doi.org/10.1073/pnas.1720962115

81) So, C. C., & Martin, A. (2019). DSB structure impacts DNA recombination leading to class switching and chromosomal translocations in human B cells. *PLoS Genetics*. https://doi.org/10.1371/journal.pgen.1008101

82) Rush, J. S., Fugmann, S. D., & Schatz, D. G. (2004). Staggered AID-dependent DNA double strand breaks are the predominant DNA lesions targeted to Sμ in Ig class switch recombination. *International Immunology*, *16*(4), 549–557. https://doi.org/10.1093/intimm/dxh057

83) Zahn, A., Eranki, A. K., Patenaude, A. M., Methot, S. P., Fifield, H., Cortizas, E. M., Foster, P., Imai, K., Durandy, A., Larijani, M., Verdun, R. E., & Di Noia, J. M. (2014). Activation induced deaminase C-terminal domain links DNA breaks to end protection and repair during class switch recombination. *Proceedings of the National Academy*

of Sciences of the United States of America. https://doi.org/10.1073/pnas.1320486111

84) Nakamura, M., Kondo, S., Sugai, M., Nazarea, M., Imamura, S., & Honjo, T. (1996). High frequency class switching of an IgM+ B lymphoma clone CH12F3 to IgA+ cells. *International Immunology*. https://doi.org/10.1093/intimm/8.2.193

85) Balasubramanian, S., Andreani, M., Andrade, J. G., Saha, T., Sundaravinayagam, D., Garzón, J., Zhang, W., Popp, O., Hiraga, S. I., Rahjouei, A., Rosen, D. B., Mertins, P., Chait, B. T., Donaldson, A. D., & Di Virgilio, M. (2022). Protection of nascent DNA at stalled replication forks is mediated by phosphorylation of RIF1 intrinsically disordered region. *ELife*. https://doi.org/10.7554/eLife.75047

86) Vettermann, C., & Schlissel, M. S. (2010). Allelic exclusion of immunoglobulin genes: Models and mechanisms. In *Immunological Reviews*. https://doi.org/10.1111/j.1600-065X.2010.00935.x

87) Dong, J., Panchakshari, R. A., Zhang, T., Zhang, Y., Hu, J., Volpi, S. A., Meyers, R. M., Ho, Y. J., Du, Z., Robbiani, D. F., Meng, F., Gostissa, M., Nussenzweig, M. C., Manis, J. P., & Alt, F. W. (2015). Orientation-specific joining of AID-initiated DNA breaks promotes antibody class switching. *Nature*. https://doi.org/10.1038/nature14970

88) Mirman, Z., & de Lange, T. (2020). 53BP1: a DSB escort. In *Genes & development*. https://doi.org/10.1101/gad.333237.119

89) Drané, P., Brault, M. E., Cui, G., Meghani, K., Chaubey, S., Detappe, A., Parnandi, N., He, Y., Zheng, X. F., Botuyan, M. V., Kalousi, A., Yewdell, W. T., Münch, C., Harper, J. W., Chaudhuri, J., Soutoglou, E., Mer, G., & Chowdhury, D. (2017). TIRR regulates 53BP1 by masking its histone methyl-lysine binding function. *Nature*. https://doi.org/10.1038/nature21358

90) Cuella-Martin, R., Oliveira, C., Lockstone, H. E., Snellenberg, S., Grolmusova, N., & Chapman, J. R. (2017). Abstract PR20: A 53BP1 integrates DNA repair and p53-dependent cell fate decisions via distinct mechanisms. *Molecular Cancer Research*. https://doi.org/10.1158/1557-3125.dnarepair16-pr20

91) Di Virgilio, M., Callen, E., Yamane, A., Zhang, W., Jankovic, M., Gitlin, A. D., Feldhahn, N., Resch, W., Oliveira, T. Y., Chait, B. T., Nussenzweig, A., Casellas, R., Robbiani, D. F., & Nussenzweig, M. C. (2013). Rif1 prevents resection of DNA breaks and promotes immunoglobulin class switching. *Science*. https://doi.org/10.1126/science.1230624

92) Chapman, J. R., Barral, P., Vannier, J. B., Borel, V., Steger, M., Tomas-Loba, A., Sartori, A. A., Adams, I. R., Batista, F. D., & Boulton, S. J. (2013). RIF1 Is Essential

for 53BP1-Dependent Nonhomologous End Joining and Suppression of DNA Double-Strand Break Resection. *Molecular Cell*. https://doi.org/10.1016/j.molcel.2013.01.002

93) Sundaravinayagam, D., Rahjouei, A., Andreani, M., Tupiņa, D., Balasubramanian, S., Saha, T., Delgado-Benito, V., Coralluzzo, V., Daumke, O., & Di Virgilio, M. (2019). 53BP1 Supports Immunoglobulin Class Switch Recombination Independently of Its DNA Double-Strand Break End Protection Function. *Cell Reports*. https://doi.org/10.1016/j.celrep.2019.06.035

94) Gupta, R., Somyajit, K., Narita, T., Maskey, E., Stanlie, A., Kremer, M., Typas, D., Lammers, M., Mailand, N., Nussenzweig, A., Lukas, J., & Choudhary, C. (2018). DNA Repair Network Analysis Reveals Shieldin as a Key Regulator of NHEJ and PARP Inhibitor Sensitivity. *Cell*. https://doi.org/10.1016/j.cell.2018.03.050

95) Noordermeer, S. M., Adam, S., Setiaputra, D., Barazas, M., Pettitt, S. J., Ling, A. K., Olivieri, M., Álvarez-Quilón, A., Moatti, N., Zimmermann, M., Annunziato, S., Krastev, D. B., Song, F., Brandsma, I., Frankum, J., Brough, R., Sherker, A., Landry, S., Szilard, R. K., … Durocher, D. (2018). The shieldin complex mediates 53BP1-dependent DNA repair. *Nature*. https://doi.org/10.1038/s41586-018-0340-7

96) Mirman, Z., Lottersberger, F., Takai, H., Kibe, T., Gong, Y., Takai, K., Bianchi, A., Zimmermann, M., Durocher, D., & de Lange, T. (2018). 53BP1–RIF1–shieldin counteracts DSB resection through CST- and Polα-dependent fill-in. *Nature*. https://doi.org/10.1038/s41586-018-0324-7

97) Dev, H., Chiang, T. W. W., Lescale, C., de Krijger, I., Martin, A. G., Pilger, D., Coates, J., Sczaniecka-Clift, M., Wei, W., Ostermaier, M., Herzog, M., Lam, J., Shea, A., Demir, M., Wu, Q., Yang, F., Fu, B., Lai, Z., Balmus, G., … Jackson, S. P. (2018). Shieldin complex promotes DNA end-joining and counters homologous recombination in BRCA1-null cells. *Nature Cell Biology*. https://doi.org/10.1038/s41556-018-0140-1

98) Ghezraoui, H., Oliveira, C., Becker, J. R., Bilham, K., Moralli, D., Anzilotti, C., Fischer, R., Deobagkar-Lele, M., Sanchiz-Calvo, M., Fueyo-Marcos, E., Bonham, S., Kessler, B. M., Rottenberg, S., Cornall, R. J., Green, C. M., & Chapman, J. R. (2018). 53BP1 cooperation with the REV7–shieldin complex underpins DNA structure-specific NHEJ. *Nature*. https://doi.org/10.1038/s41586-018-0362-1

99) Callen, E., Di Virgilio, M., Kruhlak, M. J., Nieto-Soler, M., Wong, N., Chen, H. T., Faryabi, R. B., Polato, F., Santos, M., Starnes, L. M., Wesemann, D. R., Lee, J. E., Tubbs, A., Sleckman, B. P., Daniel, J. A., Ge, K., Alt, F. W., Fernandez-Capetillo, O., Nussenzweig, M. C., & Nussenzweig, A. (2013). 53BP1 mediates productive and mutagenic DNA repair through distinct phosphoprotein interactions. *Cell*. https://doi.org/10.1016/j.cell.2013.05.023

100) Lottersberger, F., Karssemeijer, R. A., Dimitrova, N., & De Lange, T. (2015). 53BP1 and the LINC Complex Promote Microtubule-Dependent DSB Mobility and DNA Repair. *Cell*. https://doi.org/10.1016/j.cell.2015.09.057

101) Barazas, M., Annunziato, S., Pettitt, S. J., de Krijger, I., Ghezraoui, H., Roobol, S. J., Lutz, C., Frankum, J., Song, F. F., Brough, R., Evers, B., Gogola, E., Bhin, J., van de Ven, M., van Gent, D. C., Jacobs, J. J. L., Chapman, R., Lord, C. J., Jonkers, J., & Rottenberg, S. (2018). The CST Complex Mediates End Protection at Double-Strand Breaks and Promotes PARP Inhibitor Sensitivity in BRCA1-Deficient Cells. *Cell Reports*. https://doi.org/10.1016/j.celrep.2018.04.046

102) Rocha, P. P., Raviram, R., Fu, Y., Kim, J. H., Luo, V. M., Aljoufi, A., Swanzey, E., Pasquarella, A., Balestrini, A., Miraldi, E. R., Bonneau, R., Petrini, J., Schotta, G., & Skok, J. A. (2016). A Damage-Independent Role for 53BP1 that Impacts Break Order and Igh Architecture during Class Switch Recombination. *Cell Reports*. https://doi.org/10.1016/j.celrep.2016.05.073

103) Liu, X., Liu, T., Shang, Y., Dai, P., Zhang, W., Lee, B. J., Huang, M., Yang, D., Wu, Q., Liu, L. D., Zheng, X., Zhou, B. O., Dong, J., Yeap, L. S., Hu, J., Xiao, T., Zha, S., Casellas, R., Liu, X. S., & Meng, F. L. (2020). ERCC6L2 promotes DNA orientation-specific recombination in mammalian cells. *Cell Research*. https://doi.org/10.1038/s41422-020-0328-3

104) Lord, C. J., & Ashworth, A. (2017). PARP Inhibitors: The First Synthetic Lethal Targeted Therapy. *Science (New York, N.Y.)*.

105) Sartori, A. A., Lukas, C., Coates, J., Mistrik, M., Fu, S., Bartek, J., Baer, R., Lukas, J., & Jackson, S. P. (2007). Human CtIP promotes DNA end resection. *Nature*. https://doi.org/10.1038/nature06337

106) Roy, R., Chun, J., & Powell, S. N. (2012). BRCA1 and BRCA2: Different roles in a common pathway of genome protection. In *Nature Reviews Cancer*. https://doi.org/10.1038/nrc3181

107) Garcia, V., Phelps, S. E. L., Gray, S., & Neale, M. J. (2011). Bidirectional resection of DNA double-strand breaks by Mre11 and Exo1. *Nature*. https://doi.org/10.1038/nature10515

108) Nimonkar, A. V., Genschel, J., Kinoshita, E., Polaczek, P., Campbell, J. L., Wyman, C., Modrich, P., & Kowalczykowski, S. C. (2011). BLM-DNA2-RPA-MRN and EXO1-BLM-RPA-MRN constitute two DNA end resection machineries for human DNA break repair. *Genes and Development*. https://doi.org/10.1101/gad.2003811

109) Scully, R., Panday, A., Elango, R., & Willis, N. A. (2019). DNA double-strand break repair-pathway choice in somatic mammalian cells. In *Nature Reviews Molecular Cell Biology*. https://doi.org/10.1038/s41580-019-0152-0

110) Setiaputra, D., Escribano-Díaz, C., Reinert, J. K., Sadana, P., Zong, D., Callen, E., Sifri, C., Seebacher, J., Nussenzweig, A., Thomä, N. H., & Durocher, D. (2022). RIF1 acts in DNA repair through phosphopeptide recognition of 53BP1. *Molecular Cell*. https://doi.org/10.1016/j.molcel.2022.01.025

111) Lee, D., Apelt, K., Lee, S. O., Chan, H. R., Luijsterburg, M. S., Leung, J. W. C., & Miller, K. M. (2022). ZMYM2 restricts 53BP1 at DNA double-strand breaks to favor BRCA1 loading and homologous recombination. *Nucleic Acids Research*. https://doi.org/10.1093/nar/gkac160

112) Silverman, J., Takai, H., Buonomo, S. B. C., Eisenhaber, F., & De Lange, T. (2004). Human Rif1, ortholog of a yeast telomeric protein, is regulated by ATM and 53BP1 and functions in the S-phase checkpoint. *Genes and Development*. https://doi.org/10.1101/gad.1216004

113) Escribano-Díaz, C., Orthwein, A., Fradet-Turcotte, A., Xing, M., Young, J. T. F., Tkáč, J., Cook, M. A., Rosebrock, A. P., Munro, M., Canny, M. D., Xu, D., & Durocher, D. (2013). A Cell Cycle-Dependent Regulatory Circuit Composed of 53BP1-RIF1 and BRCA1-CtIP Controls DNA Repair Pathway Choice. *Molecular Cell*. https://doi.org/10.1016/j.molcel.2013.01.001

114) Hayano, M., Kanoh, Y., Matsumoto, S., Renard-Guillet, C., Shirahige, K., & Masai, H. (2012). Rif1 is a global regulator of timing of replication origin firing in fission yeast. *Genes and Development*. https://doi.org/10.1101/gad.178491.111

115) Mukherjee, C., Tripathi, V., Manolika, E. M., Heijink, A. M., Ricci, G., Merzouk, S., de Boer, H. R., Demmers, J., van Vugt, M. A. T. M., & Ray Chaudhuri, A. (2019). RIF1 promotes replication fork protection and efficient restart to maintain genome stability. *Nature Communications*. https://doi.org/10.1038/s41467-019-11246-1

116) Feng, L., Fong, K. W., Wang, J., Wang, W., & Chen, J. (2013). RIF1 counteracts BRCA1-mediated end resection during DNA repair. *Journal of Biological Chemistry*. https://doi.org/10.1074/jbc.M113.457440

117) Matsuoka, S., Ballif, B. A., Smogorzewska, A., McDonald, E. R., Hurov, K. E., Luo, J., Bakalarski, C. E., Zhao, Z., Solimini, N., Lerenthal, Y., Shiloh, Y., Gygi, S. P., & Elledge, S. J. (2007). ATM and ATR substrate analysis reveals extensive protein networks responsive to DNA damage. *Science*. https://doi.org/10.1126/science.1140321

118) Wang, J., Zhang, H., Al Shibar, M., Willard, B., Ray, A., & Runge, K. W. (2018). Rif1 phosphorylation site analysis in telomere length regulation and the response to damaged telomeres. *DNA Repair*. https://doi.org/10.1016/j.dnarep.2018.03.001

119) Ran, F. A., Hsu, P. D., Wright, J., Agarwala, V., Scott, D. A., & Zhang, F. (2013). Genome engineering using the CRISPR-Cas9 system. *Nature Protocols*. https://doi.org/10.1038/nprot.2013.143

120) Tsui, C., Inouye, C., Levy, M., Lu, A., Florens, L., Washburn, M. P., & Tjian, R. (2018). DCas9-targeted locus-specific protein isolation method identifies histone gene regulators. *Proceedings of the National Academy of Sciences of the United States of America*, *115*(12), E2734–E2741. https://doi.org/10.1073/pnas.1718844115

121) Branon, T. C., Bosch, J. A., Sanchez, A. D., Udeshi, N. D., Svinkina, T., Carr, S. A., Feldman, J. L., Perrimon, N., & Ting, A. Y. (2018). Efficient proximity labeling in living cells and organisms with TurboID. *Nature Biotechnology*. https://doi.org/10.1038/nbt.4201

122) Ummethum, H., & Hamperl, S. (2020). Proximity Labeling Techniques to Study Chromatin. In *Frontiers in Genetics*. https://doi.org/10.3389/fgene.2020.00450

123) Hung, V., Udeshi, N. D., Lam, S. S., Loh, K. H., Cox, K. J., Pedram, K., Carr, S. A., & Ting, A. Y. (2016). Spatially resolved proteomic mapping in living cells with the engineered peroxidase APEX2. *Nature Protocols*. https://doi.org/10.1038/nprot.2016.018

124) Robbiani, D. F., Deroubaix, S., Feldhahn, N., Oliveira, T. Y., Callen, E., Wang, Q., Jankovic, M., Silva, I. T., Rommel, P. C., Bosque, D., Eisenreich, T., Nussenzweig, A., & Nussenzweig, M. C. (2015). Plasmodium Infection Promotes Genomic Instability and AID-Dependent B Cell Lymphoma. *Cell*, *162*(4), 727–737. https://doi.org/10.1016/j.cell.2015.07.019

125) Xu, Z., Zan, H., Pone, E. J., Mai, T., & Casali, P. (2012). Immunoglobulin class-switch DNA recombination: Induction, targeting and beyond. In *Nature Reviews Immunology*. https://doi.org/10.1038/nri3216

126) Chu, V. T., Weber, T., Graf, R., Sommermann, T., Petsch, K., Sack, U., Volchkov, P., Rajewsky, K., & Kühn, R. (2016). Efficient generation of Rosa26 knock-in mice using CRISPR/Cas9 in C57BL/6 zygotes. *BMC Biotechnology*. https://doi.org/10.1186/s12896-016-0234-4

127) T. Das, A., Tenenbaum, L., & Berkhout, B. (2016). Tet-On Systems For Doxycycline-inducible Gene Expression. *Current Gene Therapy*. https://doi.org/10.2174/1566523216666160524144041

128) Delgado-Benito, V., Berruezo-Llacuna, M., Altwasser, R., Winkler, W., Sundaravinayagam, D., Balasubramanian, S., Caganova, M., Graf, R., Rahjouei, A., Henke, M. T., Driesner, M., Keller, L., Prigione, A., Janz, M., Akalin, A., & Virgilio, M. Di. (2020). PDGFA-associated protein 1 protects mature B lymphocytes from stress-

induced cell death and promotes antibody gene diversification. *Journal of Experimental Medicine*. https://doi.org/10.1084/JEM.20200137

129) Ramachandran, S., Haddad, D., Li, C., Le, M. X., Ling, A. K., So, C. C., Nepal, R. M., Gommerman, J. L., Yu, K., Ketela, T., Moffat, J., & Martin, A. (2016). The SAGA Deubiquitination Module Promotes DNA Repair and Class Switch Recombination through ATM and DNAPK-Mediated γH2AX Formation. *Cell Reports*. https://doi.org/10.1016/j.celrep.2016.04.041

130) Horlbeck, M. A., Gilbert, L. A., Weissman, J. S., & Berger, S. L. (2019). Combinatorial *with a novel in vivo CRISPR activation platform*. *68*(2), 663–676. https://doi.org/10.1002/hep.29626.

131) Schwenk, F., Baron, U., & Rajewsky, K. (1995). A cre-transgenic mouse strain for the ubiquitous deletion of loxP-flanked gene segments including deletion in germ cells. *Nucleic Acids Research*. https://doi.org/10.1093/nar/23.24.5080

132) Yang, S., Zhou, L., Reilly, P. T., Shen, S. M., He, P., Zhu, X. N., Li, C. X., Wang, L. S., Mak, T. W., Chen, G. Q., & Yu, Y. (2016). ANP32B deficiency impairs proliferation and suppresses tumor progression by regulating AKT phosphorylation. *Cell Death and Disease*. https://doi.org/10.1038/cddis.2016.8

133) Ohno, Y., Koizumi, M., Nakayama, H., Watanabe, T., Hirooka, M., Tokumoto, Y., Kuroda, T., Abe, M., Fukuda, S., Higashiyama, S., Kumagi, T., & Hiasa, Y. (2017). Downregulation of ANP32B exerts antiapoptotic effects in hepatocellular carcinoma. *PLoS ONE*. https://doi.org/10.1371/journal.pone.0177343

134) Kumar, R., & Fang, C. C. (2017). Dynamics of RIF1 SUMOylation is regulated by PIAS4 in the maintenance of Genomic Stability. *Scientific Reports*. https://doi.org/10.1038/s41598-017-16934-w

135) Fontana, G. A., Hess, D., Reinert, J. K., Mattarocci, S., Falquet, B., Klein, D., Shore, D., Thomä, N. H., & Rass, U. (2019). Rif1 S-acylation mediates DNA double-strand break repair at the inner nuclear membrane. *Nature Communications*. https://doi.org/10.1038/s41467-019-10349-z

136) Kalidasan, V., Ng, W. H., Ishola, O. A., Ravichantar, N., Tan, J. J., & Das, K. T. (2021). A guide in lentiviral vector production for hard-to-transfect cells, using cardiac-derived c-kit expressing cells as a model system. *Scientific Reports*. https://doi.org/10.1038/s41598-021-98657-7

137) Pausch, P., Al-Shayeb, B., Bisom-Rapp, E., Tsuchida, C. A., Li, Z., Cress, B. F., Knott, G. J., Jacobsen, S. E., Banfield, J. F., & Doudna, J. A. (2020). Crispr-casf from huge phages is a hypercompact genome editor. *Science*, *369*(6501), 333–337. https://doi.org/10.1126/science.abb1400

138) Déjardin, J., & Kingston, R. E. (2009). Purification of Proteins Associated with Specific Genomic Loci. *Cell*. https://doi.org/10.1016/j.cell.2008.11.045

139) Bothmer, A., Robbiani, D. F., Di Virgilio, M., Bunting, S. F., Klein, I. A., Feldhahn, N., Barlow, J., Chen, H. T., Bosque, D., Callen, E., Nussenzweig, A., & Nussenzweig, M. C. (2011). Regulation of DNA End Joining, Resection, and Immunoglobulin Class Switch Recombination by 53BP1. *Molecular Cell*. https://doi.org/10.1016/j.molcel.2011.03.019

140) Yang, S., Zhu, X. N., Zhang, H. L., Yang, Q., Wei, Y. S., Zhu, D., Liu, M. Di, Shen, S. M., Xia, L., He, P., Ge, M. K., Pan, Y. L., Zhao, M., Wu, Y. L., Zheng, J. K., Chen, G. Q., & Yu, Y. (2021). ANP32B-mediated repression of p53 contributes to maintenance of normal and CML stem cells. *Blood*. https://doi.org/10.1182/blood.2020010400

141) Shen, H., & G. Maki, C. (2011). Pharmacologic Activation of p53 by Small-Molecule MDM2 Antagonists. *Current Pharmaceutical Design*. https://doi.org/10.2174/138161211795222603

142) Sheppard, H. M., Corneillie, S. I., Espiritu, C., Gatti, A., & Liu, X. (1999). New Insights into the Mechanism of Inhibition of p53 by Simian Virus 40 Large T Antigen. *Molecular and Cellular Biology*. https://doi.org/10.1128/mcb.19.4.2746

143) Moiseeva, T. N., Yin, Y., Calderon, M. J., Qian, C., Schamus-haynes, S., & Sugitani, N. (2019). *An ATR and CHK1 kinase signaling mechanism that limits origin firing during unperturbed DNA replication*. *116*(27). https://doi.org/10.1073/pnas.1903418116

144) All schemes in figures were prepared in bioRender.com.

7. APPENDIX

7.1. Selbstständigkeitserklärung

Hiermit erkläre ich, dass ich die vorliegende Arbeit mit dem Titel “ Dissecting the composition, dynamics, and regulation of immunoglobulin class switch recombination” selbstständig und ohne Hilfe Dritter angefertigt habe (sofern nicht anders angegeben). Sämtliche Hilfsmittel, Hilfen sowie Literaturquellen sind als solche kenntlich gemacht. Außerdem erkläre ich hiermit, dass ich mich nicht anderweitig um einen entsprechenden Doktorgrad beworben habe. Die Promotionsordnung des Fachbereichs Biologie, Chemie und Pharmazie der Freien Universität Berlin habe ich gelesen und akzeptiert.

7.2. Abbreviations

AID: activation-induced deaminase

ATM: ataxia telangiectasia mutated

ATR: ATM- and Rad3-Related

A-EJ: Alternate end-joining

BLM: Bloom syndrome

Bp: base pair

BRCA1: breast cancer type 1 susceptibility protein

BSA: bovine serum albumin

CRISPR: clustered regularly interspaced short palindromic repeats

CSR: class switch recombination

CTC1: conserved telomere maintenance component 1

CtIP: CTBP-interacting protein

DDR: DNA damage response

DMSO: dimethyl sulfoxide

DNA: deoxyribonucleic acid

DNA-PKcs: DNA-dependent protein kinase catalytic subunit

DSB: double-strand break

dsDNA: double-stranded DNA

EXO1: exonuclease 1

FH: FLAG-2xHA

GLT: germline transcription

gDNA: genomic DNA

GFP: green fluorescent protein

gRNA: guide RNA

HMCES: 5hmC binding embryonic stem cell-specific protein

H2A.X: H2A histone family member X

HDR: Homology directed repair

HEAT: Huntingtin, elongation factor 3, protein phosphatase 2A, TOR1)-like repeats domain

HEPES: 4-(2-hydroxylethyl)-1-piperazineethanesulfonic acid

HR: homologous recombination

HRP: horseradish peroxidase

Igh: immunoglobulin heavy chain

IDR: intrinsically disordered region

IRIF: ionizing radiation-induced foci

LIG4: DNA ligase 4

MEF: mouse embryonic fibroblast

MRE11: meiotic recombination 11 homolog 1

NBS1: Nijmegen breakage syndrome 1

NHEJ: non-homologous end joining

PARPi: PARP inhibitor PAR poly-ADP ribose PARP1 poly(ADP-ribose) polymerase-1

PBS: phosphate-buffered saline

PCR: polymerase-chain reaction

PEP: posterior error probability

PP1: protein phosphatase 1

PTIP: PAX transcription activation domain interacting protein

PTM: post-translational modification

Pol: Polymerase

RAG1/2: recombination activating genes 1/2

RIF1: Rap1-interacting factor 1

RNF: ring finger protein

RPA: replication protein A

SSA: Single stranded annealing

ssDNA: single stranded DNA

TGFβ: transforming growth factor β

UDR: ubiquitylation-dependent recruitment

V(D)J: variable, diversity and joining genes

WT: wild-type

XLF: XRCC4-like factor

XRCC4: x-ray repair cross complementing 4

ZMYND8: zinc finger MYND-type containing 8

γH2AX: phosphorylated histone H2AX

3'RR: 3' regulatory region

7.3. Publications

1. Sundaravinayagam, D., Rahjouei, A., Andreani, M., Tupiņa, D., Balasubramanian, S., **Saha, T.**, Delgado-Benito, V., Coralluzzo, V., Daumke, O., & Di Virgilio, M. (2019). 53BP1 Supports Immunoglobulin Class Switch Recombination Independently of Its DNA Double-Strand Break End Protection Function. ***Cell Reports***. https://doi.org/10.1016/j.celrep.2019.06.035
2. **Saha, T.**, Sundaravinayagam, D., & Di Virgilio, M. (2021). Charting a DNA Repair Roadmap for Immunoglobulin Class Switch Recombination. In ***Trends in Biochemical Sciences***. https://doi.org/10.1016/j.tibs.2020.10.005
3. Balasubramanian S.[#], Andreani M.[#], Andrade J.G., **Saha T.**, Sundaravinayagam D., Garzón J., Zhang W., Popp O., Hiraga S., Rahjouei A., Rosen D.B., Mertins P., Chait B.T., Donaldson A.D., and Di Virgilio M. (2022). Protection of nascent DNA at stalled replication forks is mediated by phosphorylation of RIF1 intrinsically disordered region. ***eLife***. DOI: 10.7554/eLife.75047

7.4. Acknowledgments

PhD has been quite an interesting journey. I must say that the experience has also changed my perspective towards life. It was a roller coaster ride with a combination of anxiety, exhilaration and self-loathing, all at the same time. Nonetheless, it definitely made me a stronger person in life and I finally could feel adulthood hitting me hard.

I firstly would like to thank Michela for giving me the opportunity to work on these projects. You are an excellent guide and I feel very lucky to do my PhD under your supervision. But mostly I thank you for believing in me constantly even when I was at my own rock bottom. I would have given up if it was not for your motivation and mentorship. You always tell me "celebrate the little achievements, or else it will get very difficult to find happiness", "acceptance is the key" etc. Your words have always been truly inspiring that I not only implemented in my PhD life, but also generally to survive in Berlin. You always kept reminding me of my love for science that helped me to keep going. Moreover, you really make it a point to have clear communications for feedback, criticism or any kind of not-so-pleasant conversation, yet another life skill I learnt. I can't describe in words how much I look up to you.

I would like to thank Prof. Dr. Oliver Daumke for your support as my reviewer. I would like to thank my committee members: Dr. Philipp Junker and Dr. Rushad Pavri for your valuable comments and feedback on my projects that helped me to shape them better.

I would like to thank Annette and Michaela from MDC PhD office for your constant support and encouragement.

I would like to thank Jasmine and Rachida from my lab and Sylvia and Andrea from the Welcome office for all the help with bureaucracy so that I could keep staying in Berlin.

I would like to thank all my lab members, ex and current: Sandhya, Jenisha, Dev, Matteo, Vero, Julia, Marie, Giulia, Maria, Eleni, Tobias, Lisa, Ali, Omkar and Yael. Everyone is such a wonderful and helpful person. I don't know if I can ever find a lab like this, it's almost impossible! I could not have been luckier.

Maria and Tobias, thank you for joining the sports club with me. Eleni you bailed us. Going to the classes with you guys really helps me to destress from all the PhD stuffs. Maria, you have been so kind and helpful. You always know what to say to pump me up. I hope Tobias, you can finally make me swim like a pro and together we eat in all the restaurants of Berlin. Eleni,

I admire your confidence. You are a brilliant scientist and I really appreciate your criticism, even if it hurts (no it doesn't hurt, you are a great critic).

Sandhya, Sophiya and Jenisha, thank you for being there for me. You guys have been amazing friends and helped me to revive when I was at my lowest. I don't feel alone here anymore, I could see Berlin as my home because of you guys. Also thank you Max for inviting me at your place and bearing me and Sophiya share our PhD stories.

I want to thank Rishabh, Julia, Shikha, Sumeet and Kumar. I always have a great time with you guys.

Now for my four support pillars, Navo, Faiza, Kanishka and Supriya. I can't thank you guys enough for existing. You guys are my personal counsellors. No matter what, you were always there for me and stood up for me. Navo, you are the greatest empath I have ever met. You are my little sister who I grew up with (in our adulthoods). Faiza, you are basically my wife. Your unconditional love makes me feel so safe and secure in life. You are also my mother, always looking out for me. Kanishka, you have been my elder sister who is always very protective about me. It's like you adopted this introverted awkward girl into your life. Supriya, you are one of the major reason that I am in Germany. I have learnt to enjoy life and to be optimistic in life because of you. All of you have been for me through thick and thin. PhD without you guys would have been impossible. I have always been able to turn my life around after any setback because of you people. I absolutely love you guys and can't imagine my life without you all. You guys are my family.

Philipp, you have not been in my life for long. But you have been with me during a very crucial time period, the Thesis writing process! Your mere presence helped me to keep my sanity in this duration. Thank you.

Finally, I would like to thank my Maa and Baba. Thank you for having the faith in me that I could do this. I know it was not easy for you when I left to live on another continent. I always had one motive in life, to make my parents proud. I don't know if I actually did that, but I would still really want you all to be here in my defence and finally see what I did in these last 5 years.

Thank you everyone!